Application of Collagen Matrices for Enhancing Cardiac Regeneration

Ali Ahmadi

Thesis submitted to the

Faculty of Graduate and Postdoctoral Studies

in partial fulfillment of the requirements

for the Doctorate in Philosophy degree in Cellular and Molecular Medicine

Department of Cellular and Molecular Medicine

Faculty of Medicine

University of Ottawa

Abstract

Injectable biomaterials have emerged as a treatment for myocardial infarction (MI). They can be applied either as an enhancement for cell therapy or as a stand-alone treatment for MI. The main focus of this study was to apply circulating angiogenic cells (CACs) with or without an injectable collagen matrix for MI treatment in a mouse model. Furthermore, a collagen-chitosan matrix was tested for modulating the myocardial maladaptive remodeling post-MI. First, the *in vivo* thermo-gelling and retention properties of the collagen matrix were validated using positron emission tomography (PET) tracer and quantum dot (Qdot) labelled matrix in MI mouse hearts. The therapeutic potential of the matrix ± CACs was then tested in a mouse MI model. The results showed that CACs-only and matrix-only treatments were associated with cardiac function preservation. However, in combination, CAC + matrix therapy had a synergistic effect and significantly improved cardiac function (echocardiography), perfusion and viability (PET scan), increased cell engraftment and arteriole density, and reduced the infarct size. CAC-matrix interaction through the integrin $\alpha 2$ receptor was essential for the observed therapeutic effect. In a third study, the addition of chitosan (a polysaccharide) to the collagen matrix was shown to reduce maladaptive remodeling post-MI by limiting cardiac fibroblast-to-myofibroblast differentiation and scar formation. In conclusion, these collagen-based hydrogels hold promise to enhance cardiac repair as a delivery scaffold for therapeutic cells, and/or as a stand-alone treatment, which can actively modulate the environment including the fibrotic process after MI.

Acknowledgments

I would like to express my gratitude to my supervisor Dr. Erik Suuronen for giving me the opportunity to work in his lab and for providing excellent guidance and support over years. I also thank my co-supervisor Dr. Marc Ruel for his great help and support during my PhD. I would like to thank the members of my thesis advisory committee, Dr. Darryl Davis, and Dr. Maxwell Hincke for their input and advice. During my PhD, I have had the opportunity to work alongside some great people who not only helped me along the way, but also provided a very productive and pleasant working environment for all trainees including myself. Many thanks to Branka Vulesevic for her kind help and advice. I would like to thank Dr. Rob deKemp, Dr. Jean DaSilva and Dr. Rob Beanlands for their great advice and priceless help throughout my projects. Also, I would like to thank Suzanne Crowe, Brian McNeill, Rick Seymour, Joanne McBane, Donna Padavan and Eva Mathieu who helped me with many, many things. I would like to mention our Molecular Function and Imaging Program collaborators, Animal Care and Veterinary Services staff and also Drew Kuraitis, Mary Zhang, Pingchuan Zhang, Chao Deng, Tanja Sofrenovic and Celine Giordano. I would like to thank my family for their support over the years. I could not have done it without them.

Table of Content

ABSTRACT ……..…ii

ACKNOWLEDGMENTS ……...iii

LIST OF FIGURES …….ix

LIST OF TABLES ……...xi

ABBREVIATIONS …….xii

CHAPTER 1: INTRODUCTION ……1

1.1 Structure of the Heart ……...…….....2

1.2 Coronary Artery Disease: Myocardial Infarction and Remodeling …….....4

1.3 Conventional Treatment Strategies for Heart Failure ……...……7

1.4 Clinical Challenge of Heart Failure ……...…...7

1.5 Endogenous Myocardial Regeneration in Humans ……..8

1.6 Role of Endogenous Stem/Progenitor Cells in Cardiac Regeneration …….……..……....9

1.7 Cell Therapy for the Infarcted Myocardium ……...10

1.7.1 Stem Cells Applied in Clinical Trials …….……11

1.7.2 Endogenous Mobilization of Stem Cells …….12

1.7.3 CAC Therapy ……...13

1.8 Characterization of CACs ……...14

1.9 Clinical Trials with CACs ……...16

1.10 Limitations of Cell Therapy ……..18

1.11 Biomaterial Enhancement Strategies for CAC Therapy ……...18

1.12 Injectable Biomaterials ...……..21

1.12.1 General Considerations of Injectable Biomaterials …….....21

1.12.2 Injectable Biomaterials as a Scaffold for CAC Transplantation …….....23

1.12.3 Injectable Biomaterials as a Stand-alone Therapy ……..…24

1.13 ECM in Normal and Remodeling Heart ……...25

1.13.1 Normal ECM Structure ……..25

1.13.2 Integrin Receptors ……..…….....26

1.13.3 Role of Itgs in ECM and CAC Cross-Talk …….…….....26

1.13.4 ECM Alterations after Infarction …….……..28

1.14 Cardiac Fibroblasts: Key components of Cardiac Remodeling …….....30

1.14.1 Role of Cardiac Fibroblasts in Post-MI Repair …….…….30

1.14.2 Cardiac Fibroblasts as a Therapeutic Target after Infarction …….....30

1.14.3 Applying Biomaterials to Target Fibroblasts …….....31

1.15 Summary ……...31

1.16 Research Plan ……..32

1.16.1 Aims ……...32

1.16.2 Hypotheses …….……....33

1.17 Role in Research ……..33

Chapter 2: PET Imaging Reveals Effective Injection and Targeted Retention of a Collagen Matrix in a Mouse Model of Myocardial Infarction ……..34

2.1 Notes on Chapter ……..35

2.2 Contributions of Co-authors ……..36

2.3 Abstract ……..37

2.4 Introduction ……38

2.5 Methods ……..40

2.6 Results ……..44

2.7 Discussion ……...55

2.8 Supplementary Section ……...60

Chapter 3: The Role of Integrin α2 in Cell and Matrix Therapy that Improves Perfusion, Viability and Function of Infarcted Myocardium ……...63

3.1 Notes on Chapter ……64

3.2 Contributions of Co-authors ……...65

3.3 Abstract……66

3.4 Introduction ……66

3.5 Materials and methods ……68

3.6 Results ……73

3.7 Discussion ……..90

3.8 Conclusion ……..92

3.9 Supplementary Section ……...94

Chapter 4: A Collagen-Chitosan Injectable Hydrogel Improves Cardiac Remodeling in a Mouse Model of Myocardial Infarction …….....98

4.1 Notes on Chapter ……..……...99

4.2 Contribution of Co-authors ……...100

4.3 Abstract ……101

4.4 Introduction ……...103

4.5 Methods ……104

4.6 Results ……...108

4.7 Discussion ……..123

Chapter 5: General Discussion ……126

5.1 Minimally Invasive Collagen Matrix Delivery …….....127

5.2 Collagen Matrix as Enhancement Strategy for CAC Therapy ……..128

5.3 Optimum Timing of Intervention after MI ……...130

5.4 Collagen-Based Hydrogels as Cell Therapy Enhancement Strategy or Stand-alone Approach

……..131

5.5 Future Directions ……..133

References ……..140

Appendices ……179

Appendix A- Methods for the Figures of Chapter 5 ……...179

Appendix B – Authorizations …….180

List of Figures

FIGURE 1.1: Cardiac remodeling after MI ……....6

FIGURE 1.2: Biomaterial application strategies for MI ……..20

FIGURE 1.3: Biomaterial delivery methods ……..…….22

FIGURE 1.4: Integrin-ILK pathway ….…….……....29

FIGURE 2.1: Representative images of PET scans …….……...47

FIGURE 2.2: PET imaging of matrix retention and distribution properties ….……..49

FIGURE 2.3: Biodistribution …….……51

FIGURE 2.4: Qdot labeling efficiency ……...53

FIGURE 2.5: Evaluation of Qdot-labeled matrix in MI heart ……54

SUPPLEMENTARY FIGURE 2.1: Qdot-collagen matrix reaction scheme ……62

FIGURE 3.1: Combined CACs+matrix therapy improves the perfusion, glucose uptake, and function of MI mouse hearts ……79

FIGURE 3.2: CACs+matrix therapy limits adverse remodeling and improves vascular density and transplanted cell retention ……..81

FIGURE 3.3: Integrin α2β1 is required for the functional enhancement of CACs on collagen matrix ……83

FIGURE 3.4: The synergistic effect of CACs+matrix therapy in MI mouse heart is lost when integrin α2 is blocked in CACs ……85

FIGURE 3.5: Collagen matrix-enhanced function of CACs is dependent on integrin α5 ……..87

FIGURE 3.6: Collagen matrix-enhanced integrin α5 expression involves Itgα2 signaling and the ERK pathway ……89

SUPPLEMENTARY FIGURE 3.1: Integrin α2 is required for increased ILK expression in matrix-cultured mouse BM-CACs ……94

SUPPLEMENTARY FIGURE 3.2: The ability of CACs+matrix therapy to limit adverse remodeling is inhibited when itgα2 is blocked in CACs ……..95

FIGURE 4.1: Cardiac fibroblast culture ……..…112-113

FIGURE 4.2: Left ventricular EF and FS in MI mice injected with different treatments …….114

FIGURE 4.3: Infarct size assessment 1wk and 3wks after treatment delivery …….115

FIGURE 4.4: Arteriole density in mouse MI hearts …….117

FIGURE 4.5: $CD68^+$ cells in mouse MI hearts …….119

FIGURE 4.6: MMP9 and TIMP2 levels in the treated hearts ……...121

FIGURE 5.1: Ratio of $C\text{-}kit^+$ cells in the infarcted myocardium to the entire ventricles …….135

FIGURE 5.2: Circulating serum levels of VEGF and G-CSF in MI mice 3wks after treatment delivery……137

LIST OF TABLES

SUPPLEMENTARY TABLE 3.1: Summary of qPCR primers ……96

Abbreviations

^{13}NH3	[^{13}N]-ammonia
^{18}F-FDG	2-[^{18}F]fluoro-2-deoxy-D-glucose
^{18}F-HFB	hexadecyl-4-[^{18}F]fluorobenzoate
^{18}F-NaF	^{18}F- sodium fluoride
ACE	angiotensin-converting enzyme
Ang-1	angiopoietin-1
AP1	activator protein 1
ATP	adenosine 5’-triphosphate
BM	bone marrow
CACs	circulating angiogenic cells
CDCs	cardiosphere-derived cells
CMR	cardiac magnetic resonance
COX	cyclooxygenase
CSCs	cardiac resident stem cells
CXCR4	CXC chemokine receptor type 4
DAPI	4'6-diamidino-2'-phenylindole

EBM-2	endothelial basal medium 2
ECM	extracellular matrix
EDC	ethyl(dimethylaminopropyl) carbodiimide
EF	ejection fraction
ELISA	enzyme-linked immunosorbent assay
eNOS	endothelial nitric oxide synthase
EPCs	endothelial progenitor cells
FACS	fluorescence activated cell sorting
FAK	focal adhesion kinase
FGF	fibroblast growth factor
FISH	fluorescence in situ hybridization
FOV	field-of-view
FS	fractional shortening
G-CSF	granulocyte colony-stimulating factor
GFP	green fluorescent protein
GSK3	glycogen synthase kinase 3
HGF	hepatocyte growth factor

HIF-1	hypoxia-inducible factor 1
HMG-CoA	5-hydroxy-3-methylglutaryl-coenzyme A
HPS	hematoxylin-phloxine-saffron
HSCs	hematopoietic stem cells
HUVECs	human umbilical vein endothelial cells
IGF	insulin-like growth factor
IL	interleukin
Itg	integrin
ILK	integrin-linked kinase
LDL	low density lipoprotein
LVEF	left ventricular ejection fraction
MBq	millibecquerel
MHC	myosin heavy chain
MI	myocardial infarction
MNCs	mononuclear cells
MMP	matrix metalloproteinase
MSCs	mesenchymal stem cells

mTOR	mammalian target of rapamycin
NF-κB	nuclear factor kappa-light-chain-enhancer of activated B cells
NHS	N-Hydroxysuccinimide
NOS	nitric oxide synthase
PBS	phosphate buffered saline
PCI	percutaneous coronary intervention
PDGF	platelet-derived growth factor
PET	positron emission tomography
Qdots	quantum dots
RMV	real-time microvisualization
ROIs	regions of interest
ROS	reactive oxygen species
SCID	severe combined immunodeficiency
SD	standard deviation
SDF	stromal cell-derived factor
SEM	standard error of the mean
SM	skeletal myoblast

SMA	smooth muscle actin
SPECT	single-photon emission computed tomography
TGF	transforming growth factor
TIMPs	tissue inhibitor of metalloproteinases
VEGF	vascular endothelial growth factor
VEGFR-2	vascular endothelial growth factor receptor 2
vWF	von Willebrand factor

Chapter 1: General Introduction

1.1 Structure of the Heart

The heart is a fibromuscular cone-shaped organ situated in the middle thoracic mediastinum (Mahadevan, 2012). Its inferior surface lies on the diaphragm central tendon and its base is adjacent to the esophagus and descending aorta. The left atrium and a part of right atrium constitute the base. The heart's left and right surfaces lie medial to a lung and a phrenic nerve. The sternum and the costal cartilages protect the anterior surface of the heart (Whitaker, 2010).

There are four chambers in the heart: the right and left atria and the right and left ventricles. These are separated by atrioventricular valves: the tricuspid valve on the right and the mitral valve on the left. Each ventricle is separated from its great artery by a semilunar valve with crescent-shaped cusps: the pulmonary valve between the right ventricle and the pulmonary artery and the aortic valve between the left ventricle and the aorta (Katz, 2006).

The heart wall is made up of three layers: epicardium, myocardium and endocardium. The epicardium is the visceral layer of the pericardium which is a double-walled enclosing sac around the heart. The outer pericardium is a fibrous protective connective tissue which anchors the heart to the diaphragm and great vessels; and the inner pericardium is a thin serous membrane composed of two layers: the parietal layer (lining the inner surface of the fibrous pericardium) and the visceral pericardium (epicardium). Between the two layers of the visceral pericardium there is a serous fluid that allows the two membranes to glide smoothly (Des Jardins, 2008). The myocardium is the muscular part of the ventricle walls and is made up of overlapping spiral sheets which sweep from the heart base to the apex. The muscle fibers at the outer surface of the left ventricle are arranged parallel to the base-apex axis of the heart. At the inner surface of ventricular myocardium, the muscle fibers are oriented circumferentially (Katz,

2006). As a result of this myocardial fiber pattern, when the left ventricle contracts it twists and turns toward the chest wall and to create the apical impulse (Opie, 2004).

The oxygenated blood from the lungs flow into the left atrium and subsequently enters the left ventricle as the mitral valve opens. The mitral opening happens only during the left ventricle relaxation phase (diastole) that reduces the left ventricular pressure. During left ventricular contraction (systole), the two mitral valve cusps are forced to close which prevents the blood from flowing back to the left atrium (Opie, 2004). The ventricular cusps are tethered at the margins by thin fibrous structures (chordae tendinae) that attach to long muscular projections of the ventricular inner wall (papillary muscle) (Des Jardins, 2008). As the mitral valve is shut by left ventricular contraction, the aortic valve is forced to open by the increasing ventricular pressure and the blood travels throughout the circulation (Opie, 2004).

The myocardium is irrigated by the coronary arteries which arise from the aorta. Sinus of Valsalva is located behind each of the three aortic valve cusps. The anterior and left posterior sinuses give rise to the right and left coronary arteries while no coronary artery originates from the right posterior sinus (Katz, 2006). The left coronary artery divides into the left anterior descending and the circumflex coronary arteries. The former runs on the anterior wall and supplies the apex and the interventricular septum and the latter irrigates the posterior wall of the left ventricle and also the left atrium. The right coronary artery supplies the right atrium and then divides into the posterior descending and marginal arteries (Des Jardins, 2008); in about 10% of human hearts the posterior descending artery originates from the circumflex artery (Katz, 2006). The posterior descending artery supplies the posterior wall of both ventricles and the marginal branch supplies the lateral wall of the heart (Des Jardins, 2008).

1.2 Coronary Artery Disease: Myocardial Infarction and Remodeling

Atherosclerosis is the most prevalent cause of morbidity and mortality in the developed world. Briefly, formation of the atherosclerotic plaque is initiated by endothelial dysfunction, intimal accumulation of lipoproteins, leukocyte recruitment and accumulation of lipoprotein particles in monocytes (foam cell formation) (Strom, 2011). As the plaque progresses, smooth muscle cells migrate into the intima and extracellular matrix (ECM) synthesis and degradation is altered. Finally, calcification, fibrosis and smooth muscle cell death occur which may be accompanied by hemodynamic stresses leading to plaque disruption and thrombus formation (Libby et al., 2002). The clinical manifestation of coronary artery plaque rupture is an acute cardiac event such a myocardial infarction (MI) (Libby, 2002), which is characterized at the cellular level by myocyte necrosis due to severe impairment of blood flow to the myocardium. The progression of cell death from sustained ischemia often starts in the sub-endocardium (sub-endocardial infarct) (Rhee, 2011) and spreads toward the sub-epicardium in a wave front (transmural infarct) (Opie, 2004, Rhee, 2011). The wave front phenomenon is caused by increasing intraventricular pressure and progressive failure of left ventricle. Therefore, the larger the initial infarct zone is, the larger and faster the wave front is (Opie, 2004).

Occlusion of a major coronary artery leads to cell death by apoptosis, necrosis, or a combination of both (Nadal-Ginard et al., 2003). Apoptosis induces acute modification in the myocardial structure and impairment of myocardial force development (Cheng et al., 1995). Necrosis causes inflammation, macrophage infiltration, fibroblast activation, and finally scar formation (Nadal-Ginard et al., 2003). Different mechanisms have been proposed for the irreversible myocardial damage in the context of severe prolonged ischemia: (1) inhibition of the sodium pump; (2) substantial loss in the reservoir of adenosine 5’-triphosphate (ATP); (3) metabolically or

mechanically damaged cell membrane; (4) free radical formation; and (5) calcium overload. The amount of tissue which is irreversibly damaged by the severe ischemia is referred to as the infarct size. Therefore, upon occlusion of a major coronary artery, the whole area supplied by that artery is at risk of infarction. In a typical rabbit model, about 60% of the ischemic area will undergo infarction after coronary artery occlusion (Opie, 2004).

The irreversible damage of functional myocardial cells quickly leads to impaired contractile function of the ventricle and results in systolic dysfunction, which is characterized by cardiac output decrease and loss of synchronous myocardial contraction. Therefore, the damaged myocardium becomes hypokinetic (reduced contraction), akinetic (no contraction at all) or dyskinetic (bulging out of the infarcted region) during contraction of the remaining functional ventricular tissue. Furthermore, diastolic dysfunction of the left ventricle develops because ventricular diastolic relaxation is an energy dependent process; the heart's function is adversely affected by reduced ventricular compliance and elevated filling pressures. After MI, cardiac remodeling eventually occurs and the abnormal loading conditions change the geometry of both infarcted and non-infarcted regions (Rhee, 2011). Within days, the infarct area begins to expand and becomes thinner. Within days to months, global remodeling results in overall ventricular dilation, mitral valve dysfunction, augmentation of wall stress, formation of aneurysms and ventricular arrhythmias (Jessup and Brozena, 2003, Rhee, 2011). A recent study using contrast enhanced cardiac magnetic resonance (CMR) imaging showed that adverse cardiac remodeling in remote areas starts as early as 5 days post-MI (Chan et al., 2012). These structural and functional abnormalities ultimately lead to heart failure (Jessup and Brozena, 2003) (Figure 1.1).

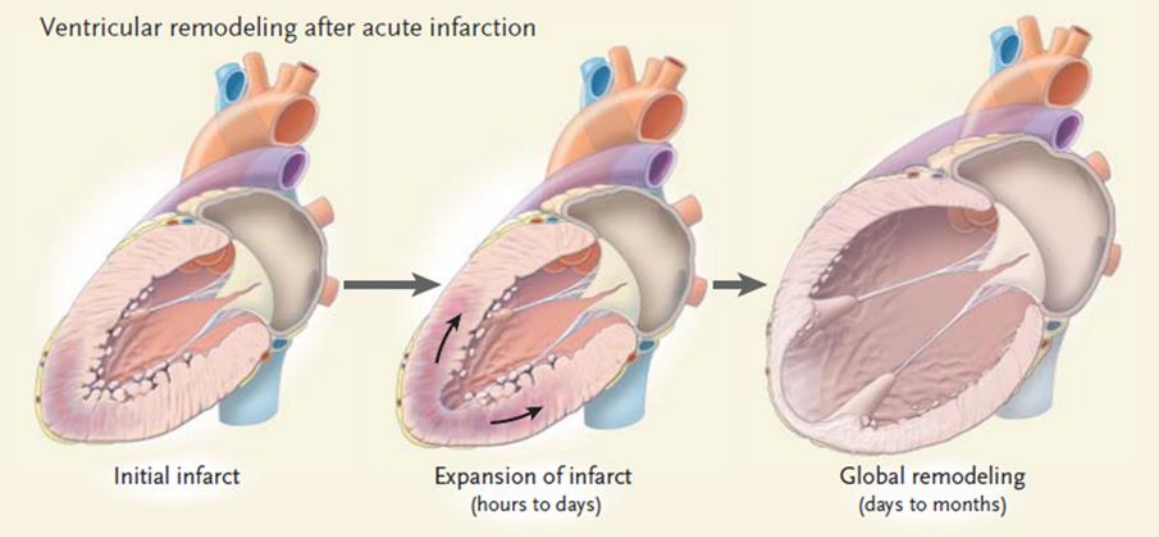

Figure 1.1 Cardiac Remodeling after MI. In the infarcted area of the myocardium, cardiomyocytes undergo cell death (apoptosis and necrosis) and the infarct area expands and becomes thinner within days. The remodeling continues over a period of weeks, which leads to morphologic and physiologic alteration of the entire LV.

Reproduced with permission from (Jessup and Brozena, 2003); Copyright Massachusetts Medical Society

1.3 Conventional Treatment Strategies for Heart Failure

Thrombolysis treatment has been shown to decrease the transmural MI mortality from 11% to less than 7%, if applied within a few hours of the onset of infarction (Bohula, 2012). Mortality and morbidity was even further reduced by the advent of acute percutaneous coronary intervention and also with the addition of anti-platelet agents (e.g. glycoprotein IIb/IIIa inhibitors) (Schomig et al., 2000). Conventional post-discharge therapy for MI patients targets controlling lipids (statins), blood pressure (angiotensin-converting enzyme (ACE) inhibitors), heart rate (beta blocker), and blood coagulation (anti-platelet therapy) (Bohula, 2012). Furthermore, rigorous attention to underlying risk factors like diabetes and smoking is essential (Rhee, 2011). The use of implantable automatic defibrillators has also been shown to further reduce the mortality rate by about 7% over five years (Bardy et al., 2005).

Despite conventional treatment strategies, heart failure has increased in prevalence in North America and worldwide (Kannel, 2000, Mendez and Cowie, 2001). This is due to: (1) a significant decrease in mortality results in the survival of patients with a large MI who progress to heart failure; (2) an increase in the number of patients at risk of MI as the population ages; and (3) the development of cardiac risk factors at a younger age (Bohula, 2012).

1.4 Clinical Challenge of Heart Failure

In spite of recent advances in conventional therapies for acute and chronic heart failure, the mortality rate remains significant: ~4% in hospital, ~10% in the first two months after discharge, and up to 30% after one year (Jong et al., 2002, Yancy et al., 2006). Although ACE inhibitors are proven to be efficient in reducing the mortality associated with heart failure (Shearer et al.,

2013), current therapies can only slow the progression of cardiomyocyte loss, but they fail to reverse the process of cardiac remodeling (Bohula, 2012).

It has been shown that a left ventricular ejection fraction of ≤30% is associated with a high risk of sudden cardiac death (Rhee, 2011), which warrants heart transplantation as the definitive treatment (Bohula, 2012). Heart transplantation has a survival rate of 85% at the end of first year and 50% after ten years (Taylor et al., 2008). The major limitation of transplantation is that the demand largely surpasses the donor supply (Langone and Helderman, 2003).

1.5 Endogenous Myocardial Regeneration in Humans

Myocardial regeneration has emerged as a potential treatment for heart failure since the myocardium of both non-mammalian and mammalian hearts has shown regenerative capacity (Bohula, 2012). Several studies suggest that the human heart has some degree of cellular turnover: (1) the measurement of carbon-14 (generated by nuclear bomb tests) integrated into human cardiomyocyte DNA has shown that cardiomyocyte renewal occurs at the rate of 1% at the age of 25 and decreases to 0.45% at the age of 75, which suggests a renewal of more than half of the cardiomyocytes during an average life span (Bergmann et al., 2009); (2) in human aortic stenosis, a small level of cardiomyocyte mitosis and division has been demonstrated (Urbanek et al., 2003); (3) in human end-stage heart ischemia the number of mitotic cardiomyocytes increases to 10 times that in the normal heart (Kajstura et al., 1998); and (4) biopsies of patients who underwent heart transplantation demonstrated that in nearly 30% of cardiomyocytes, DNA synthesis and replication occur in the context of heart failure (Beltrami et al., 1997).

1.6 Role of Endogenous Stem/Progenitor Cells in Cardiac Regeneration

An experimental study used a double transgenic mouse model in which constitutive expression of β-galactosidase was replaced by green fluorescent protein (GFP) expression in cardiomyocytes upon tamoxifen treatment. This study showed that MI induced the formation of new cardiomyocytes in the peri-infarct and non-infarcted areas from an immature endogenous myocyte or progenitor cell pool (Hsieh et al., 2007). Results such as these have led to greater research into understanding the potential for endogenous stem/progenitor cells to contribute to cardiac regeneration in response to injury or disease.

In the human body, adult progenitor cells that exist in the circulation or within niches in the bone marrow (BM), home to damaged tissues in response to appropriate induction signals (Koyanagi, 2012). Hematopoietic stem cells (HSCs), endothelial progenitor cells (EPCs) and mesenchymal stem cells (MSCs) have all been reported to be mobilized and/or recruited by various signals such as granulocyte-colony stimulating factor (G-CSF) and stromal cell-derived factor-1 (SDF-1) (Koyanagi, 2012).

The contribution of marrow-derived circulating cells to cardiomyocytes and endothelium formation was shown in a study of male recipients of female BM allograft by applying dual color fluorescence in situ hybridization (FISH) (X and Y chromosome-specific probes) (Thiele et al., 2004). A similar study indicated that in male recipients of female heart transplantation, the endothelial cells and vascular smooth muscle cells show a high degree of chimerism (24.3±8.2% and 11.2±2.1%, respectively) from extracardiac sources (Minami et al., 2005). Similarly, in another study, Y chromosome positive nuclei were detected in post-mortem transplanted hearts of male patients who had heart transplantation from female donors. This chimeric study

concluded that 18% of cardiomyocytes, 20% of coronary arterioles and 14% of capillaries originated from male cells, indicating recruitment from the male host into the female donor heart (Quaini et al., 2002). These findings have been challenged by a more recent study using HSCs carrying a fusion gene consisting of the α-myosin heavy chain (MHC) promoter and a modified β-galactosidase gene. The cells were injected to the peri-infarct myocardium in mice 5h after MI surgery. Tracking of the transplanted cells up to 28 days post-MI showed no cardiomyocyte transdifferentiation of HSCs (Murry et al., 2004). Although marrow-derived progenitor cells may not transdifferentiate to cardiomyocytes after MI, it is suggested that their main therapeutic effect is through the release of growth factors and induction of angiogenesis (Balsam and Robbins, 2005).

1.7 Cell Therapy for the Infarcted Myocardium

Although the body mounts an endogenous regenerative response, it is insufficient to prevent progression of heart disease. Therefore, regenerative therapies are an attractive approach to restore tissues and cardiac function. Multiple clinical and experimental studies have focused on cell therapy for improvement of myocardial regeneration after infarction (Bohula, 2012). In this context, there are three main therapeutic aspects to be addressed: (1) the best cell or cardiac tissue to be targeted; (2) the most efficient method of stimulating regeneration; (3) the optimum timing for intervention (Kuraitis et al., 2010).

Presumably, the best cardiac regeneration strategy involves the replacement of the lost cardiomyocytes (Bohula, 2012). However, experimental and clinical studies have also highlighted the importance of angiogenesis in the inadequately perfused myocardium (Suuronen et al., 2007, Erbs et al., 2007, Kawamoto et al., 2003).

1.7.1 Stem Cells Applied in Clinical Trials

Different cell types including BM-derived HSCs, MSCs, resident cardiac stem cells (CSCs), skeletal myoblasts (SMs) and circulating angiogenic cells (CACs) have been tested and shown to improve heart function in humans (Segers and Lee, 2008). Undifferentiated marrow-derived mononuclear cells (MNCs) have been shown to improve left ventricular ejection fraction (LVEF) (Seeger et al., 2007). $CD133^+$ cells, which constitute a primitive subtype of MNCs, were applied in a non-randomized clinical trial, and improved LVEF and enhanced myocardial glucose uptake were observed (Bartunek et al., 2005). MSCs are stromal cells which can be isolated from bone marrow and adipose tissue and have the capacity to exert paracrine effects to suppress inflammation and apoptosis (Amado et al., 2005). Several clinical studies are investigating the safety and feasibility of MSC delivery in MI patients. Current published data has indicated that a high dose (6×10^{10}) but not a low dose (5×10^{6}) MSC injection is associated with a significant improvement in LVEF (Tongers et al., 2011). CSCs, which are $lineage^-$ $ckit^+$, have shown a capacity to generate cardiomyocytes (Beltrami et al., 2003). Since the total number of CSCs in the heart is low, CSCs have been expanded *ex vivo* from endomyocardial biopsies (Bearzi et al., 2007). The Marban group has identified a CSC population that can be isolated from self-adherent clusters (cardiosphere-derived stem cells (CDCs)), and which show cardiomyogenic potential (Davis et al., 2010). A recent randomized controlled trial of CDC therapy in 17 MI patients has showed promising results in terms of decreased scar tissue and increased viable myocardium (Malliaras et al., 2014). SMs are isolated from muscle biopsies, and have been expanded *ex vivo* and delivered to the infarcted heart (Murry et al., 1996). The most comprehensive SM Phase II clinical trial has indicated no improvement in LVEF after 6 months and even a significant LVEF deterioration in the high dose group (Menasche et al., 2008). Since the myoblast injection has

also been associated with increased arrhythmic events in patients (Menasche et al., 2003), SM application for MI patients is controversial (Tongers et al., 2011). The characterization and application of CACs, which are a heterogeneous population of angiogenic cells, will be discussed later in this chapter. These results indicate, for the most part, that cell therapy can be safe and effective at improving cardiac function in patients; however, improvements are still needed to further enhance the degree to which cell therapies can promote repair and regeneration.

1.7.2 Endogenous Mobilization of Stem Cells

In addition to cell transplantation, strategies are being developed to attract greater numbers of endogenous stem cells to the injured or diseased tissue. G-CSF is the major mobilizing agent that has been used in clinical trials. One study showed a modest improvement in LVEF, wall motion and infarct zone wall thickness in patients that received G-CSF for 6 consecutive days following angioplasty. This effect was attributed to higher mobilization of $CD34^+$ MNC into the systemic circulation (Ince et al., 2005). In contrast, a meta-analysis conducted in 2008, indicated no therapeutic benefit associated with G-CSF therapy in the context of MI (Zohlnhofer et al., 2008). Yet, a more recent meta-analysis on the clinical outcomes of G-CSF treatment indicated non-significant trends towards LVEF improvements in 3-6 months after injection (Zimmet et al., 2012). Another potential approach is to target the SDF-1 pathway, which is known to enhance progenitor cell trafficking. It has been shown that recruitment of angiogenic cells via the SDF-1 signaling pathway is required for myocardial regeneration; competitive inhibition of SDF-1 by a mutant form of the chemokine, delivered on a lentiviral plasmid, was associated with a decreased regenerative response and reduced cardiomyocyte repopulation in a fetal sheep model of MI (Allukian et al., 2013). In a recent clinical study, a non-viral DNA plasmid encoding human

SDF-1 was delivered to 17 ischemic cardiomyopathy patients via endomyocardial injection. Four months after treatment, the patients' 6-minute walk distance and quality of life were reported to be improved. These therapeutic benefits persisted at 12 months post-treatment (Penn et al., 2013).

Adult stem cells secrete a multitude of growth factors, chemokines, and enzymes that not only play an important role in different stages of tissue regeneration, angiogenesis and cardiac remodeling, but also recruit more progenitor cells to the ischemic site (Gnecchi et al., 2008). In fact, paracrine signaling is believed to be the main mechanism by which transplanted cells exert their positive effects on the MI heart, rather than direct tissue generation/replacement (Cho et al., 2007). In summary, the recruitment of endogenous progenitor cells constitutes an essential element of myocardial regeneration. The types of cells contributing to regeneration may vary depending on the pathophysiologic state of the heart. In the normal heart, resident CSCs are responsible for myocardial turnover. In the infarcted myocardium, a regenerative response arises from CSCs and circulating endogenous progenitor cells which are recruited to the damaged tissue (Malliaras et al., 2013).

1.7.3 CAC Therapy

In this context, CACs have emerged as a promising cell source for myocardial repair and regeneration. They release growth factors with multiple positive effects including cardiomyocyte survival, neovascularization, the prevention of adverse remodeling, and the induction of endogenous progenitor cell mobilization (Shintani et al., 2001, Takahashi et al., 1999, Jujo et al., 2008). Furthermore, there is evidence that CACs have the potential for differentiation into endothelium, therefore directly contributing to new tissue formation (Cho et al., 2003). The

safety of CAC therapy has been demonstrated by multiple clinical trials (Tongers et al., 2011), and will be discussed in detail later in this chapter.

1.8 Characterization of CACs

Endothelial precursors, positive both for hematopoietic stem cell marker (CD34) and endothelial markers (vascular endothelial growth factor receptor-2 (VEGF-R2)), were first isolated from human peripheral blood in 1997 by Asahara et al. The isolated $CD34^+$ cells (first termed endothelial progenitor cells (EPCs)) showed potential for endothelial differentiation *in vitro* and also incorporation to newly formed blood vessels *in vivo* (Asahara et al., 1997). Several studies to identify putative markers for human EPCs have been conducted using hematopoietic marker CD133 (Gehling et al., 2000, Shi et al., 1998). EPCs are often characterized as $CD133^+$ and VEGF-$R2^+$ cells, which in the presence of appropriate growth factors, can differentiate to endothelial cells which express CD34 and von Willebrand factor (vWF) markers and incorporate acetylated low-density lipoprotein (LDL)(Shi et al., 1998). However, a study demonstrated that $CD133^+CD34^+$VEGF-$R2^+$ cells isolated from umbilical cord or from peripheral blood after G-CSF stimulation, do not differentiate into endothelial cells *in vitro* (Case et al., 2007). Concurrently, another group demonstrated that only $CD34^+CD45^-$ cells and not the $CD34^+CD45^+$ cells show the potential to form endothelial cell colonies (Timmermans et al., 2007). Another study indicated that $CD133^+CD34^-$VEGR-2^+ cells are precursors for $CD133^+CD34^+$VEGFR-2^+ cells, but the $CD34^-$ cells show a higher potency with respect to homing and vascular repair in patients with limb ischemia and also in an artery injury mouse model (Friedrich et al., 2006).

These findings are not consistent in identifying EPC specific markers. The complexity of EPC characterization is, to some degree, attributable to differences between *in vitro* culture conditions

and *in vivo* environments; the growth factors and chemokines secreted in the damaged tissue can alter cell differentiation and function in a fashion which is not reproducible *in vitro*. The transplanted cells, on the other hand, interact with other cells of the tissue by paracrine mechanisms which further adds to the complexity of *in vivo* environment (Koyanagi, 2012). These are some of the reasons why pro-angiogenic cells obtained from the culture of peripheral blood mononuclear cells are commonly referred to as circulating angiogenic cells (CACs), to reflect their heterogeneity and function, rather than their status as true endothelial precursors. Typically, CACs are generated from the culture of bone marrow-derived mononuclear cells (from BM or peripheral circulation) on fibronectin; the adherent cells after 4-7 days are referred to as early CACs. These CACs express endothelial markers (e.g. VEFG-R2, vWF, and CD31) (Kalka et al., 2000) and myeloid markers (e.g. CD45 and CD14). After 14 days of culture, late CAC cultures form large colonies on the plate. These cells express a higher level of VEGFR-2 and demonstrate a higher potential to incorporate in the capillaries; however, late CACs secretes less cytokines compared to early CACs (Koyanagi, 2012).

The characterization and identification of CACs has been controversial. None of the current identifying and quantifying methods has shown a reliable capacity to predict the *in vivo* behavior of the cells. Moreover, it is unknown whether the culture-modified cells only represent an artificial phenotype or they naturally exist in the circulation or BM (Fadini et al., 2012). Overall, the main difference between the types of CACs is the culture time. The short-term protocols (4-7 days) yield myeloid/hematopoietic cells and the long-term protocols (more than 14 days) give a more homogenous population of CACs with a reduced cytokine release profile (Koyanagi, 2012). The *in vivo* capacity of CACs to enhance angiogenesis differs with respect to their culture protocol. It has been shown that short-term culture CACs mainly enhance tissue perfusion by

providing potent growth factors that promote angiogenesis (Di Santo et al., 2009, Urbich et al., 2005, Rehman et al., 2003). The cells gained by long-term culture contribute to the structure of new blood vessels by differentiating to endothelial cells (Yoon et al., 2005b, Hur et al., 2004). Despite the existence of different methods for CAC isolation and culture, defining CACs has been challenging because of the following reasons: 1) although it has been shown that a variable percentage of endothelial cells is derived from BM (Gunsilius et al., 2000), a common precursor for marrow-derived blood cells and endothelial cells has not been identified (Fadini et al., 2012); 2) growing evidence indicates a new concept that mature endothelial cells can dedifferentiate and enter the circulation with an overlapping endothelial-hematopoietic phenotype (e.g. CD34 expression) in case of tissue injury (Chao and Hirschi, 2010); and 3) many cell surface markers are expressed by both hematopoietic and endothelial cells which complicates the determination of lineage difference between the two (Fadini et al., 2012).

1.9 Clinical Trials with CACs

Several clinical studies have demonstrated the efficacy and feasibility of CAC therapy. Autologous $CD133^+$ cell injection in combination with bypass surgery resulted in improved cardiac function and perfusion in a group of myocardial ischemia patients (Stamm et al., 2003). Another clinical study has tested the therapeutic benefit of autologous $CD133^+$ cell implantation in patients who were candidates for limb amputation due to critical limb ischemia. This treatment improved treadmill walking time and prevented leg amputation (Burt et al., 2010). A non-randomized clinical trial (TOPCARE-AMI trial) indicated improved LV function in patients treated with a heterogeneous population of CACs (Schachinger et al., 2004). In the REPAIR-AMI randomized trial, intracoronary injection of marrow-derived progenitor cells improved LV function significantly (Schachinger et al., 2006). In this context, not only CACs, but also

marrow-derived MNCs have shown the capacity for moderate but significant improvement of LV function (Assmus et al., 2006). Moreover, the efficacy of marrow-derived MNCs for moderately increasing LV function (~3%) and slightly improving the quality of life, has been shown in a randomized double-blind clinical trial (van Ramshorst et al., 2009). In the BOOST trial, intracoronary delivery of unselected marrow-derived progenitor cells after percutaneous coronary intervention (PCI) was associated with a transient increase in LV function at 6 month; however, this effect did not persist until month 18 post-injection (Meyer et al., 2006). A phase I double-blind randomized controlled trial was conducted using CACs in patients with severe inoperable coronary heart disease. The autologous CACs were collected from peripheral blood MNCs and injected directly to the ischemic myocardium using an electromechanical mapping system. This treatment was associated with improved clinical parameters such as reduced angina frequency and increased exercise duration and overall showed a trend favoring the CAC therapy (Losordo et al., 2007, Losordo et al., 2011). Overall, clinical studies reported an enhanced recovery in cardiac function after CAC therapy (Dimmeler et al., 2008). Despite these promising results, the long-term therapeutic effects of CAC therapy is not elucidated yet (Koyanagi, 2012); it has been suggested that the cell therapy benefit may be sustained for at least two years following treatment delivery (Assmus et al., 2010). However, the effect of CAC therapy is variable due to different subtypes of CACs used in clinical trials and also because the cells have been applied at different stages of myocardial ischemia (Koyanagi, 2012). Several clinical trials are underway to further study the prospect of cell therapy in patients with different types of ischemic disease, including coronary artery disease. As discussed before, the most important issue to be addressed in these second generation trials, is to maximize sustainable therapeutic benefits for the patients (Wollert and Drexler, 2010b). Given the variation in clinical outcomes

with similar cell isolation protocols in previous trials (Hirsch et al., 2008, Huikuri et al., 2008, Lunde et al., 2006, Schachinger et al., 2006), it is essential to establish a standard protocol for cell isolation, characterization and delivery to the target tissue (Wollert and Drexler, 2010b). This is also confirmed by a recent meta-analysis on marrow-derived stem cells indicating that clinical trials with more discrepancies in patient selection and study design yield larger variances in results compared to studies with fewer discrepancies (Nowbar et al., 2014).

1.10 Limitations of Cell Therapy

Cell therapy is mainly limited by poor cell engraftment and survival after delivery, regardless of the cell type used (Wollert and Drexler, 2010b). Moreover, co-morbidities (e.g. diabetes), advanced patient age and heart failure have a negative impact on the functional activity of marrow-derived progenitor cells, including CACs. The cells isolated from patients with diabetes and heart failure demonstrate impaired activity in repairing denuded arteries when transplanted into mice (Dimmeler and Leri, 2008), which is associated with reduced *in vitro* functionality such as decreased colony formation and impaired migration capacity (Assmus et al., 2007). Cell therapy enhancement strategies are, therefore, required to augment the therapeutic potential of progenitor cells (Wollert and Drexler, 2010b).

1.11 Biomaterial Enhancement Strategies for CAC Therapy

Strategies for enhancing the efficacy of transplanted progenitor cells are needed in order to overcome the challenges posed by the hostile environment of the infarcted myocardium, which include: (1) ischemia and reduced perfusion of the infarcted area; (2) inflammatory response due to oxidative stress and cytotoxic cytokines and (3) loss of normal ECM (Wollert and Drexler, 2010b). These conditions reduce cell engraftment and function, thus limiting the therapeutic

potential of cell transplantation. The use of biomaterials presents an opportunity to address all of these limitations. Biomaterials are being designed to improve the host environment into which the cells are being transplanted, to enhance the therapeutic potential of the transplanted cells, and to increase the engraftment of the transplanted cells. Theoretically, an ideal biomaterial will improve the secretion of growth factors and cytokines from the cells, promote their engraftment and survival and guide their phenotype and function (Wollert and Drexler, 2010b). Several different biomaterial approaches have been tested for cell delivery in the context of MI, including: (1) transplantable cell sheets generated *in vitro* from cells that have been stimulated to produce their own ECM; (2) culturing cells on a scaffold *in vitro* and then suturing the cultured tissue on the epicardial surface of the heart; (3) decellularized cardiac ECM; and 4) injectable biomaterials as delivery scaffolds (Christman and Lee, 2006) (Figure 1.2).

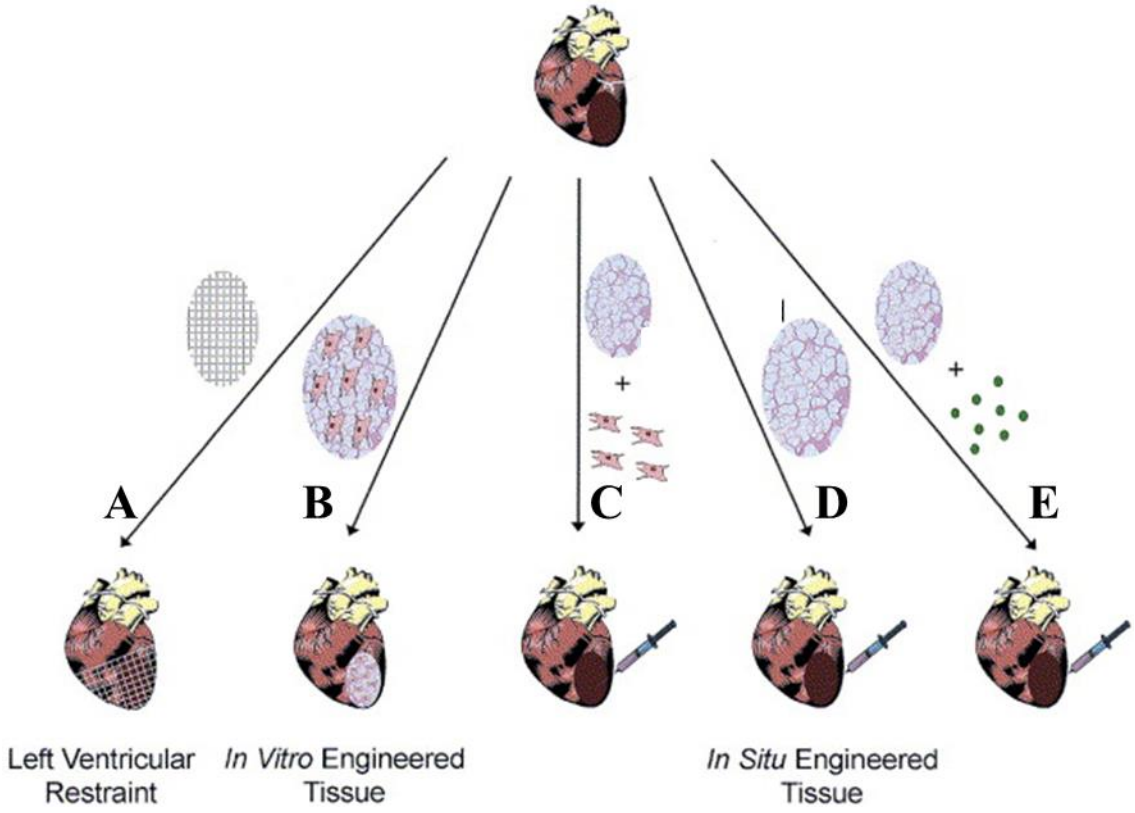

Figure 1.2 Biomaterial application strategies for MI. (A) A biocompatible mesh can be fixed around the infarted heart to prevent LV dilation. (B) Progenitor cells are cultured on biomaterials to form a tissue *in vitro*. The tissue is grafted on the epicardial surface of the heart. (C) Progenitor cells are delivered within an injectable matrix. (D) Injectable biomaterial can be used as a stand-alone therapy for MI. (E) Injectable scaffold have also shown the capacity to act as a vehicle for growth factors and/or chemokine delivery.

Reprinted with permission from (Christman and Lee, 2006); Permission from Elsevier

1.12 Injectable Biomaterials

1.12.1 General Considerations of Injectable Biomaterials

The injectable biomaterial approach is less invasive than implanting a polymer mesh or an epicardial patch and is therefore more favorable for clinical application (Christman and Lee, 2006); injectable materials have the potential to be delivered via catheter. This also allows for direct treatment delivery to the damaged myocardium. Injectable biomaterials are mainly hydrogels, which are made of cross-linked polymer networks from natural or synthetic sources. Within the body, the hydrogel is solidified by a variety of ways depending on how the hydrogel is cross-linked and also its chemical makeup. Hydrogel cross-linking may be achieved by covalent bonds, physical entanglements or ionic interactions which can respond to triggers like pH or temperature (Radisic and Christman, 2013).

Possible non-invasive methods for hydrogel delivery are intracoronary infusion (Leor et al., 2009) and transendocardial injection (Seif-Naraghi et al., 2013) (Figure1.3). The disadvantages of both methods are: (1) risk of leakage to the blood stream at the time of injection; (2) risk of solidification due to exposure to the body heat during the time the hydrogel flows through the catheter to its target area at the infarcted myocardium. Therefore, a very quick gelling injectable material may not be compatible with these two delivery methods and also the challenge of being hemocompatible to reduce the risk of emboli is a major concern. The preferable biomaterial delivery method is via direct myocardial injection that reduces the exposure of injected material to the circulation (Johnson and Christman, 2013). Finally, the depth and quantity of injected material must be carefully monitored to minimize the risk of cardiac arrhythmia after injection (Radisic and Christman, 2013).

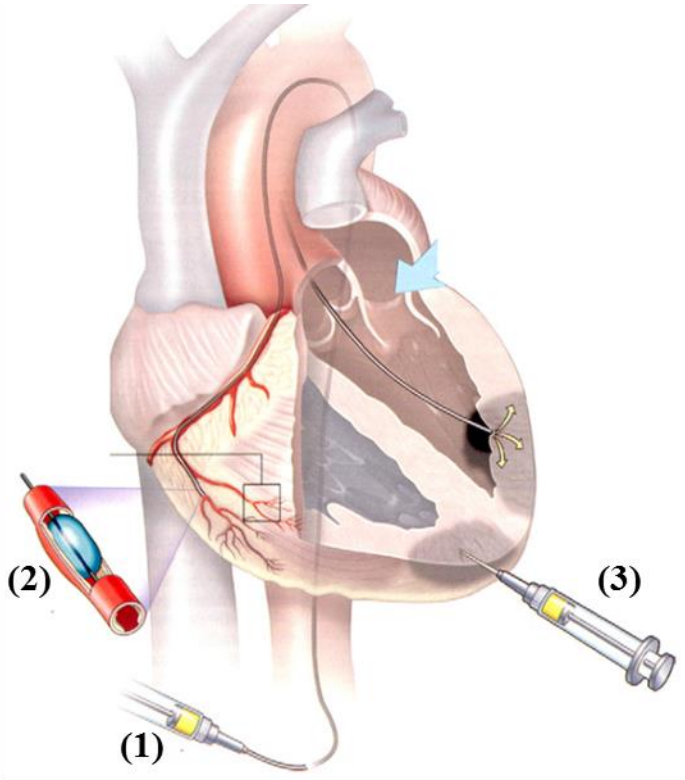

Figure 1.3 Biomaterial delivery methods. Injectable biomaterials can be injected in experimental models via 3 routes: 1) transendocardial injection; 2) intracoronary delivery by using an inflated percutaneous transluminal coronary balloon; and 3) direct injection to the infarcted myocardium.

Reprinted from (Stamm et al., 2009); Permission from Elsevier

1.12.2 Injectable Biomaterials as a Scaffold for CAC Transplantation

Many materials have been tested for the delivery of multiple cell types (Radisic and Christman, 2013). Of particular interest to the present work are biomaterials for CAC therapy. The injection of CACs with a fibrin matrix (used commercially as a sealant) resulted in improvement of cardiac function and angiogenesis (Chekanov et al., 2003). Another study investigated CAC delivery within a thermo-gelling collagen matrix in a rat ischemic hindlimb model; results showed that the CACs (labeled with a positron emission tomography (PET) tracer) were mostly retained at the injection site in the hindlimb, whereas the cell-only injection showed a poor cell retention after 4hrs (Zhang et al., 2008b). The injection of a collagen-based matrix to the ischemic hindlimb of rats increased arteriole density, and this effect was further improved by adding $CD133^{+}$ cells to the collagen matrix. The same study also demonstrated the positive effect of the collagen matrix on the retention of transplanted cells in the target tissue compared to the cell-only group (Suuronen et al., 2006). CAC delivery within a macroporous alginate scaffold has been shown to be associated with augmented blood vessel density, improved perfusion and prevention of foot necrosis in a severe combined immunodeficiency (SCID) mouse model of hindlimb ischemia (Silva et al., 2008). Kim et al. have developed a biosynthetic material as a scaffold for CAC therapy in a murine dermal injury model. The scaffold increased the survival and retention of injected cells and improved their vascular repair potential (Kim et al., 2009). An injectable polylactic coglycolic acid-based injectable matrix has also been used as a vehicle for delivering CACs and angiogenic growth factors (VEGF, hepatocyte growth factor (HGF) and angiopoietin-1 (Ang-1)). The therapeutic benefits of CAC delivery in the scaffold (enhanced incorporation to blood vessels and higher capillary density) is improved when the pro-angiogenic growth factors are also delivered (Saif et al., 2010). In the same animal model, co-injection of

MSCs and EPCs within a thermo-gelling engineered peptide hydrogel (PuraMatrix) show synergistic effects in promoting angiogenesis compared to either element injected alone (Allen et al., 2011). The focus of another study was the fate of EPCs after injection within an injectable fibrin matrix; the cells were transfected with β-galactosidase *in vitro* and the mixture of cells and matrix was injected subcutaneously at the dorsum of rats. The cells within the matrix formed blood vessels and also migrated along the intermuscular septa and differentiated to mature endothelial cells (Bleiziffer et al., 2011). A therapy consisting of $CD133^+$ cells in a collagen type 1 patch was favorable for blood vessel formation, but it did not promote the formation of cardiomyocytes or vascular smooth muscle cells in a rat MI model (Pozzobon et al., 2010). Overall, the use of a biomaterial appears promising for improving the benefits that can be obtained from cell therapy.

1.12.3 Injectable Biomaterials as a Standalone Therapy

Although injectable biomaterials were first developed to improve cell survival and engraftment after transplantation by providing a temporary ECM (Radisic and Christman, 2013), it was later discovered that they can also be utilized as a stand-alone therapy as well, to support the left ventricular wall and prevent the negative effects of cardiac remodeling (Johnson and Christman, 2013). For example, an injectable fibrin glue has been shown to preserve cardiac function and left ventricular geometry in a rat model of heart ischemia (Christman et al., 2004). In a rat model of hindlimb ischemia, a collagen-based matrix containing sialyl $Lewis^X$ which binds L-selectin membrane receptor on progenitor cells, improved the recruitment of endogenous and exogenous L-$selectin^+$ cells and improved arteriole density and perfusion in the ischemic tissue (Suuronen et al., 2009).

The exact mechanism by which certain hydrogel-only treatments in experimental models show therapeutic effects is still under debate. A recent study indicated that the myocardial injection of an alginate-chitosan hydrogel prevents adverse cardiac remodeling in a rat MI model potentially by improving angiogenesis, attenuating inflammation and reducing cardiac cell apoptosis (Deng et al., 2014). Although some studies suggest mechanical wall support by thickening the infarct wall as a potential mechanism involved in the therapeutic benefits conferred from myocardial injection of hydrogels, more recent studies indicated that bioactivity of injected materials plays an essential role in attenuating the negative cardiac remodeling (Radisic and Christman, 2013). For example, in one study, a bio-inert and non-degradable synthetic polymer was injected to the infarcted rat myocardium one week after MI surgery. The results indicated that passive reinforcement of myocardial structure could preserve infarct wall thickness, but it was not sufficient to prevent adverse post-MI remodeling and restore normal ECM (Rane et al., 2011). Therefore, bioactivity appears to be an important consideration in the development of injectable biomaterials to be used as stand-alone therapies; insight into the required functions of such biomaterials may come from a better understanding of the role of the native ECM.

1.13 ECM in Normal and Remodeling Heart

1.13.1 Normal ECM Structure

Normal cardiac ECM is made up of basement membrane and stromal matrix. The former provides a support for tissues' peripheral cells such as the outer layer of blood vessels and the latter maintains structural support for the cells within a tissue (Kuraitis et al., 2012b). The ECM key components include collagens (e.g. collagen type 1 and 4), non-collagenous glycoproteins (e.g. fibronectin, laminin, vitronectin), proteoglycans (e.g. transmembrane transforming growth

factor beta receptor), glycosaminoglycans (e.g. chondroitin sulfate) and matrix-bound growth factors (e.g. VEGF, interleukin-1 (IL-1)). The ECM provides essential structural support and also a regulatory system for the cells; it not only regulates cells by transducing signal through integrin (Itg) receptors but also act as a reservoir for growth factors and ligands (Friedman, 2010).

1.13.2 Integrin Receptors

Integrins (Itgs) are adhesion receptors composed of non-covalently bound α and β subunits. The Itg family is made up of 18 α and 8 β subunits which form 24 different Itg heterodimers. The amount of α subunits is generally the determinant of heterodimer formation since the β subunits are more abundant in the cells. Upon ligand binding to a region at the intersection of two subunits, the β subunit undergoes conformational changes which trigger multiple signaling cascades. The major ECM-integrin binding sites (and some of their corresponding integrins) are: (1) the RGD sequence (e.g. α5β1) on fibronectin, vitronectin and fibrinogen; and (2) the GFOGER sequence (e.g. α1β1, α2β1) on the fibrillar collagens. In summary, the Itg receptors interact actively with ECM and relay cell-specific signaling which can alter the conformation of the receptor itself, leading to cell functional changes (Barczyk et al., 2010).

1.13.3 Role of Itgs in ECM and CAC Cross-Talk

CACs contribute to the angiogenic process through four inter-related phases: (1) mobilization from the BM reservoir to the blood stream in response to chemoattractant agents; (2) homing to the damaged tissue; (3) migration through the ECM; and (4) differentiation to endothelial cells and/or provision of paracrine signaling. During this process, CACs need to interact with adjacent cells and also the ECM (Caiado and Dias, 2012).

Itg receptor subunits α2, β1 and β2 have been shown to play a major role in CAC interaction with the ECM (Carmona et al., 2008, Chavakis et al., 2005). A recent *in vitro* study has shown that collagen type 1 induces the self-renewal of mouse embryonic cells through activation of α2 β1 Itg which up-regulates integrin-linked kinase (ILK) (Suh and Han, 2011). ILK is a serine threonine kinase that has been shown to bind to the intracellular domain of β Itgs (Hannigan et al., 2005) and its activation is stimulated by the interaction of cells with the ECM (Cho et al., 2005). ILK activation plays an important role in promoting pro-survival (Akt/NFκB) and inhibiting pro-apoptotic signaling (Chiarugi and Giannoni, 2008) (Figure 1.4).

In a rat MI model, the injection of adenoviral vector expressing ILK to the myocardial peri-infarct areas one week post-MI was associated with reduced infarct size, LV mass preservation, and enhanced angiogenesis. However, ILK over-expression in this MI model did not result in significant improvement in cardiac function (Ding et al., 2009). Moreover, in a mouse model of hindlimb ischemia, CACs which were transfected with the ILK gene showed enhanced survival, reduced apoptosis and higher capacity to restore blood flow (Cho et al., 2005). It has also been shown that ILK is down-regulated in CACs isolated from patients with coronary artery disease. This is associated with CAC dysfunction which can be rescued by restoration of ILK expression *in vitro* (Werner et al., 2008).

Itg α5 is also highly expressed in CACs and plays a pivotal role in the cell-ECM interaction which is required for homing to the injury site, regulation of gene expression and angiogenesis (Caiado and Dias, 2012). A study has indicated that statins improve endothelial repair in a rat model of arterial denudation by recruiting marrow-derived CACs to the injury site. Notably, the

CACs had increased expression of Itg α5 and β1 at the protein and the mRNA level (Walter et al., 2002). Blocking Itg α5 in marrow derived CACs has been shown to decrease the therapeutic capacity of CACs to repair blood vessel endothelium in a mouse model of pulmonary vascular injury (Wary et al., 2009). Knowledge of CAC-matrix interactions and the integrins involved is likely to help optimize biomaterials designed to enhance CAC therapy.

1.13.4 ECM Alterations after Infarction

Disruption of the normal matrix after MI leads to LV geometry alteration and cardiac dysfunction. A severe inflammatory reaction is triggered by cardiomyocyte death and leads to activated leukocyte infiltration; the acute inflammatory phase lasts almost 4 days in large mammals. This activates matrix metalloproteinases (MMPs) which mediate matrix degradation. The matrix debris and dead cells are subsequently cleared by macrophages; myofibroblasts then accumulate and generate a large quantity of type I and type III collagen. As the reparative phase continues, a mature infarct scar develops and myocardial mechanical properties change, which results in LV dilation and sphericity. In this context, it has been shown that ECM proteins play a major role in modulating fibroblast/myofibroblast phenotype and gene expression (Dobaczewski et al., 2010).

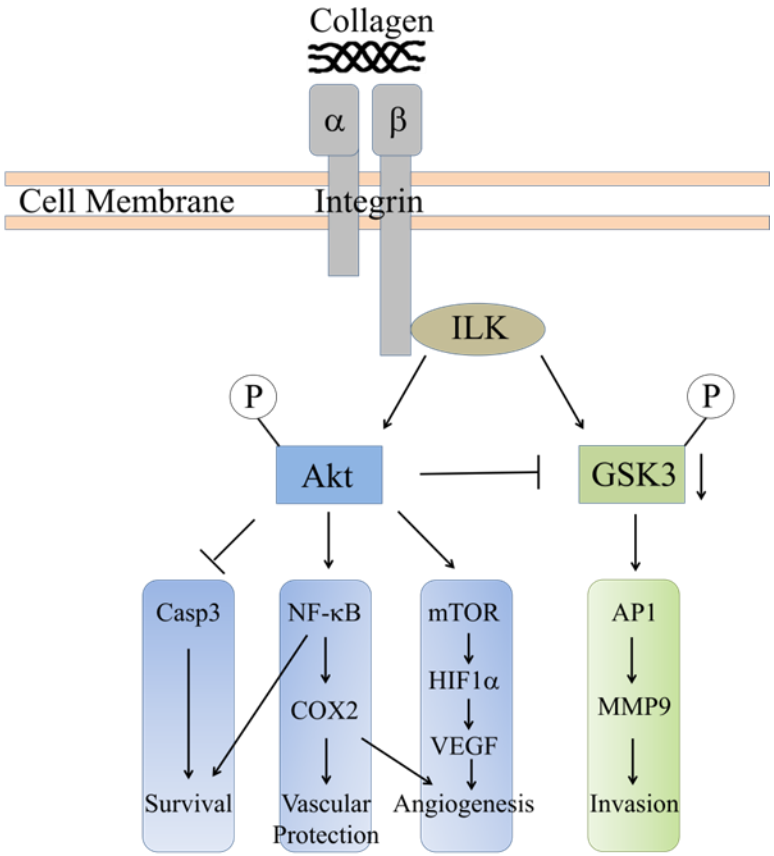

Figure 1.4 Integrin-ILK pathway. Upon adhesion of collagen to Itg receptor, the β subunit undergoes a conformation change leading to ILK activation, which then phosphorylates Akt and GSK3. Akt phosphorylation increases its activity, which ultimately results in cell survival, angiogenesis and vascular protection. GSK3 phosphorylation relieves the negatively regulated MMP9 pathway. (AP1: activator protein 1; Casp3: caspase 3; COX2: Cyclooxygenase 2; MMP9: matrix metalloproteinase 9; GSK3: glycogen synthase kinase 3; HIF1: hypoxia-inducible factor 1; ILK: integrin linked kinase; mTOR: mammalian target of rapamycin; NF-κB: nuclear factor kappa-light-chain-enhancer of activated B cells; VEGF: vascular endothelial growth factor)

1.14 Cardiac Fibroblasts: Key components of Cardiac Remodeling

1.14.1 Role of Cardiac Fibroblasts in Post-MI Repair

As the post-MI inflammation subsides (mainly due to activation of IL-10 and transforming growth factor (TGF)-β), fibroblasts proliferate and differentiate to myofibroblasts which secrete a substantial amount of ECM proteins. Simultaneously, IL-10 and TGF-β induce the secretion of tissue inhibitor of metalloproteinases (TIMPs) that improve matrix deposition and preservation. This proliferative phase lasts 4-14 days which is succeeded by the maturation phase, characterized by matrix cross-linking and fibroblast quiescence (Dobaczewski et al., 2010). In the aging myocardium, fibroblasts respond poorly to growth factors; this leads to decreased collagen deposition, defective scar formation and ventricular dilation (Chen and Frangogiannis, 2013).

1.14.2 Cardiac Fibroblasts as a Therapeutic Target after Infarction

Targeting fibroblasts may be a promising strategy for post-MI cardiac remodeling since cardiac fibroblasts are the main effector cells of the reparative phase (Chen and Frangogiannis, 2013). For example, targeting TGF-β1 has been shown to be an effective approach to modify cardiac remodeling (Bujak and Frangogiannis, 2007). However, inhibition of fibroblast function may induce adverse cardiac remodeling by reducing the tensile strength of the scar (Chen and Frangogiannis, 2013). The time frame of intervention is also important since inhibition of TGF-β signaling at the early stages of infarction prolongs the inflammatory reaction (Ikeuchi et al., 2004). Late TGF-β1 inhibition may be ineffective because fibrosis and advanced scar formation

have occurred. Thus, improved/preserved cardiac function depends on optimal anti-fibrotic intervention, which remains elusive (Chen and Frangogiannis, 2013).

1.14.3 Applying Biomaterial to Target Fibroblasts

A scaffold-based 3D human fibroblast culture has been tested as an epicardial patch in immunodeficient mice after MI surgery; the patch delivery was associated with increased angiogenic response compared to control mice; however, the mechanisms of this angiogenic effect were not investigated (Kellar et al., 2001). A potential mechanism is the release of angiogenic factors from the transplanted fibroblasts, such as fibroblast growth factor (FGF). In another study, FGF was delivered within an injectable chitosan hydrogel to a rat MI model and resulted in improved cardiac function, reduced fibrosis and higher arteriole density (Wang et al., 2010). The animals injected with growth factor alone did not show a significant improvement compared to the control, indicating that biomaterials can provide a means to prevent rapid washout and sustain FGF release over the course of study (Wang et al., 2010). A similar study confirmed that FGF delivery within a pH- and thermo-sensitive injectable hydrogel improves angiogenesis by controlling the release of the growth factor in rat model of MI. This was also associated with cardiac function improvement (Garbern et al., 2011).

1.15 Summary

The objective of cell therapy is to limit adverse cardiac remodeling, repair/regenerate tissue and maintain/enhance cardiac function in infarcted hearts. Clinical trials have indicated the overall safety and moderate efficiency of cardiac cell therapy in terms of cardiac function improvement and infarct size reduction (Jeevanantham et al., 2012). However, cell therapy typically suffers from low cell retention and engraftment in the hostile ischemic myocardium. Furthermore, post-

MI ECM alteration is known to be an important modulatory component not only to cell survival but also to inflammatory, reparative and fibrotic responses. The use of injectable hydrogels has the potential to improve the post-MI environment as well as support the survival and therapeutic efficacy of cells transplanted for cardiac regeneration.

1.16 Research Plan

1.16.1 Aims

The primary goal of this research was to test an injectable collagen-based matrix for application in the heart. Specifically, there were 3 main objectives: 1) to examine the injection and retention properties of the collagen matrix when applied to the beating myocardium; 2) to use the matrix to enhance CAC therapy for infarcted hearts; and 3) to test a collagen-chitosan matrix as a stand-alone therapy for treating established myocardial scar post-MI. These 3 aims are summarized as follows:

Aim (1): A minimally invasive ultrasound-guided injection technique was used to deliver a thermo-gelling collagen matrix to the infarcted mouse myocardium (Chapter 2). This aim focused on: (I) labeling the collagen matrix either with hexadecyl-4-[(18)F]fluorobenzoate (^{18}F-HFB) PET radiotracer or with Qdot® 525 ITK™ carboxyl quantum dots (q-dots) for tracking matrix distribution in the heart after injection; and (II) measuring the retention (matrix in the target tissue) and leakage (matrix in off-target tissue) relative to total injected matrix.

Aim (2): The collagen matrix was used as an enhancement strategy for CAC therapy in a mouse MI model (Chapter 3). The therapeutic benefits of CAC delivery within the collagen matrix was assessed in terms of myocardial perfusion and viability, cardiac function, cell engraftment,

infarct size and arteriole density. Furthermore, the role of integrins in the therapeutic benefit of CACs+matrix treatment was examined.

Aim (3): A collagen-chitosan matrix was delivered to the MI mouse heart as a strategy to repair the established myocardial scar produced after MI (Chapter 4). The effect of fibronectin (control), collagen and collagen-chitosan on fibroblasts/myofibroblast differentiation was investigated *in vitro*; and the therapeutic benefit of collagen-chitosan injection to infarcted myocardium during reparative phase was assessed.

1.16.2 Hypotheses

It was hypothesized that: (1) a collagen thermo-gelling hydrogel would demonstrate favorable retention and distribution properties after injection to the infarcted mouse heart; (2) the collagen matrix would enhance the therapeutic efficacy of CACs delivered in a mouse model of myocardial infarction by improving integrin and ILK signaling; and (3) a collagen-chitosan matrix would alter adverse cardiac remodeling after MI mediated through its interaction with cardiac fibroblasts.

1.17 Role in research

At the beginning of each chapter, the role of co-authors is described for the respective studies. Other than the stated co-author contributions, the experiments were designed, performed and analyzed by myself.

Chapter 2

PET Imaging Reveals Effective Injection and Targeted Retention of a Collagen Matrix in a Mouse Model of Myocardial Infarction

At the time of thesis preparation, this chapter was submitted for consideration of publication in a peer-reviewed journal as per following citation:

Ali Ahmadi, Stephanie Thorn, Myra Kordos, Donna T. Padavan, Tayabeh Hadizad, Gregory O. Cron, Rob S. Beanlands, MD, Jean N. DaSilva, Marc Ruel, Robert A. deKemp, Erik J. Suuronen. PET Imaging Reveals Effective Injection and Targeted Retention of a Collagen Matrix in a Mouse Model of Myocardial Infarction. 2014; under review.

2.1 Notes on Chapter

Injectable matrices have emerged not only as a promising vehicle to deliver transplanted cells and other therapeutic agents to damaged or diseased tissue, but also as stand-alone therapies. However, no study has ever addressed the accuracy and efficiency of biomaterial injection to the dynamic environment of the contracting myocardium. The retention and distribution of our collagen matrix after ultra-sound guided delivery to the infarcted mouse myocardium is reported in this chapter.

2.2 Contributions of Co-authors

S. Thorn assisted with PET image analysis.

M. Kordos operated PET scans with my assistance.

R. deKemp provided technical advice on optimizing PET experimentations and was involved in PET data generation and analysis, and manuscript writing.

D. Padavan designed the matrix q-dot labeling experiments.

T. Hadizad and J.N. DaSilva developed and provided the PET radiotracers.

G.O. Cron performed the *in vivo* fluorescence imaging with my assistance.

R.S. Beanlands provided clinical perspective on the data and manuscript editing.

M. Ruel was involved in experimental planning and provided a clinical perspective on the data.

E.J. Suuronen was involved in experimental planning, analysis and manuscript writing/editing.

2.3 Abstract

Background—Injectable biomaterials have shown promise for cardiac regeneration therapy. However, little is known regarding their retention and distribution *in vivo*. Matrix imaging would be a useful tool for evaluating these important properties. Herein, hexadecyl-4-[^{18}F]fluorobenzoate (^{18}F-HFB) and Qdot labeling was used to evaluate collagen matrix delivery in a mouse model of myocardial infarction (MI).

Methods and Results—MI was surgically induced in C57BL/6J mice. At 1wk post-MI, mice received myocardial injections of a collagen matrix labeled with ^{18}F-HFB or Qdots to assess its early retention and distribution (at 10min and 2h) by positron emission tomography (PET) and biodistribution, or fluorescence imaging, respectively. For PET, mice were injected with ^{18}F-NaF to demarcate the skeleton (for image co-registration) and with ^{13}N-NH_3 to delineate the infarct prior to the ^{18}F-HFB-matrix imaging. ^{18}F-HFB matrix labeling efficiency was 81.6±1.9%. PET imaging showed that the bolus of matrix at 10min (74.4±1.9% of injected activity) re-distributed evenly within the ischemic territory by 2h (70.7±1.9% activity). *Ex vivo* biodistribution revealed greater myocardial matrix retention (65.2±1.7%) compared to other tissues, which correlated strongly with PET results. For covalently linked Qdots, labeling efficiency was 96.1±1.6%. *Ex vivo* Qdot signal quantification showed that 84.1±7.4% of the injected matrix was retained in the myocardium.

Conclusions—Serial non-invasive PET imaging and validation by fluorescence imaging confirmed the effectiveness of the collagen matrix to be retained and redistributed within the infarcted myocardium. This study identifies matrix-targeted imaging as a promising modality for assessing the biodistribution of injectable biomaterials for application in the heart.

Key Words: biomaterials; collagen matrix; fluorescence imaging; injectable; PET imaging

2.4 Introduction

Despite the success of interventional and pharmacological therapy for acute myocardial infarction (MI), many patients still suffer irreversible damage. Consequently, the prevalence of congestive heart failure is growing (Nabel and Braunwald, 2012). This highlights the need for new therapies to better prevent progression of the disease and to regenerate the damaged heart. The use of biomaterials has been shown to be a promising strategy for treating the infarcted myocardium in different experimental models (Rane and Christman, 2011). Injectable extracellular matrix (ECM)-like hydrogels are particularly attractive due to their property to undergo a gel phase transition within the body, potentially allowing them to be delivered non-invasively to the heart (Johnson and Christman, 2013). Upon injection, such hydrogels can serve as instructive scaffolds to guide cell behavior through the provision of structural and biochemical cues, and their biodegradability allows tissue remodeling and regeneration. Various injectable materials have been used as stand-alone therapies, as cell delivery vehicles, and as growth factor release scaffolds, and have achieved multiple positive effects on the infarcted heart including increased vascularization, less inflammation, increased progenitor cell recruitment, reduced scar size, and improved cardiac function (Badylak et al., 2009, Johnson and Christman, 2013, Wall et al., 2006).

Collagen-based matrices are highly suitable for use as injectable hydrogels for cardiac repair as they mimic the native ECM environment (Kuraitis et al., 2012a). We and others have demonstrated that the application of a collagen matrix can improve the vascularization of ischemic tissues, show minimal immunogenicity after transplantation, enhance cell function, and ameliorate the geometry and function of the MI heart (Kuraitis et al., 2011a, Dai et al., 2005, Huang et al., 2005, Ahmadi et al., 2014). Recently, it was reported that an injectable ECM

hydrogel derived from decellularized myocardium applied in a porcine MI model resulted in improved cardiac function; and notably, the hemocompatibility and thromboembolic properties were shown to be favorable (Seif-Naraghi et al., 2013). Despite the promise of these and other biomaterials for cardiac regeneration, there is limited information on their injectability, retention and distribution upon delivery into the myocardium. These are important considerations, particularly during the material's gelation phase, due to the possible immediate physical extrusion following injection into the contracting myocardium. Knowing these properties would be of critical importance in firmly establishing the safety, biocompatibility and efficacy for their eventual clinical use.

A few tools for labeling and tracking biodegradable materials *in vivo* have been reported. For example, fluorescence-based imaging has been used to monitor the degradation of chitosan, collagen, and polyethylene:dextran materials following implantation (Artzi et al., 2011, Cunha-Reis et al., 2011). Also, MRI has been employed to visualize the location and degradation of a collagen scaffold labeled with ultrasmall super-paramagnetic iron oxide nanoparticles (Mertens et al., 2014). These are promising imaging strategies for following the fate of erosive materials *in vivo*; however, all were tested in subcutaneous implant models, and imaging approaches have not been reported for studying the properties of injectable biomaterials applied in cardiac tissue.

Previously, we used a minimally invasive ultrasound-guided injection technique for the delivery of matrix ± cells to the MI heart in mice (Ahmadi et al., 2014). In the present study, we used the same matrix delivery and MI model, and two imaging strategies were developed to track the fate of the matrix early after its injection. The matrix was labeled with i) hexadecyl-4-[(18)F]fluorobenzoate (^{18}F-HFB), or ii) fluorescent quantum dots (Qdots) for *in vivo*

visualization by positron emission tomography (PET) or fluorescence imaging, respectively, and its injectability, retention and distribution properties were evaluated.

2.5 Methods

Matrix Preparation

Following previous methods (Kuraitis et al., 2011a), type I rat tail collagen (0.34%, wt/vol; Becton Dickinson) and chondroitin sulfate-C (CS-C; Wako) were cross-linked with 0.02% glutaraldehyde on ice for 45min. Glycine was added and pH adjusted to ~7.2. The final concentrations of collagen and CS-C were 2.49 mg/ml and 11.49mg/ml, respectively. The matrices were thermo-sensitive and solidified upon injection (*in vivo*) or allowed to gel at 37^{o}C for *in vitro* use.

Radiotracer Syntheses

^{18}F-NaF is produced following elution of the ^{18}F-fluoride ion from a quaternary ammonium anion exchange Sep-Pak column (Waters) with 8.4% sodium bicarbonate using the Tracerlab-MX unit (GE Healthcare) into a vial containing 0.9% sodium chloride. ^{13}N-NH_3 is produced as reported (Lamoureux et al., 2012). ^{18}F-HFB was prepared by ^{18}F substitution of the triflate precursor followed by semi-preparative high-performance liquid chromatography as reported (Zhang et al., 2012). Pure ^{18}F-HFB was dissolved in 10% dimethylsulfoxide/saline. All tracers were prepared in high radiochemical and chemical purities.

^{18}F-HFB-labeled Collagen Matrix

For *in vitro* study, 44.9±8.3 MBq of ^{18}F-HFB was mixed with the collagen matrix (1:50 vol/vol), added to a 12-well plate (250µl/well) and incubated at 37^{o}C for 10min or 2h to assess the efficiency of radio-labeling. The solidified gel was rinsed with phosphate buffered saline (PBS), and radioactivity was measured both in the gel and in the PBS rinse using a dose calibrator (Capintec) and decay-corrected. For the PET scan, a final concentration of 3.0±0.9 MBq of ^{18}F-HFB in 50µl of collagen hydrogel (1:50 vol/vol) was prepared and the mixture was kept on ice until injection.

Qdot-labeled Collagen Matrix

Qdot® 525 ITK™ carboxyl quantum dots (500, 250, 125, and 62.5 nM; Invitrogen) were covalently linked to the collagen amine groups using a 1:1 mixture of *N*-ethyl-*N´*-(3-dimethylaminopropyl) carbodiimide (EDC) and N-hydroxysuccinimide (NHS; Sigma; 0.7M). Persistent Qdot retention was confirmed using a microplate reader (MTX Lab Systems) at 10min and 2h. See Online Appendix.

Myocardial Infarction Animal Model and Echo-guided Matrix Injection

Procedures were performed with the approval of the University of Ottawa Animal Care Committee, in accordance with the Canadian Council on Animal Care's Guide to the Care and Use of Experimental Animals. Female C57BL6/J mice (9-wk old; Jackson Laboratory) were anesthetized (2% isoflurane), and MI was induced by ligation of the left anterior descending coronary artery, as previously described (Ahmadi et al., 2014). One week after MI surgery, transthoracic echocardiography was performed with a Vevo770 system (VisualSonics) in B

mode with the use of a 707B series real-time microvisualization (RMV) scanhead probe. Using an ultrasound-guided closed-chest procedure, mice received ^{18}F-HFB- or Qdot-labeled collagen matrix injections (3 adjacent spots along the left ventricular long axis and the apex; 50μl total), according to published methods (Ahmadi et al., 2014). See Online Appendix.

PET Imaging of ^{18}F-HFB-labeled Collagen Matrix In Vivo

An intra-peritoneal injection of sodium-[^{18}F]fluoride (^{18}F-NaF; 7.5±1.4 MBq) was performed one hour before acquiring PET [^{13}N]ammonia (^{13}N-NH_3) and ^{18}F-HFB-matrix images to demarcate the skeleton as fiducial markers for co-registration of the different scans. Mice were anesthetized (2% isoflurane) and the tail vein was cannulated for the injection of ^{13}N-NH_3 (42.5±4.8 MBq). A 30min dynamic PET acquisition was performed using the Small Animal INVEON™ scanner (Siemens) for rest myocardial perfusion imaging. After a 30min ^{13}N-NH_3 washout period, 60min dynamic PET images were acquired at 10min and 2h after ultrasound-guided myocardial injections of ^{18}F-HFB-labeled collagen matrix. Mice were recovered from anesthesia between the 2 scans. Images were reconstructed and analyzed in three axes (axial, coronal, and sagittal) with the Inveon Research Workplace software. Regions of interest (ROIs) were drawn manually around the injection site of ^{18}F-HFB-labeled collagen matrix within the myocardium as visualized on the co-registered NH_3 perfusion images. The quantity of matrix was calculated as the percentage of the injected activity per gram tissue multiplied by ROI volume (cm^3) assuming a tissue density of 1g/cm^3.

Biodistribution Assessment

After PET scan completion (~2.5h after matrix injection), mice were sacrificed and tissues were harvested. Biodistribution of the radioactivity accumulation in the tissues was measured by a

gamma counter (PerkinElmer), and the tissues were weighed. For each organ, the data were expressed as the percentage of the total injected activity.

In vivo Imaging and Quantification of Qdot-labeled Matrix

Qdot-labeled matrix (50µl) was injected to the infarcted mouse heart, as described above. Based on *in vitro* results, a Qdot concentration of 250nM was used. Animals were sacrificed at 10min and 2h after matrix injection, and hearts were harvested and imaging by IVIS® Spectrum (PerkinElmer) to visualize the matrix distribution pattern within the heart *ex vivo* (excitation: 400-440nm; emission: 520-540 nm).

For quantifying Qdot-labeled matrix retention, there were 3 MI groups. Two groups of mice received echo-guided injections: 1 group with PBS (negative control), and 1 group with Qdot-labeled matrix. After 2h, mice were sacrificed and the hearts and lungs were harvested. The third group received no injection and served as positive control; these mice were sacrificed and 50µl of Qdot-labeled matrix was injected to the hearts *ex vivo* (100% retention). Separately, heart and lung tissues were minced and incubated for 45min at 37^{o}C in a digesting solution containing collagenase A (6mg/ml; Roche), collagenase B (6mg/ml; Roche), dispase II (2mg/ml; Roche), and HEPES (0.2M; Sigma) in Hank's balanced salt solution (Sigma). Fluorescence measurement of the samples was performed using a plate reader, as described above. The results were normalized to the negative control and then reported as the ratio of fluorescence measured in the sample vs. the average of the positive controls.

Histology

Hearts were preserved in Tissue-Tek® O.C.T. Compound. Slides of tissue sections were prepared in 10μm serial cryo-sections, and used for infarct assessment (Masson Trichrome staining) or for Qdot visualization by fluorescence microscopy (cell nuclei were labeled with 4´,6-di-amidino-2´-phenylindole (DAPI; Sigma).

Statistical Analysis

Values are expressed as mean ± standard error of the mean. Comparisons of data between groups were performed with a one-way analysis of variance adjusted for repeat measures. Individual two group comparisons were analyzed with a Student's t-test. Correlation analysis was performed by linear regression. Statistical significance was given for $p<0.05$.

2.6 Results

^{18}F-HFB Collagen Matrix Labeling Efficiency

In vitro experiments showed that 82.2±1.8% of ^{18}F-HFB was retained by the collagen matrix immediately after transition from an aqueous phase to a hydrogel (measured at 10min). Two hours after solidification, no change in the tracer retention was observed (81.6±1.9%; $p=0.8$; $n=4$), confirming the persistent labeling by ^{18}F-HFB.

^{18}F-HFB-labeled Matrix PET Imaging

Representative images for the PET imaging protocol are provided in Figure 2.1. One week after induction of MI, ^{18}F-NaF was delivered to the mice. Its preferential absorption in the skeleton (Grant et al., 2008) allowed it to serve as a fiducial marker for co-registration of the subsequent

^{13}N-NH_3 and ^{18}F-HFB-matrix PET images. The ischemic area in the infarcted mouse heart was delineated by a 20min ^{13}N-NH_3 PET scan as an anteroapical perfusion defect. The subsequent ^{18}F-HFB-matrix scans defined the location of matrix at 10min and 2h after ultrasound-guided injection. The images demonstrate that the injection technique was effective for the targeted delivery of the matrix to the infarcted heart.

Retention and Distribution of ^{18}F-HFB-labeled Matrix

After 10min, a bolus of matrix was observed at the site of injection, which spread through the ischemic myocardium and conformed to the shape of the heart's apical region within 2h (Figure 2.2A, B). ROI quantification of ^{18}F-HFB-labeled matrix indicated that 74.4±1.9% of the injected activity was retained in the myocardium 10min after injection (Figure 2.2C). This was not changed (70.7±1.9%) at 2h post-delivery (p=0.2). This represents a relative retention of 95.1±1.2% in the myocardium between 10min and 2h. Radioactivity in the lungs and pleural cavity was much lower than in the myocardium (p<0.0001) and did not change between 10min and 2h (4.8±1.5% and 5.8±1.4%, respectively; p=0.6, Figure 2.2C).

Biodistribution Analysis

Ex vivo biodistribution of tissues collected after the last PET scan revealed that 65.2±1.7% of the total injected radioactivity was in the heart, which was higher than in all other tissues including lungs, liver, and kidneys (Figure 2.3A). The level of matrix retention in the heart correlated significantly with the results from the PET imaging analysis (70.7±1.9%; r=0.996, $p<2.2\times10^{-12}$, Figure 2.3B).

Qdot Matrix Labeling

To validate the results obtained from the ^{18}F-HFB-labeled matrix PET imaging studies, we further evaluated the hydrogel retention properties using Qdots that were covalently bound to the matrix. Several concentrations of Qdots were tested *in vitro* (500, 250, 125, and 62.5 nM) and it was determined that 250nM was the highest concentration that could be incorporated within the matrix before the leakage of Qdots became significant (Figure 2.4). At this concentration, minimal loss of Qdots from the matrix after gelation occurred at a low rate of 1.8±0.7% and 3.8±1.6% at 10min and 2h, respectively. A reduction in Qdot concentration did not improve the labeling efficiency (Figure 2.4).

Ex Vivo Fluorescence Imaging of Qdot-labeled Matrix and Histology

Ex vivo fluorescence imaging of MI hearts injected with Qdot-labeled matrix demonstrated the same distribution pattern as the PET images (Figure 2.5A). The matrix was observed to spread from its injection site in the infarcted myocardium to the surrounding ischemic area between 10min and 2h post-injection. Quantification revealed that Qdot signal intensity in the myocardial tissues was 84.1±7.4% that of the positive control samples (Figure 2.5B). The fluorescence intensity in the lungs (9.8±3.9%) was lower than the targeted myocardium (Figure 2.5B). Fluorescence microscopy performed on heart tissue sections showed the presence of Qdot-labeled matrix in the infarct and peri-infarct area of the myocardium (Figure. 2.5C). Masson Trichrome staining of the next serially sectioned myocardial slice confirmed the morphology of the MI heart and the localization of the Qdot fluorescence (Figure 2.5D).

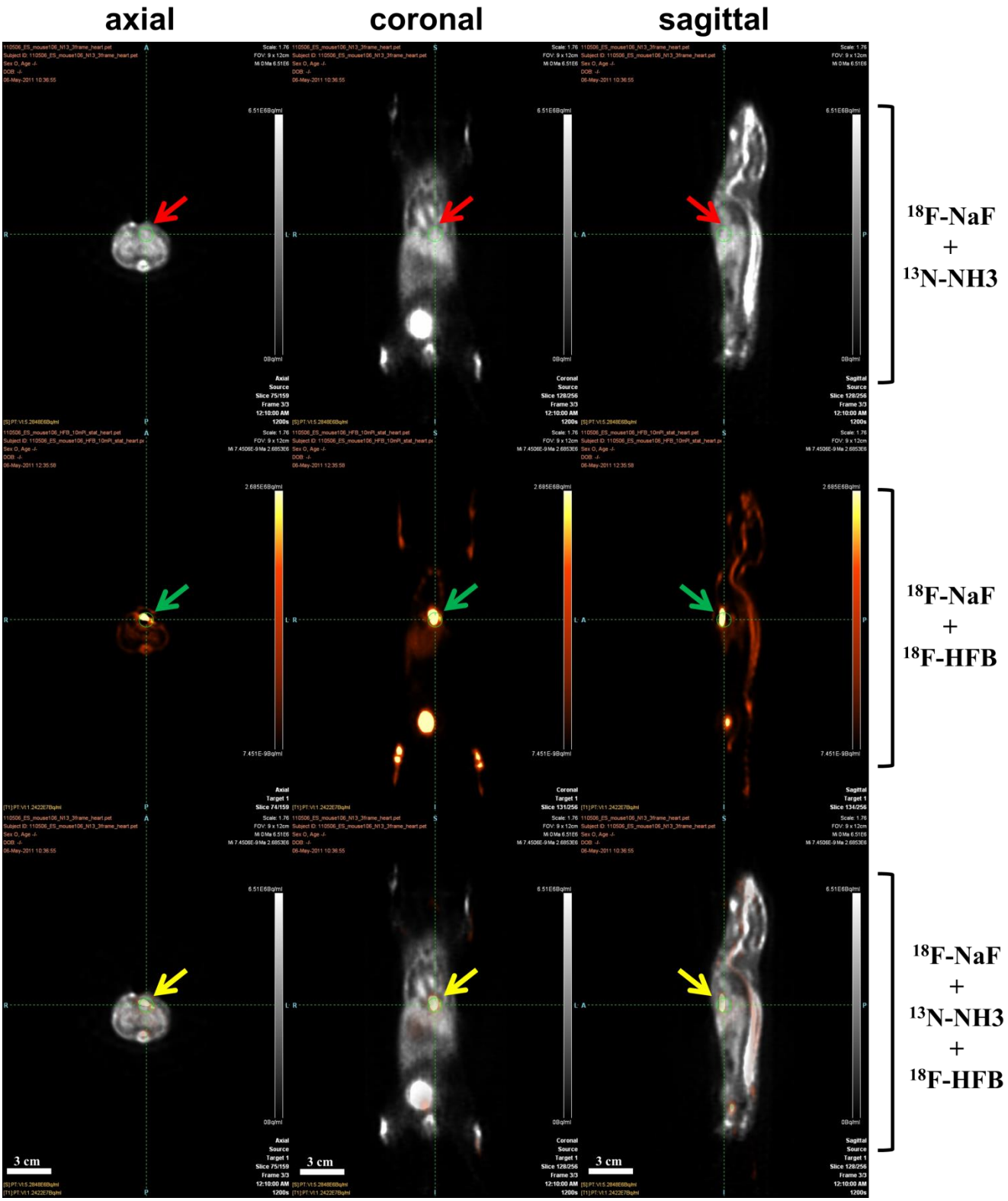
axial
coronal
sagittal
^{18}F-NaF
+
^{13}N-NH3
^{18}F-NaF
+
^{18}F-HFB
^{18}F-NaF
+
^{13}N-NH3
+
^{18}F-HFB
3 cm
3 cm
3 cm

Figure 2.1 Representative images of PET scans. Representative axial, coronal and sagittal images of an infarcted mouse heart injected sequentially with ^{18}F-NaF, ^{13}N-NH_3 and ^{18}F-HFB-matrix. The ^{13}N-NH_3 scan defined the ischemic/infarct area (red arrows). The ^{18}F-HFB labeled collagen matrix was then injected to the infarcted myocardium (green arrows). Images of ^{18}F-NaF accumulation in the skeleton were used for merging the scans and visualizing ^{18}F-HFB-matrix in the heart (yellow arrows).

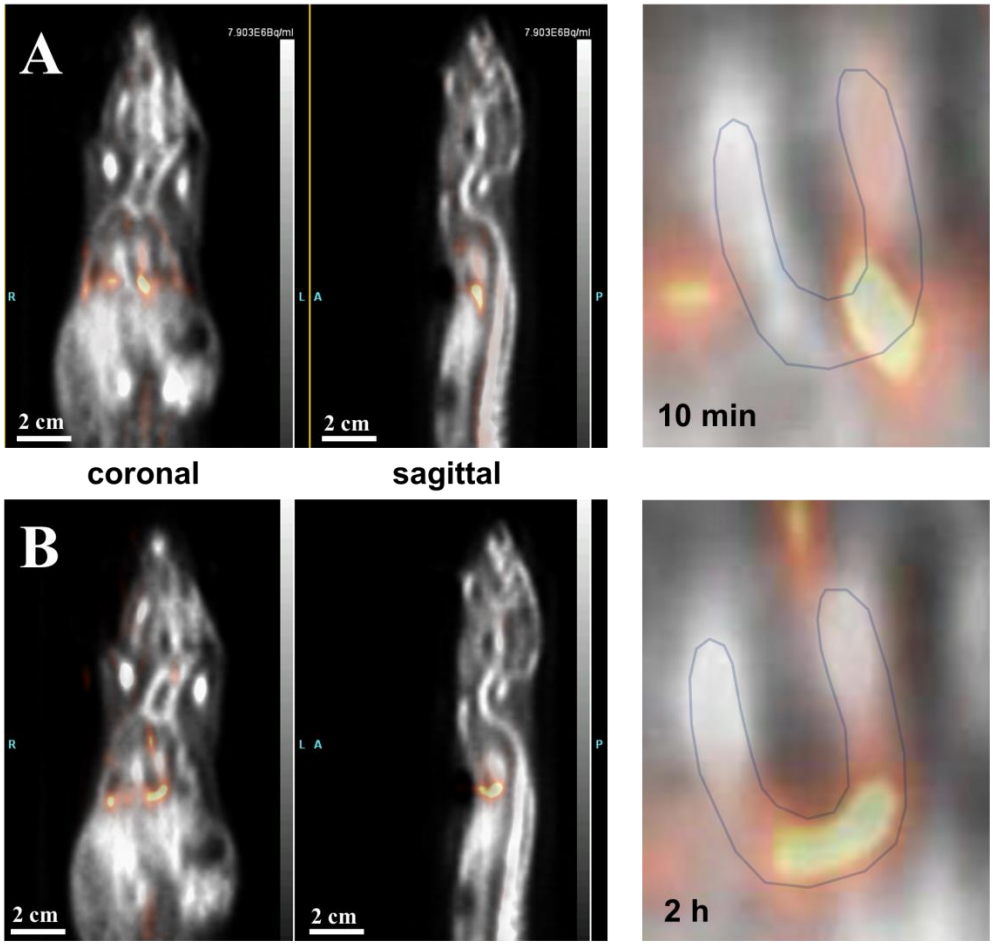
A
7.903E6Bq/ml
7.903E6Bq/ml
R
L
A
P
2 cm
2 cm
coronal
sagittal
10 min
B
R
L
A
P
2 cm
2 cm
2 h

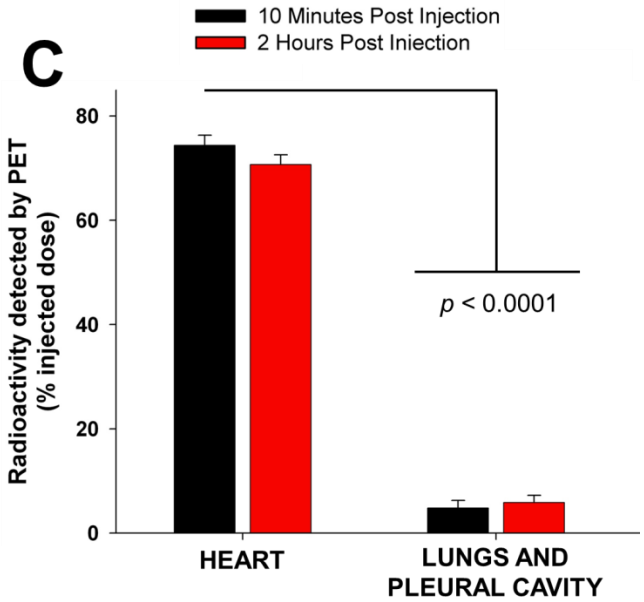
C
10 Minutes Post Injection
2 Hours Post Iniection
Radioactivity detected by PET
(% injected dose)
80
60
40
20
0
p < 0.0001
HEART
LUNGS AND
PLEURAL CAVITY

Figure 2.2 PET imaging of matrix retention and distribution properties. Whole body PET images of ^{18}F-HFB-labeled matrix 10min (**A**) and 2h (**B**) after intramyocardial injection into MI mouse hearts. The right panel close-ups depict the myocardial perfusion contour (light blue line) and the spreading of the matrix within the ischemic region between 10min and 2h. In **C**, ROI quantification revealed significantly higher ^{18}F-HFB-matrix activity in the heart compared to other thoracic tissues, but no change within tissues between the 2 time points (n=11).

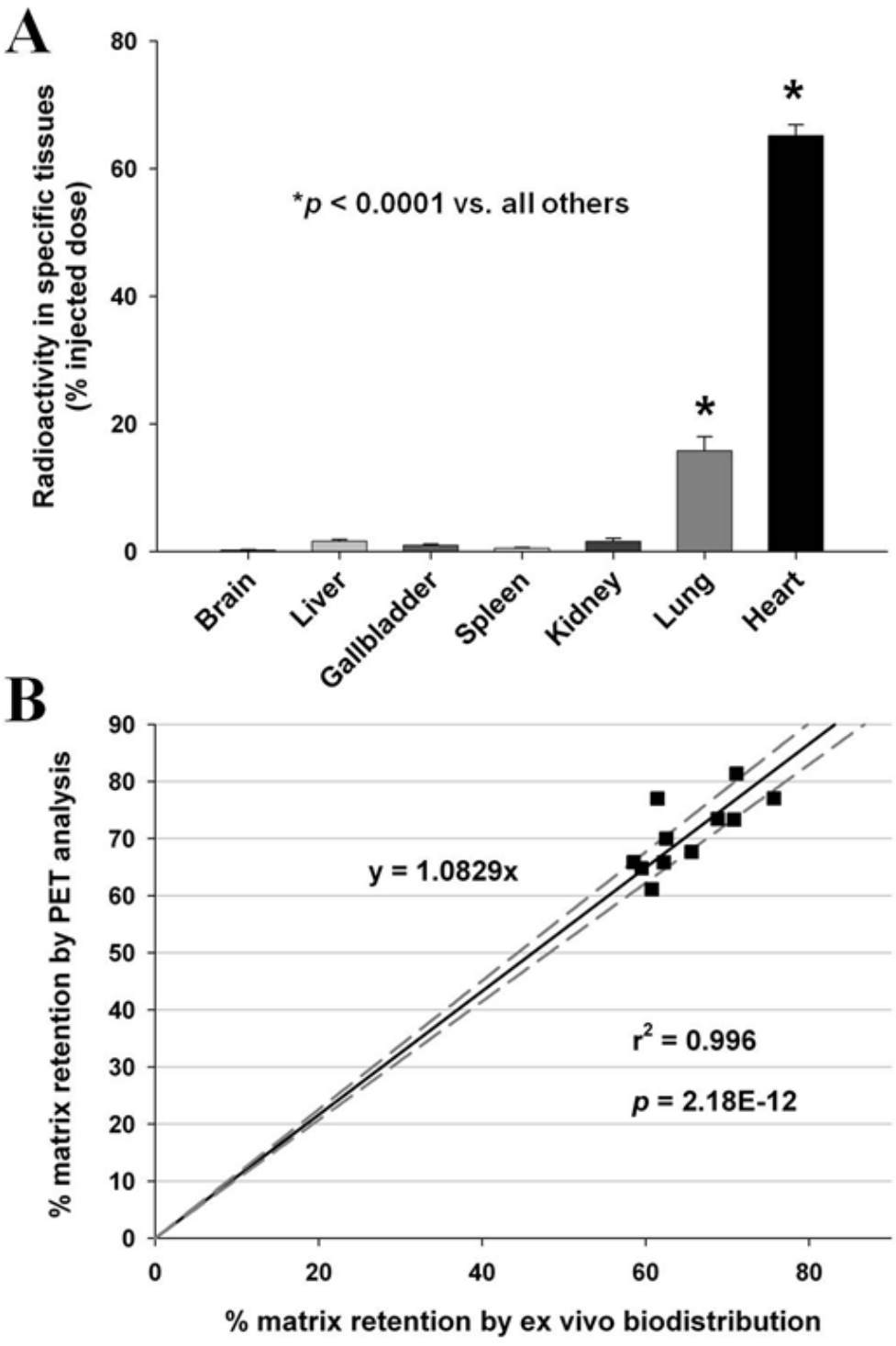
A
Radioactivity in specific tissues (% injected dose)
80
60
40
20
0
*p < 0.0001 vs. all others
*
*
Brain
Liver
Gallbladder
Spleen
Kidney
Lung
Heart
B
% matrix retention by PET analysis
90
80
70
60
50
40
30
20
10
0
y = 1.0829x
r2 = 0.996
p = 2.18E-12
0
20
40
60
80
% matrix retention by ex vivo biodistribution

Figure 2.3 Biodistribution. Biodistribution analysis (**A**) revealed greater ^{18}F-HFB-matrix activity (% injected dose) in the heart compared to all other tissues (*n*=11). (**B**) ^{18}F-HFB-matrix activity measured by biodistribution correlated strongly with the values obtained from the ROI quantification of PET images (dashed lines represent the 95% confidence intervals; *n*=11).

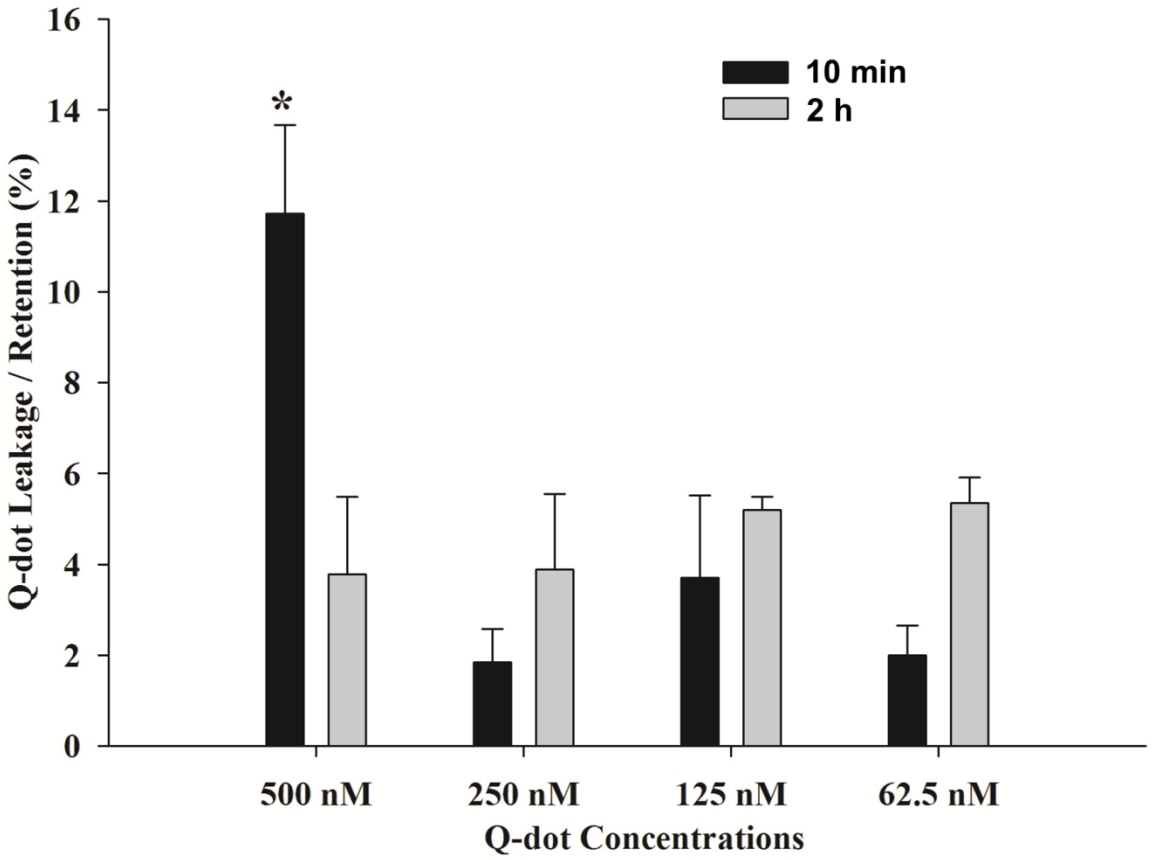

Figure 2.4 Qdot labeling efficiency. The efficiency of Qdot labeling was determined by measuring the amount of Qdots released from matrices 10min and 2h after solidification (leakage), and calculated as the concentration of Qdots in matrix supernatants ÷ total concentration of Qdots loaded (4 loading concentrations tested; *****$p \leq 0.03$ vs. all others; $n=3$).

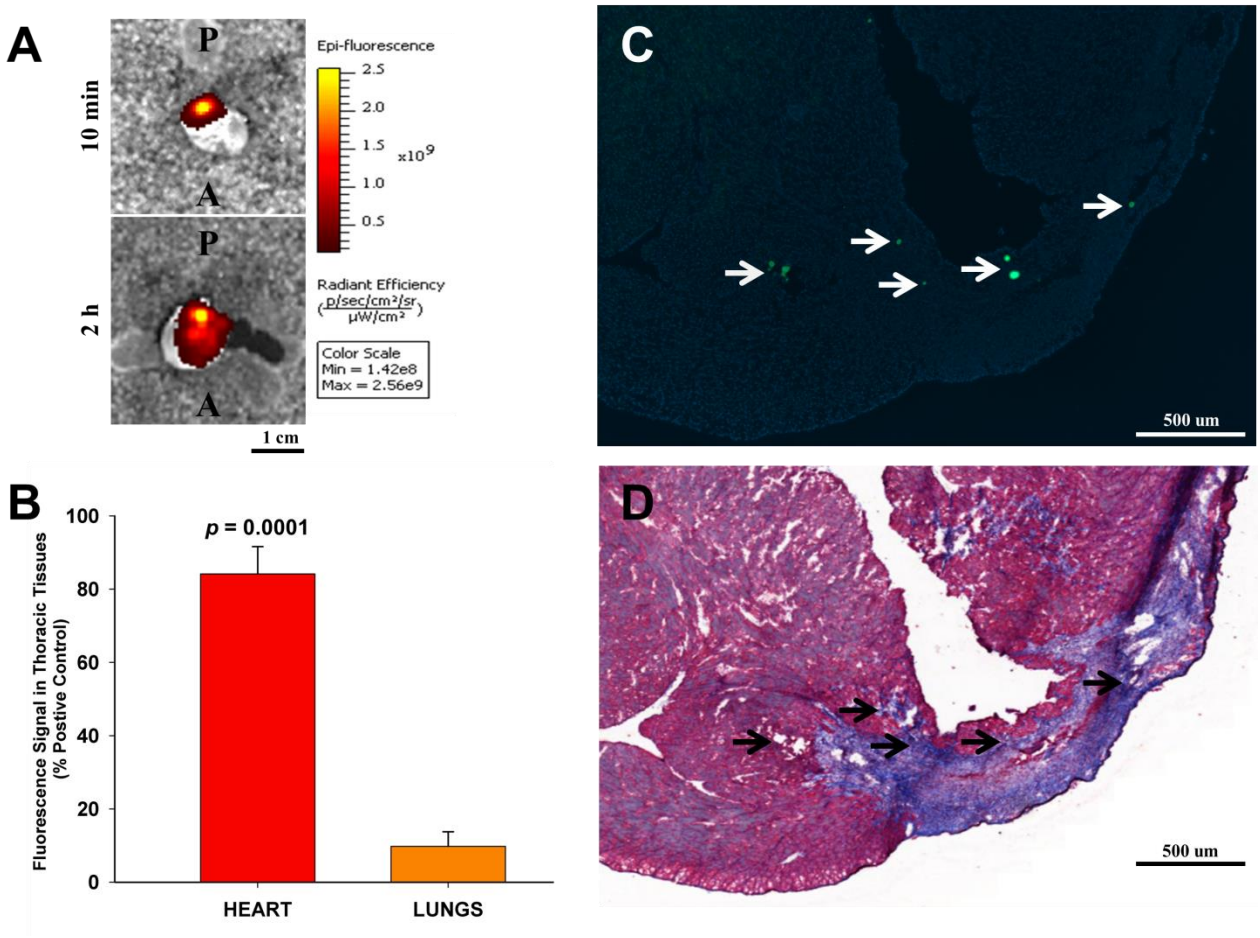

Figure 2.5 Evaluation of Qdot-labeled matrix in MI heart. In **A**, representative *ex vivo* fluorescence images show the distribution pattern of the matrix at 10min and 2h after injection into the MI mouse heart (A: anterior; P: posterior). Fluorescent signal quantification of Qdot-labeled matrix injected MI hearts revealed a high retention (~84%) of matrix in the myocardium (**B**; *n*=4). Serial sections visualized by immunofluorescence (**C**) and bright field microscopy (Masson Trichrome staining; **D**) show Qdot-labeled matrix in the infarct (dense bluish color) and peri-infarct myocardium (white and black arrows) 2h after injection. Note: in the crosslinking reaction, Qdots label the collagen molecule within the matrix at specific sites (see Supplemental); therefore, dispersed Qdot staining of the matrix is observed in sections of tissue.

2.7 Discussion

Imaging techniques for tracking the fate of injectable biomaterials are evolving (Artzi et al., 2011, Cunha-Reis et al., 2011, Mertens et al., 2014), but none have been assessed for application in the beating myocardium. The availability of imaging strategies to monitor biomaterial properties and function is forecast to significantly advance the development of injectable hydrogel therapies (Johnson and Christman, 2013). In this study, ^{18}F-HFB and Qdot labeling methods were devised to evaluate collagen matrix biodistribution following local delivery in a mouse MI model. The main findings were: 1) non-invasive PET imaging of ^{18}F-HFB-labeled matrix was successfully applied to investigate the short-term biologic re-distribution of an injectable matrix delivered to the MI mouse heart; 2) an invasive Qdot labeling method validated the PET imaging findings and provided robust quantification of hydrogel retention; and 3) matrix imaging demonstrated that the matrix's thermogelling properties allowed it to be effectively retained and distributed in the target tissue upon injection to the infarcted myocardium.

Recent progress in the development and pre-clinical testing of injectable hydrogels for cardiac therapy suggests that human trials are imminent (Radhakrishnan et al., 2014, Seif-Naraghi et al., 2013, Radisic and Christman, 2013). However, little is known regarding the basic injection, retention, re-distribution and integration properties of the various biomaterials *in vivo*. A balanced gelation property is desired for minimizing leakage and also for injectability of the hydrogel through a needle or narrow catheter (Singelyn and Christman, 2010). Leakage following injection directly into the contracting myocardium may lead to the material entering the systemic circulation, raising possible safety concerns associated with thromboembolic potential and hemocompatibility, or other unwanted off-target side-effects. Although a certain level of matrix in the circulation may be tolerated and safe, as was shown for a myocardium-

derived ECM biomaterial (Seif-Naraghi et al., 2013), this may be specific to the individual nature of different biomaterials.

In addition to site-specific retention, the re-distribution of a material after injection may play a role in its therapeutic efficacy. Gelation that occurs too quickly may compromise the distribution of the matrix throughout the target area. The application of hydrogels to the infarcted myocardium can serve as bulking agents to alleviate wall stress (Lee et al., 2013, Kichula et al., 2013), which likely depends on the appropriate physical distribution of the applied material, as has been proposed by modeling systems (Miller et al., 2013). Furthermore, the distribution of an injected material throughout the damaged tissue region would allow for greater contact area with the host tissue and a more uniform dispersal of deliverables such as stem cells, growth factors or drugs. Typically, the distribution of an injected biomaterial within the target tissue is assessed by invasive or *ex vivo* histological methods. The availability of non-invasive imaging methods for the visualization of the materials upon injection, such as the PET imaging procedures reported here, would address this and could help optimize the injectability and retention properties of hydrogel-based therapies.

The lipophilic nature of the ^{18}F-HFB radiotracer (Zhang et al., 2012) allows it to be physically maintained within the hydrogel during the liquid-gelation transition period. However, complete radiotracer retention was not achieved: ^{18}F-HFB matrix labeling efficiency was ~82%. Therefore, the initial loss of cardiac radioactivity detected by PET imaging (~74% of initial injected radioactivity at 10min) was likely from the combination of leakage of free ^{18}F-HFB (major; based on *in vitro* labeling efficiency) plus incomplete injection and early redistribution of ^{18}F-HFB-matrix (minor). Our previous study showed that free ^{18}F-HFB radiotracer rapidly clears from the MI heart and is redistributed mostly to the lungs and the liver (Zhang et al., 2012); this,

combined with the *in vitro* results of the present study, makes it unlikely that free ^{18}F-HFB would be contributing significantly to the radioactivity measured in the heart.

As a consequence of the highly specific PET 'hot spot' imaging signal from the ^{18}F-HFB-labeled matrix, precise co-registration with the infarct zone seen on the ^{13}N-NH_3 images would be exceedingly difficult without additional anatomic landmarks. For this reason, ^{18}F-NaF was pre-injected to specifically label and visualize the cortical bones, and used as internal fiducial markers to accurately align the ^{18}F-HFB and ^{13}N-NH_3 PET images. The one hour delay between ^{18}F-NaF injection and PET imaging ensured virtually complete clearance from the systemic tissues, with no significant uptake or interference with the measured PET signals in the heart. Although ^{18}F-NaF has been reported recently to image active calcification in some atherosclerotic arteries (Joshi et al., 2014), this process is not typically activated in the normal or early post-MI heart. X-ray CT imaging could potentially be used as an alternative to provide high-resolution anatomic co-registration of the ^{18}F-HFB-labeled matrix with the ^{13}N-NH_3 perfusion images; however, the local radiation dose to the heart from CT imaging would be much higher compared to ^{18}F-NaF PET, and might interfere with the biologic processes of remodeling or regenerative therapies delivered with the proposed matrix.

Due to the loss of some free ^{18}F-HFB during matrix solidification, it appears likely that PET imaging analysis may have underestimated matrix retention. Therefore, Qdots were used to covalently label the collagen hydrogel for fluorescence imaging to validate the PET imaging results and more accurately quantify matrix retention. Permanent Qdot labeling efficiency was high (~96-98%), so that the fluorescence imaging signal or plate reader analysis is reliably indicative of the presence of the injected matrix. Qdot quantification revealed that the hydrogel retention at 2h (~84%) was higher than that detected by PET imaging (~71%) and *ex vivo*

biodistribution assessment (~65%). Although the Qdot labeling approach was more accurate for the quantification of matrix retention, fluorescence imaging is not currently translatable to the clinic due to its limited depth penetration. In contrast, PET imaging is widely applied in the clinic and may currently offer the best combination of sensitivity, resolution, and whole body imaging to assess biomaterial therapy. In the present study, PET effectively allowed visualization of the matrix's retention and distribution, and the ROI quantification strongly correlated with the *ex vivo* biodistribution analysis. It must be noted that PET imaging with our ^{18}F-labelling strategy can monitor matrix delivery only in the short-term, i.e. several hours following injection, owing to the 2 hour half-life. Injectability and early retention/distribution are very important considerations as discussed above, but longer-lived PET isotopes such as ^{124}I and ^{89}Zr, or other non-invasive imaging strategies will be needed for longer-term *in vivo* assessment of biomaterial therapy.

In conclusion, a collagen matrix delivered via ultrasound guidance to the MI mouse heart was effectively retained and distributed within the ischemic myocardium, with minimal leakage to non-target tissues, highlighting its suitability for use in cardiac therapy. Furthermore, matrix imaging was shown to be a promising approach for assessing the properties and potential of injectable biomaterials for application in the heart, which may be critical in pre-clinical testing and clinical trials.

Acknowledgements

The authors wish to thank Drs. Joanne McBane and Yan Zhang, and the radiochemistry staff for their technical assistance.

Source of Funding

This work was supported by the Heart & Stroke Foundation of Canada (grant T6793 to Dr. Suuronen; program grant PRG 6242 to Dr. Beanlands), and the Canadian Institutes of Health Research (grant MOP-77536 to Drs. Ruel and Suuronen and MOP-79311 to Dr. deKemp). Dr. Beanlands is a Career Investigator of the Heart and Stroke Foundation of Ontario. Dr. Thorn was supported by a Canadian Graduate Scholarship from the Canadian Institutes of Health Research, and Dr. Padavan by a University of Ottawa Cardiology Research Endowment Fellowship.

Disclosures

None.

2.8 Supplementary Section

Supplemental Methods

Qdot-labeled Collagen Matrix

Qdot® 525 ITK™ carboxyl quantum dots (Invitrogen) were covalently linked to the collagen fibril amine groups using a 1:1 mixture of *N*-ethyl-*N´*-(3-dimethylaminopropyl) carbodiimide (EDC) and N-hydroxysuccinimide (NHS; Sigma; 0.7M; see Supplemental Figure 2.1). Briefly, EDC and NHS were dissolved separately in 0.1M 2-(N-morpholino) ethanesulfonic acid buffer (pH=6.0). EDC was first blended with the collagen matrix. A mixture of NHS and Qdots was then added to the collagen matrix and left on ice for 10sec before plating in 12-well plates or being used for mouse injections.

In vitro, Qdot concentrations of 500, 250, 125, and 62.5 nM in the matrix were tested. After solidification, the matrix was rinsed with PBS for 10min and 2h, and Qdot retention and leakage was evaluated using a microplate reader (MTX Lab Systems) at 510nm (excitation: 390nm). Based on the results on these experiments, the 250nM concentration was used *in vivo* because it offered the highest concentration option with limited Qdot leakage.

Myocardial Infarction Animal Model and Echo-guided Matrix Injection

Procedures were performed with the approval of the University of Ottawa Animal Care Committee, in accordance with the Canadian Council on Animal Care's Guide to the Care and Use of Experimental Animals. Female C57BL6/J mice (9-wk old; Jackson Laboratory) were anesthetized (2% isoflurane), intubated and ventilated, and then the heart was exposed via fourth intercostal thoracotomy. Subsequently, MI was induced by ligation of the left anterior

descending coronary artery using a 7.0 suture just below its emergence from the left atrium, as previously described (Ahmadi et al., 2014). One week after MI surgery, mice were anesthetized and fixed in a supine position. Transthoracic echocardiography was performed with a Vevo770 system (VisualSonics) in B mode with the use of a 707B series real-time microvisualization (RMV) scanhead probe. Using an ultrasound-guided (long axis view) closed-chest procedure, mice received ^{18}F-HFB- or Qdot-labeled collagen matrix injections, according to published methods (Ahmadi et al., 2014). Briefly, the syringe was secured in a micromanipulator (VisualSonics), and both the needle (27G × 1½ in; Becton Dickinson) and RMV scanhead probe were aligned along the heart long axis before the injection procedure. The needle was retracted from the ultrasound field-of-view with the use of the micromanipulator until the needle tip was in the desired location within the heart. The matrix mixture (50μl total) was injected into three adjacent spots along the left ventricular long axis and the apex.

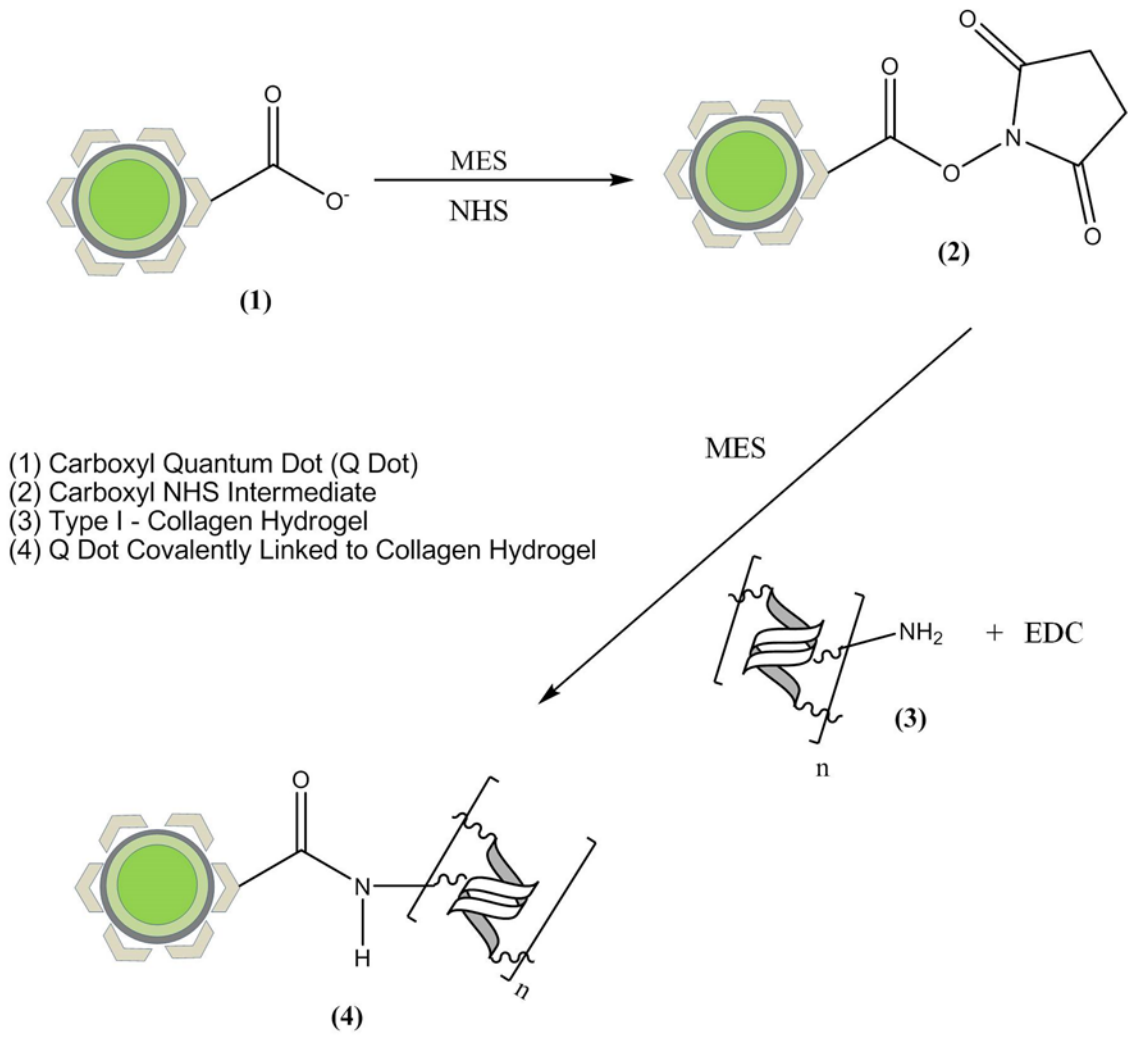

Supplemental Figure 2.1 Qdot-collagen matrix reaction scheme. Schematic of the cross-linking reaction involved in the Qdot labeling of collagen matrix. Qdots (1) are blended with NHS to produce an intermediate (2) that is then reacted with the collagen hydrogel and EDC (3) via carbodiimide coupling chemistry to form the major Qdot-labeled matrix product (4). Note: in the crosslinking reaction, Qdots label the collagen molecule at specific sites (amine groups). Therefore, Qdot staining of the matrix, after it has spread and solidified within the host tissue, is sparse when observed in thin sections of tissue. The Qdot staining pattern (at nM concentrations) is similar to another study that used EDC-NHS crosslinking to attach oligosaccharides to a collagen matrix (at mM concentration) (Suuronen et al., 2009).

Chapter 3

The role of integrin α2 in cell and matrix therapy that improves perfusion, viability and function of infarcted myocardium

This chapter has been published in the journal *Biomaterials*, as per the following citation:

Ali Ahmadi, Brian McNeill, Branka Vulesevic, Myra Kordos, Laura Mesana, Stephanie Thorn, Jennifer M. Renaud, Emily Manthorp, Drew Kuraitis, Hadi Toeg, Thierry G. Mesana, Darryl R. Davis, Rob S. Beanlands, Jean N. DaSilva, Robert A. deKemp, Marc Ruel, Erik J. Suuronen. *Biomaterials* 2014;35:4749-58.

3.1 Notes on Chapter

An injectable collagen-based matrix has previously been used to increase the retention of transplanted CACs, and enhance neovascularization, perfusion and function in models of hindlimb ischemia. Furthermore, it has been shown that collagen matrix-cultured CACs are phenotypically more enriched for endothelial and progenitor markers and also more resistant to apoptosis due to Akt and ERK1/2 pathway activation. Therefore, the study in this chapter sought to evaluate the potential therapeutic benefits of CAC treatment with or without collagen matrices in a mouse MI model. Furthermore, the mechanisms by which the collagen matrix conferred improved phenotype/survival for transplanted cells were examined.

3.2 Contributions of Co-authors

B. McNeill contributed to manuscript writing and to results presented in Figures 3.3, 3.4, 3.5 and 3.6.

B. Vulesevic was involved in manuscript preparation and providing results presented in Figure 3.3B-C.

M. Kordos operated mouse PET scans with my assistance.

L. Mesana performed experiments presented in Figure 3.3C.

S. Thorn, J.M. Renaud and R.A. deKemp were involved in PET data generation and analysis.

E. Manthrop and D. Kuraitis helped with designing ILK protocols and *in vitro* cytokine release experiments.

H. Toeg was involved in ultrasound guided injection design and helped with supplemental video preparation.

T.G. Mesana provided a clinical perspective on the data.

D.R. Davis was involved in experimental planning.

R.S. Beanlands provided a clinical perspective on the data and helped with PET data analysis.

J.N. DaSilva provided radiotracers and helped with PET data analysis.

M. Ruel and E.J. Suuronen were involved in experimental planning, analysis and manuscript writing/editing.

3.3 Abstract

Injectable delivery matrices hold promise in enhancing engraftment and the overall efficacy of cardiac cell therapies; however, the mechanisms responsible remain largely unknown. Here we studied the interaction of a collagen matrix with circulating angiogenic cells (CACs) in a mouse myocardial infarction model. CACs + matrix treatment enhanced CAC engraftment, and improved myocardial perfusion, viability and function compared to cells or matrix alone. Integrin-linked kinase (ILK) was up-regulated in matrix-cultured CACs. Integrin $\alpha 2\beta 1$ blocking prevented ILK up-regulation, significantly reduced the adhesion, proliferation, and paracrine properties of matrix-cultured CACs, and negated the benefits of CACs + matrix therapy in vivo. Furthermore, integrin $\alpha 5$ was essential for the angiogenic potential of CACs on matrix. These findings indicate that the synergistic therapeutic effect of CACs + matrix therapy in MI requires the matrix to enhance CAC function via $\alpha 2\beta 1$ and $\alpha 5$ integrin signaling mechanisms, rather than simply delivering the cells.

3.4 Introduction

The clinical feasibility and safety of cell therapy for treating myocardial infarction (MI) has been demonstrated (Jeevanantham et al., 2012). Meta-analysis of randomized controlled clinical trials, mostly using bone marrow cell products, revealed a 2.2-3.9% improvement in left ventricular ejection fraction (LVEF) at 6-12 months post-MI, and 1.9% beyond 12 months (Delewi et al., 2013). The lack of a more significant outcome can be attributed, in part, to the low survival, engraftment and function of transplanted cells (Aicher et al., 2003, Li et al., 2009). Therefore, it appears that the limited benefits are largely due to the release of cardioprotective and angiogenic cytokines that stimulate enhanced regenerative and survival responses in host cells (Cho et al.,

2007, Loffredo et al., 2011). As such, it has been postulated that strategies for improving cell retention are needed to increase transplanted cell effects and therapeutic outcome (Strauer and Steinhoff, 2011, Wollert and Drexler, 2010a). In response to this need, a diversity of biomaterials is being developed. The concept is that providing a scaffold will improve cell retention and viability, thus prolonging their therapeutic effects. Combined cell and biomaterial therapy in small animal models has been successful (Kuraitis et al., 2010, Rane and Christman, 2011, Segers and Lee, 2011). The outcomes in large animal models (Lin et al., 2010, Shudo et al., 2011, Takehara et al., 2008) and in one clinical trial (MAGNUM trial) (Chachques et al., 2008, Chachques et al., 2007) have also been positive, but are modest in comparison. This highlights the necessity to better understand the underlying mechanisms driving the repair and regeneration.

Injectable extracellular matrix (ECM)-like hydrogels hold promise for local and minimally-invasive cell delivery for MI. The ECM-mimicking composition is expected to contribute: 1) natural binding sites for improved cell engraftment; and 2) specific cues that enhance cell therapeutic effects and direct regeneration (Kuraitis et al., 2012b). Cells interact with the ECM through surface adhesion molecules, primarily integrins, which initiate downstream signaling events that regulate their function (Geiger et al., 2009, Stupack and Cheresh, 2002). *In vitro* work has advanced our understanding in this area, which has been applied in the design of materials to direct cell fate; however, these concepts are minimally investigated in the context of *in vivo* regenerative therapy applications (Lutolf et al., 2009).

This study sought to examine the role of integrins in MI mouse hearts treated with bone marrow (BM)-derived circulating angiogenic cells (CACs) delivered with a type I collagen matrix. The material is fitting since type I collagen is the most abundant ECM protein in the healthy heart (Herpel et al., 2006), and it has been used previously to enhance cell therapy in ischemic tissue

(Zhang et al., 2008a, Kuraitis et al., 2011a, Suuronen et al., 2006). Specifically, α-integrin expression and signaling through the integrin-linked kinase (ILK) pathway was investigated to elucidate matrix-mediated mechanisms that may enhance the adhesion, proliferation, angiogenic signaling and therapeutic potential of CACs.

3.5 Materials and methods

Matrix preparation

Following previous methods (Kuraitis et al., 2011a), type I rat tail collagen (0.34%, wt/vol; Becton Dickinson) and chondroitin sulfate-C (CS-C; Wako) were cross-linked with 0.02% glutaraldehyde on ice for 45min. Glycine was added and pH adjusted to ~7.2. The final concentrations of collagen and CS-C were 2.49 mg/ml and 11.49mg/ml, respectively. The matrices were thermo-sensitive and solidified upon injection (*in vivo*) or allowed to gel at 37^{o}C for *in vitro* use.

Mouse BM-CAC preparation

BM-derived CACs for *in vivo* mouse MI experiments were collected from 9-wk old male eGFP mice (C57BL/6-Tg(CAG-EGFP)1Osb/J (Jackson Laboratories). Briefly, tibias and femurs were dissected from mice and bone marrow was extruded using phosphate-buffered saline (PBS; Sigma). Mononuclear cells (MNCs) were then isolated by Histopaque 1083 (Sigma) density-gradient centrifugation. MNCs contained in the buffy coat were collected, washed with a PBS buffer and cultured (at 1×10^{6} cells/cm^{2}) on plates coated with 10 μg/ml fibronectin (Sigma). Cultures were incubated at 37^{o}C in endothelial basal medium (EBM-2, Clonetics) supplemented with EGM-2-MV-SingleQuots (Clonetics). After 4 days of culture, the adherent cells (hereafter

referred to as CACs) were collected with sterile PBS and their number and viability measured (Vi-CELL, Beckman Coulter). For α2 blocking experiments, cells were treated with a mouse-specific anti-integrin α2β1 antibody (Abcam) for 1h before transplantation. Blocking efficiency was confirmed by Western blot analysis for ILK expression.

Animal model and surgical procedures

All experimental procedures were performed in accordance with the National Institute of Health Guide for the Care and Use of Laboratory Animals. Female C57BL6/J mice (9-wk old; Jackson Laboratories) were anesthetized (2% isoflurane), intubated, and the heart was exposed via fourth intercostal thoracotomy. MI was induced by ligation of the left anterior descending coronary artery (LAD) just below its emergence from the left atrium. At 1-wk post-MI (baseline), echocardiography was performed with a Vevo770 system (VisualSonics) in B mode with the use of a 707B series real-time microvisualization (RMV) scanhead probe. Using an ultrasound-guided closed-chest procedure, mice randomly received one of the following 50μl treatments (in 5 equivolumetric injections by a 27G needle) into the infarct border zone: (1) 5×10^5 GFP^+ CACs; (2) collagen matrix only; (3) 5×10^5 GFP^+ CACs + collagen matrix; or (4) PBS (Sigma) as control. The syringe was secured in a micromanipulator (VisualSonics), and both the needle and RMV scanhead probe were aligned along the heart long axis before the injection procedure. A subset of mice received treatment consisting of 5×10^5 CACs pre-treated for 1h with an Itgα2 blocking antibody (Abcam), delivered with or without the collagen matrix. Left ventricular ejection fraction (LVEF) and fractional shortening (FS) were also determined in a blinded fashion by echocardiography (Vevo 770 system; VisualSonics) at baseline (1-wk post-MI) and follow-up (4-wk post-MI).

^{13}N-NH_3 and ^{18}F-FDG PET imaging

PET imaging was performed on randomly selected animals. Mice were anesthetized (2% isoflurane) and the tail vein was cannulated for injection of ^{13}N-NH_3 (1mCi). A 30min dynamic PET acquisition was performed using the Small Animal INVEON™ scanner (Siemens) for rest myocardial perfusion imaging. After a 30min ^{13}N-NH_3 washout period, 60min dynamic PET images were acquired after intravenous injection of ^{18}F-fluorodeoxyglucose (^{18}F-FDG; 1mCi). Images were reconstructed and polar maps were generated using FlowQuant software showing the time course of NH_3 and FDG activity in each sector of the myocardium (Klein et al., 2010).

Infarct Histology

Mice were sacrificed at 4 weeks. Hearts were collected, snap frozen in OCT, and slides were prepared with 10μm sections at different levels. Masson's Trichrome staining was performed to measure the anterior to posterior myocardial wall thickness ratio. Using section images, 3 lines perpendicular to the infarct (one in the middle and one at each end) were used to measure the anterior and posterior wall thickness. All three lines converged at the center of left ventricle and continued to the posterior wall. The average anterior wall thickness was divided by the average posterior wall thickness. To assess the relative infarct area, images of hematoxylin-phloxine-saffron (HPS)-stained heart sections were used to calculate the pixel number of the infarct area, which was then divided by the pixel number for the total myocardium.

Immunohistochemistry

Sections were stained with anti-GFP (1:100; Abcam), anti-von Willebrand factor (1:50; Abcam) and anti-α-smooth muscle actin (1:200; Abcam) monoclonal antibodies followed by secondary

antibody staining. GFP staining identified engrafted transplant cells, and vWF stained for endothelial cells. Arterioles were identified by SMA^+ staining combined with characteristic vessel morphology and quantified in 4 random microscopic fields-of-view.

In vitro human CAC cultures

Procedures for the isolation of human CACs were approved by the Human Research Ethics Board of the University of Ottawa Heart Institute. With informed consent, total peripheral blood mononuclear cells were freshly isolated from the blood of healthy human volunteers by Histopaque 1077 (Sigma) density-gradient centrifugation, as previously described (Kuraitis et al., 2011a). Cells contained in the buffy coat were collected, washed and cultured on fibronectin-coated plates with EBM-2, as described above. After 4 days in culture, adherent CACs were collected.

In vitro human CAC assays

CACs were cultured in 50 µg/ml of 4',6-diamidino-2-phenylindole (DAPI; Sigma-Aldrich) to stain the nucleus. Adhesion: 5×10^4 DAPI-stained CACs were seeded on fibronectin or matrix for 1h prior to 4% paraformaldehyde (PFA) fixation and quantification. Proliferation: CACs were cultured on fibronectin or collagen matrix for 4 days, then plated onto Superfrost+ slides and incubated for 45min at 37oC to allow adhesion. Cells were then fixed with 4% PFA for 10min, washed with PBS and processed for Ki67 staining using a sodium citrate microwave antigen retrieval technique. Primary incubation with rabbit anti-Ki67 (Abcam) was performed overnight at 4oC followed by several RT washes before 1h incubation with the anti-rabbit secondary (Cell Signaling). Migration: 5×10^4 CACs, after 4-day culture on fibronectin or matrix, were lifted and re-suspended in growth factor-free EBM, and placed in the top compartment of a 24-well

Boyden chamber (Corning). The lower chamber contained 0.05μg/ml of VEGF (Cedarlane) in EBM. After 24h, CACs were fixed with PFA and the number migrating to the lower chamber was quantified. Angiogenesis: CACs lifted after 4-day culture on fibronectin or collagen matrix were co-cultured with human umbilical vein endothelial cells in an ECMatrix™ angiogenesis assay (Chemicon) as previously described (Kuraitis et al., 2011a). SDF-1 Immunoassay: To quantify SDF-1 release by CACs cultured on fibronectin vs. collagen matrix, media collected after 48h culture in hypoxia (1% O_2) was immediately used to measure supernatant SDF-1 levels. Determination of SDF-1 concentration was carried out by quantitative sandwich enzyme-linked immunosorbent assay (ELISA) using the Quantikine kit (R&D Systems), according to the manufacturer's recommendations.

For α1- and α2-blocked *in vitro* experiments, human CACs were treated with blocking antibodies against integrin α1 (Abcam) or α2β1 (Abcam) for 1h, then rinsed before use in the assays. For *in vitro* α5 blocking experiments, human CACs were treated with a specific α5 blocking antibody (BIIG2; Developmental Studies Hybridoma Bank) for 1h then rinsed before use. For ERK/MEK inhibition, CACs were cultured with a MEK inhibitor (U0126; Tocris Bioscience), and an ERK inhibitor (Calbiochem) for 1h then rinsed before use.

qPCR and RT-qPCR analysis

CACs were cultured on fibronectin or matrix for 24h, and total RNA was then extracted using Tri-reagent (Sigma). First strand cDNA was synthesized from 2μg total RNA using GoScript™ reverse transcriptase (Promega) and random hexamer primers (IDT). DNA was isolated using QIAamp DNA extraction kit (Qiagen). Target gene mRNA levels were assessed by RT-qPCR, and Y chromosome by q-PCR (McBride et al., 2003), using BRYT Green GoTaq® qPCR Master

Mix (Promega) and a LightCycler 480 Real-Time PCR system (Roche). Primer pairs (Supplemental Table 1) were designed using DNAMAN software (Lynnon Biosoft) and primer3 (v.0.4.0). Relative changes in mRNA expression were determined using the Δ-ΔCt method, expressed as levels relative to 18S and GAPDH.

Flow cytometry

For evaluation of Itgα5 surface expression, CACs were lifted after 24h culture on fibronectin or collagen matrix, and stained with an Itgα5-FITC antibody (Millipore). In controls, isotype-matched FITC-conjugated antibodies were used. All flow cytometry was performed on a FACSAria™ (BD Biosciences) immediately after sample staining was complete. Data was analyzed using FACSDiva software.

Statistical analysis

Values are expressed as mean ± standard error. Comparisons of data between groups were performed with a one-way analysis of variance with Tukey's *post-hoc* test, and individual two group comparisons with a 2-tailed Student's t-test, unless otherwise indicated. Statistical significance was given for $p<0.05$.

3.6 Results

Morphology and function of MI hearts following therapy

CACs are a heterogeneous cell population of bone marrow (BM) origin that can stimulate cardiac repair (Cho et al., 2007, Fadini et al., 2012). CACs (2.4% $CD34^+$, 0.6% $CD133^+$, 0.1% c-kit^+, 0.04% $CXCR4^+$) were obtained from BM mononuclear cells of green fluorescent protein

(GFP) expressing male mice and delivered ±matrix into female mouse hearts 1-week post-MI (matrix and PBS treatment served as controls). CACs+matrix treatment significantly improved left ventricular ejection fraction (LVEF) and fractional shortening (FS) (Figure 3.1A and 3.1B). In contrast, function in the PBS-treated group deteriorated, and there was no change for mice treated with CACs or matrix only. Representative echocardiograms demonstrating improved LV wall contractility in hearts treated with CACs+matrix, but not PBS, are shown in the Supplemental Video. PET imaging of myocardial perfusion using ^{13}N-NH_3 and of glucose metabolism using ^{18}F-FDG was also performed at 1 and 4 weeks post-MI (Figure 3.1C). CACs+matrix treatment improved myocardial perfusion (by 22%) and glucose uptake (by 26%; indicative of viability) at 4 weeks, whereas no change was observed with other treatments (Figure 3.1D, E). Analysis of tissue sections revealed a reduced infarct size (% scar/total myocardial area) in the CACs+matrix group compared to all other treatments (Figure 3.2A and 3.2B). Furthermore, wall thickness was better preserved with CACs+matrix treatment (Figure 3.2C). Overall, these results reveal that treatment with CACs or matrix prevented further loss of function in MI hearts; whereas combining them had a synergistic effect in improving myocardial perfusion, glucose uptake and function.

Transplanted cell engraftment and vascular density

As was the initial intended purpose, the collagen matrix increased the retention of transplanted CACs in the infarcted myocardium. Transplanted cell engraftment was quantified by Y-chromosome qPCR analysis, and revealed a ~9-fold increase in Y-chromosome copy number in the CACs+matrix group compared to CACs-only 3 weeks after delivery (Figure 3.2E). Neovascularization is a major mechanism mediating the effects of CAC therapy via endothelial differentiation of transplanted cells and by paracrine signaling to augment angiogenesis (Cho et

al., 2007, Fadini et al., 2012, Yoon et al., 2005a). The number of smooth muscle actin $(SMA)^+$ arterioles in CACs+matrix treated hearts was ≥1.8-fold greater than in CACs, matrix, or PBS groups (Figure 3.2D). The matrix- and CACs-only treated hearts also had enhanced vascularity compared to PBS treatment. In both cell treatment groups, evidence of CACs differentiating into endothelial cells (i.e. GFP^+vWF^+ cells) and contributing to blood vessel growth was observed (Figure 3.2F).

Integrin α2/ILK signaling in CAC-matrix interaction

Specific alpha integrins (Itg), Itgα1, Itgα2, Itgα10, and Itgα11, form heterodimeric proteins with Itgβ1 to generate transmembrane receptors (McCall-Culbreath and Zutter, 2008), which bind ECM collagen and activate various intracellular signaling pathways. Compared to fibronectin, collagen-cultured CACs had increased *Itgα1* and *Itgα2* expression, but no difference in *Itgα10* and *Itgα11* mRNA levels (Figure 3.3A). To assess the role of Itgα1 and Itgα2 in regulating CAC-matrix interaction, blocking studies were performed. Following 1h treatment with an Itgα1 blocking antibody, CAC adhesion to the matrix was unaffected; in contrast, application of an Itgα2 blocking antibody for 1h reduced CAC adhesion by ~82% (Figure 3.3B). This reduced adhesion was matrix-specific, as their ability to bind to fibronectin was unaltered (Figure 3.3B). This suggests that Itgα2 is the main α-integrin involved in controlling CAC-matrix interaction. Functional assessment revealed that α2-blocking resulted in ~77% less proliferation in matrix-cultured CACs and ~20% less secretion of stromal cell-derived factor-1α (SDF-1α), a pro-angiogenic cytokine (Figure 3.3C). Integrin-linked kinase (ILK) is a key downstream mediator of integrin signaling (Qin and Wu, 2012); therefore the effect of matrix culture (±Itgα2 blocking) on its expression in CACs was evaluated. Compared to fibronectin, matrix culture increased ILK protein levels in CACs by ~2-fold, while Itgα2 blocking reduced this increase (Figure 3.3D and

3.3E). Consistent with ILK's role in regulating endothelial progenitor survival and vasculogenesis (Cho et al., 2005), the ability of our matrix to enhance the function and therapeutic potential of CACs appears to be dependent on Itgα2 signaling mediated through an ILK pathway.

Role of integrin α2 in CACs+matrix therapy

Using the same mouse MI model described earlier, hearts were injected (±matrix) with mouse BM-CACs pretreated with an Itgα2 blocking antibody for 1h prior to transplantation. The ability of Itgα2 blocking to decrease ILK expression in mouse CACs was confirmed (Supplement Figure 3.1). Inhibiting Itgα2 abolished the benefits previously observed with CACs+matrix therapy. Heart function 3 weeks after being treated with Itgα2-blocked CACs+matrix was not different from baseline (1-wk post-MI) as determined by LVEF and FS (Figure. 3.4A and 3.4B), nor was there a difference compared to hearts treated with Itgα2-blocked CACs. Treatment with Itgα2-blocked CACs reduced infarct size (Figure 3.4C and Supplemental Figure 3.2) and improved ventricular wall thickness (Figure 3.4D) versus PBS; however, matrix delivery of Itgα2-blocked CACs conferred no additional improvement. Compared to PBS, arteriole density was greater with Itgα2-blocked CACs treatment, but CACs+matrix conferred no further effect (Figure 3.4E and 3.4F). qPCR analysis for Y-chromosome copy number revealed negligible transplanted cell retention for both groups (data not shown). This suggests that CACs need to interact with the matrix, specifically through Itgα2, to achieve long-term engraftment and confer the enhanced benefit of CACs+matrix therapy.

Integrin α5 and matrix-cultured CAC function

Having examined various collagen-binding integrins, we next assessed expression of the remaining α-integrins. Compared to fibronectin, the mRNA expression of *Itgα4*, *Itgα5*, *Itgα7* and *ItgαV* were up-regulated, and *Itgα3* was down-regulated in matrix-cultured CACs (Figure 3.5A). Itgα5 was chosen for further study based on its established role in endothelial progenitor biology, including homing and angiogenic functions (Choi et al., 2009, Caiado and Dias, 2012). *Itgα5* mRNA up-regulation translated to a 3-fold increase in total Itgα5 protein (Figure 3.5B and 3.5C). The increased Itgα5 expression in matrix-cultured CACs was associated with superior adhesion when re-plated on fibronectin (Figure 3.5D), consistent with Itgα5 being a strong RGD/fibronectin binding receptor (Caiado et al., 2011, Li et al., 2011). Blocking Itgα5 reduced the ability of CACs to adhere to matrix and to fibronectin, to proliferate, and to participate in capillary-like structure formation in an angiogenesis assay (Figure 3.5D and 3.5E). Migration of matrix-cultured CACs was superior to that of CACs from fibronectin, but this function was not affected by blocking Itgα5 (Figure 3.5E). In summary, these data reveal that despite Itgα5 not being known as a collagen-binding protein, it is increased in CACs through interaction with the collagen matrix, and it plays an important role in the matrix-enhanced function of CACs.

Integrin α5 signaling pathway in matrix-cultured CACs

Previously, we found that CACs cultured on collagen matrix more rapidly stimulated neovascularization *in vivo* (Kuraitis et al., 2011a). Although a role for the ERK pathway was identified, it remained unknown how CACs and matrix interact to obtain the functional enhancement. Given the CAC-matrix interaction involves Itgα2 and Itgα5 (this study) and the ERK pathway (Kuraitis et al., 2011a), we examined the possibility that they are linked. The

percentage of CACs expressing α5 at the cell membrane was >2-fold higher for matrix-cultured cells compared to fibronectin; however, when ERK was blocked, the Itgα5^{+} cell number dropped to levels similar to that observed on fibronectin (Figure 3.6A). Furthermore, protein levels of Itgα5 were reduced in matrix-cultured CACs when either Itgα2 or ERK was blocked (Figure 3.6B). This strongly suggests that binding to collagen matrix through Itgα2 activates the ERK pathway in CACs leading to up-regulation of Itgα5. A schematic is provided to summarize some of the many activated pathways and enhanced CAC functions that have been identified as resulting from interaction with the collagen matrix (Figure 3.6C).

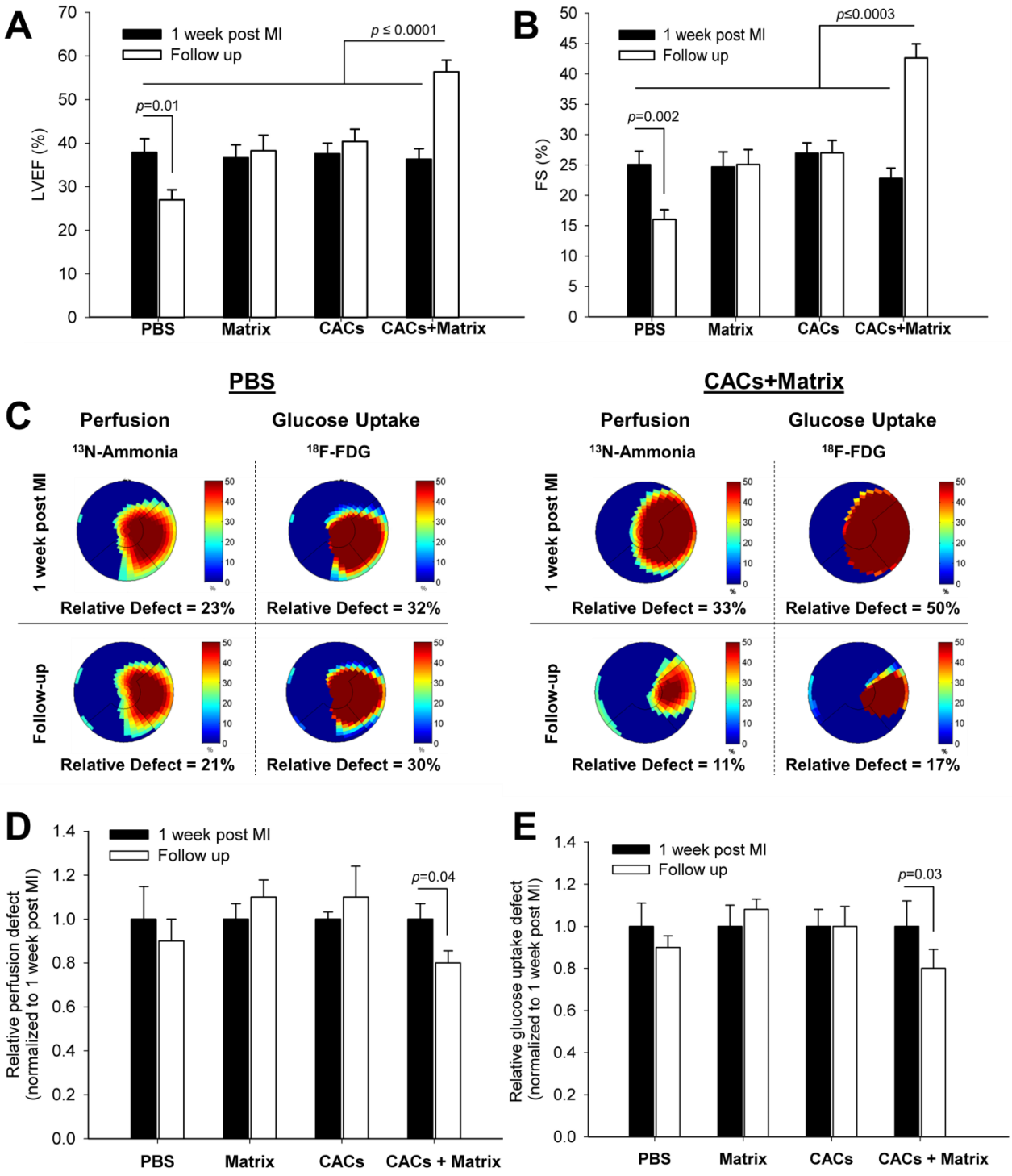
A
1 week post MI
Follow up
p ≤ 0.0001
p=0.01
LVEF (%)
PBS
Matrix
CACs
CACs+Matrix
B
1 week post MI
Follow up
p≤0.0003
p=0.002
FS (%)
PBS
Matrix
CACs
CACs+Matrix
C
PBS
CACs+Matrix
Perfusion
Glucose Uptake
13N-Ammonia
18F-FDG
1 week post MI
Follow-up
Relative Defect = 23%
Relative Defect = 32%
Relative Defect = 21%
Relative Defect = 30%
Relative Defect = 33%
Relative Defect = 50%
Relative Defect = 11%
Relative Defect = 17%
D
1 week post MI
Follow up
p=0.04
Relative perfusion defect (normalized to 1 week post MI)
PBS
Matrix
CACs
CACs + Matrix
E
1 week post MI
Follow up
p=0.03
Relative glucose uptake defect (normalized to 1 week post MI)
PBS
Matrix
CACs
CACs + Matrix

Figure 3.1 Combined CACs+matrix therapy improves the perfusion, glucose uptake, and function of MI mouse hearts. (A) LVEF at baseline (1 week post-MI) and at follow-up (3-wk post-treatment) measured by echocardiography (*n*=14-29). (B) FS at baseline (1 week post-MI) and at follow-up (3-wk post-treatment) measured by echocardiography (*n*=14-29). See also video S 3.1 [avaialable online]. (C) Representative perfusion (^{13}N-NH3) and glucose uptake (^{18}F-FDG) polar maps generated by PET imaging analysis of PBS (left) and CACs+matrix (right) treated hearts at 1-wk post-MI (day of treatment) and at 3-wk post-treatment (follow-up). (D) Relative perfusion defect (% of LV) calculated from polar map images (*n*=4-9). (E) Relative glucose uptake defect (% of LV) calculated from polar map images (*n*=4-9). Statistical analysis for defect size (D and E) was performed using a paired t-test.

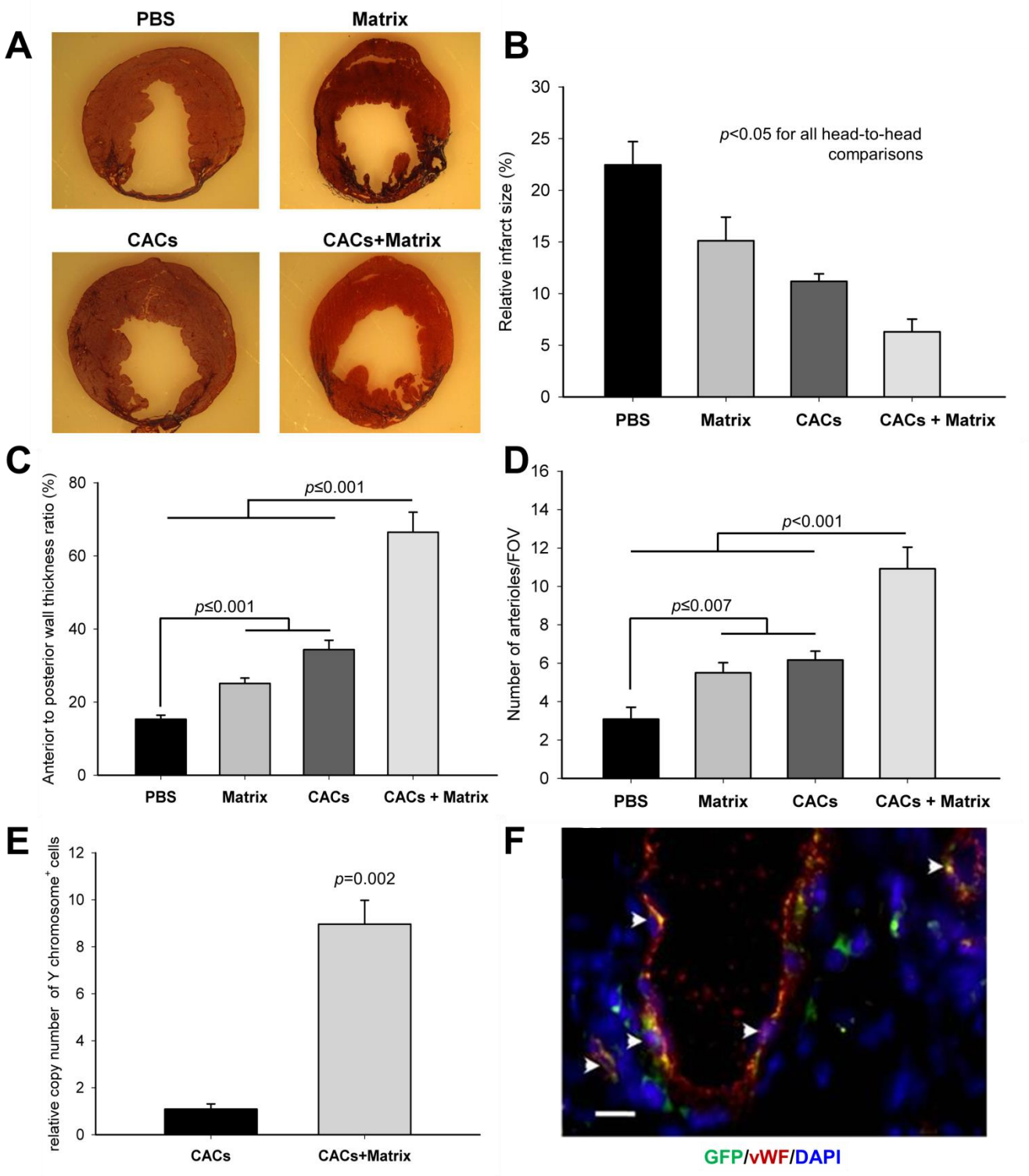
A
PBS
Matrix
CACs
CACs+Matrix
B
Relative infarct size (%)
p<0.05 for all head-to-head comparisons
PBS
Matrix
CACs
CACs + Matrix
C
Anterior to posterior wall thickness ratio (%)
p≤0.001
p≤0.001
D
Number of arterioles/FOV
p<0.001
p≤0.007
E
relative copy number of Y chromosome+ cells
p=0.002
F
GFP/vWF/DAPI

Figure 3.2 CACs+matrix therapy limits adverse remodeling and improves vascular density and transplanted cell retention. (A) Representative Masson Trichrome-stained transverse myocardial mid-papillary (3.8mm from the apex) sections of treated hearts; images show greater preservation of infarct wall thickness and smaller infarct size with CACs+matrix treatment. (B) Size of the infarct relative to the complete ventricle area 3 weeks after treatment (n=7-15). (C) Anterior-to-posterior wall thickness ratio as an indicator of wall thinning, 3 weeks after treatment (n=7-15). (D) Arteriole density in MI mouse hearts 3 weeks after treatment (n=12). (E) Y-chromosome qPCR for detection of male donor CACs in the MI mouse heart (n=3). (F) Transplanted GFP^+ cells were observed to incorporate into vWF^+ blood vessel structures (arrowheads); green=GFP; red=vWF, blue=DAPI nuclei, yellow=GFP^+vWF^+. Scale bar = 10μm.

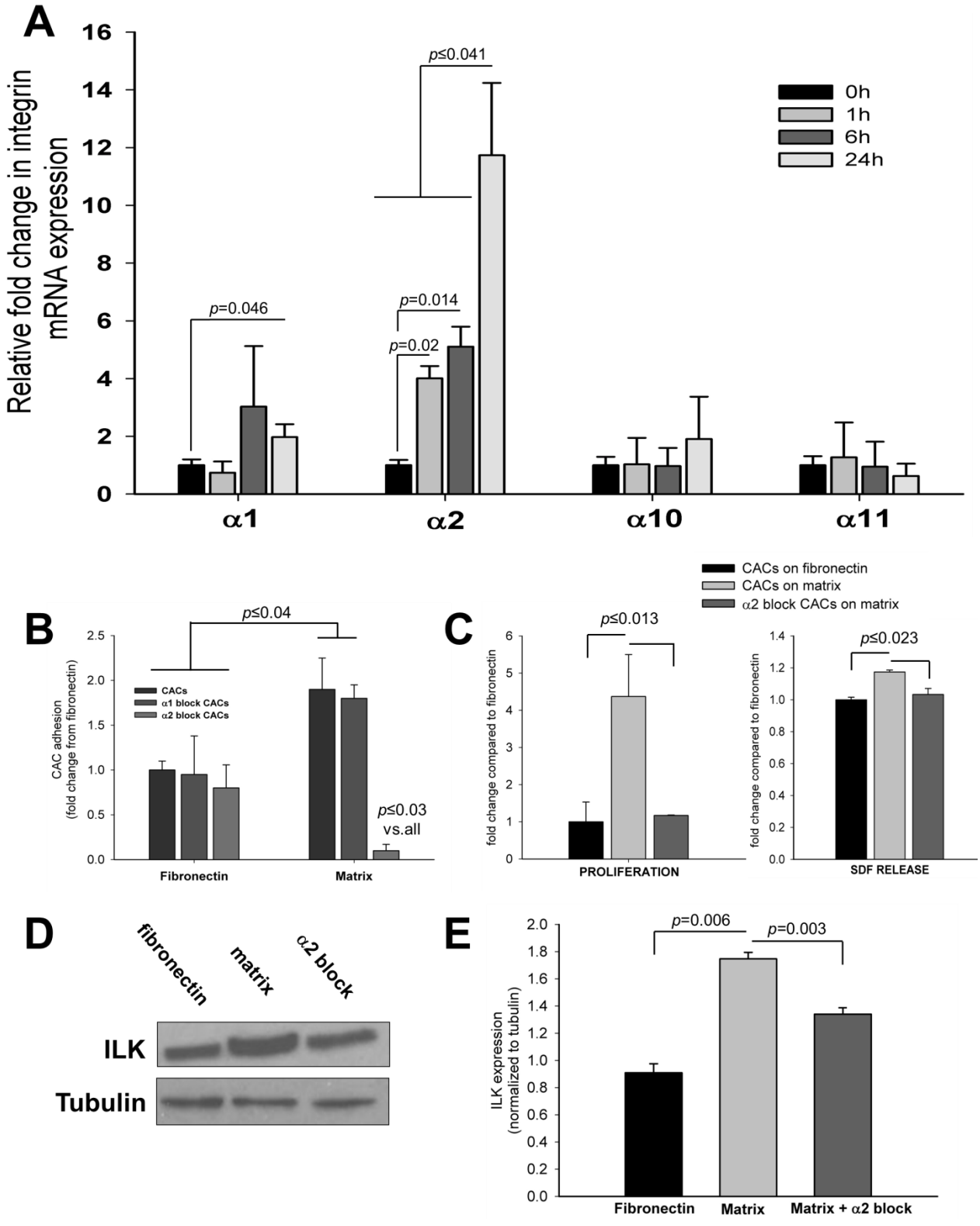
A
Relative fold change in integrin mRNA expression
0h
1h
6h
24h
p≤0.041
p=0.046
p=0.014
p=0.02
α1
α2
α10
α11
B
p≤0.04
CAC adhesion (fold change from fibronectin)
CACs
α1 block CACs
α2 block CACs
p≤0.03 vs.all
Fibronectin
Matrix
C
CACs on fibronectin
CACs on matrix
α2 block CACs on matrix
p≤0.013
fold change compared to fibronectin
PROLIFERATION
p≤0.023
SDF RELEASE
D
fibronectin
matrix
α2 block
ILK
Tubulin
E
p=0.006
p=0.003
ILK expression (normalized to tubulin)
Fibronectin
Matrix
Matrix + α2 block

Figure 3.3 Integrin α2β1 is required for the functional enhancement of CACs on collagen matrix. (A) Expression profile for collagen-binding α-integrin mRNA in CACs cultured on collagen matrix over 24h relative to fibronectin (n=5). (B) Adhesion of CACs, CACs with Itgα1 blocking (α1 block), and CACs with Itgα2 blocking (α2 block) 1h after addition to collagen matrix or fibronectin (n=3). (C) Proliferation in CACs, assessed by enumerating Ki-67^{+} cells after 24h of culture (n=4); and SDF-1 secretion by CACs, measured by ELISA in the supernatant of 24h cultures (n=3). (D) Representative immunoblot of ILK protein expression in CACs after 1h culture on fibronectin, matrix or matrix+α2 block, with tubulin as a loading control. (E) Quantification of ILK protein expression in CACs after 1h culture on fibronectin, matrix or matrix+α2 block (n=3).

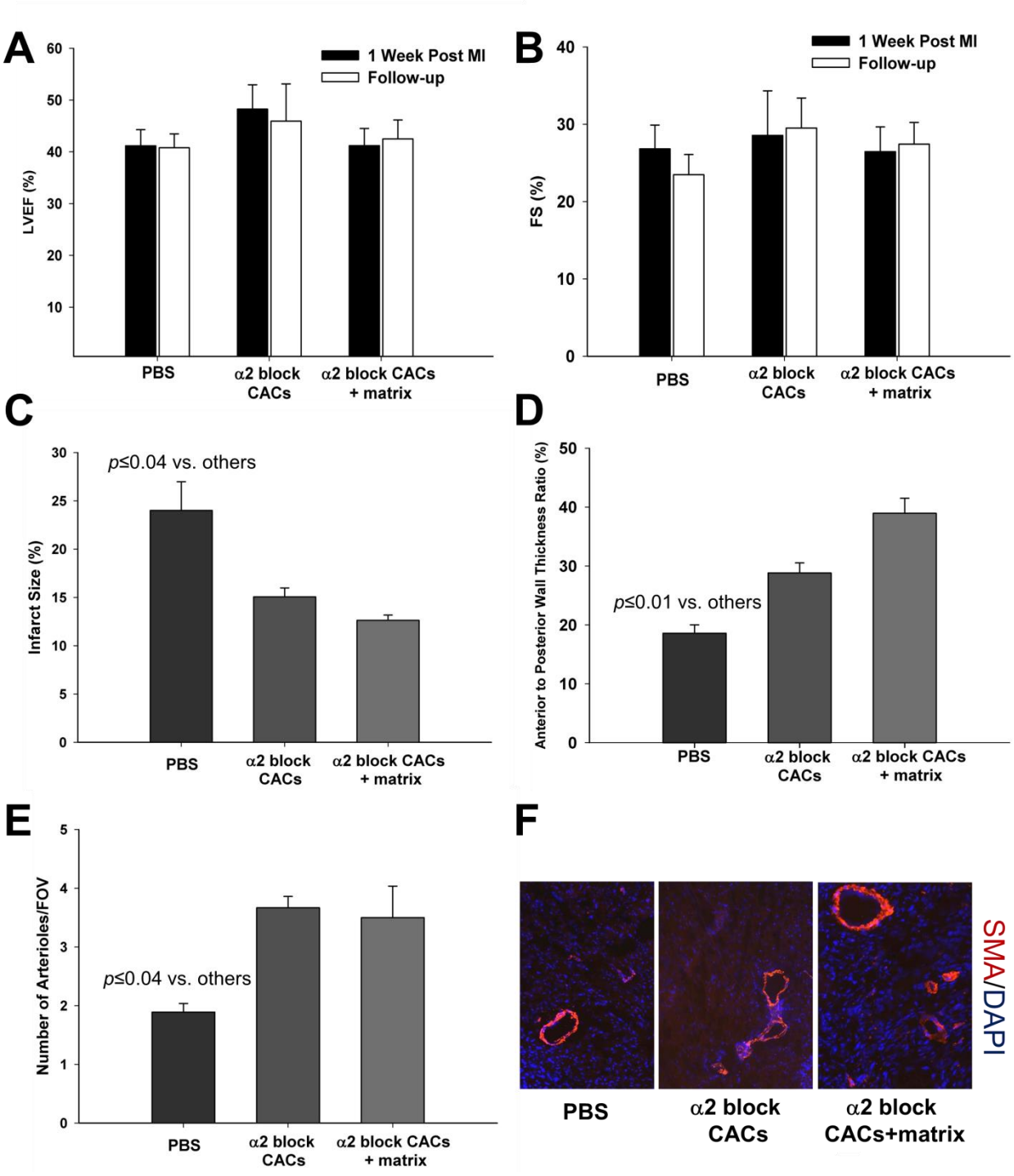
A
1 Week Post MI
Follow-up
LVEF (%)
60
50
40
30
20
10
PBS
α2 block CACs
α2 block CACs + matrix
B
1 Week Post MI
Follow-up
FS (%)
40
30
20
10
0
PBS
α2 block CACs
α2 block CACs + matrix
C
p≤0.04 vs. others
Infarct Size (%)
30
25
20
15
10
5
0
PBS
α2 block CACs
α2 block CACs + matrix
D
p≤0.01 vs. others
Anterior to Posterior Wall Thickness Ratio (%)
50
40
30
20
10
0
PBS
α2 block CACs
α2 block CACs + matrix
E
p≤0.04 vs. others
Number of Arterioles/FOV
5
4
3
2
1
0
PBS
α2 block CACs
α2 block CACs + matrix
F
SMA/DAPI
PBS
α2 block CACs
α2 block CACs+matrix

Figure 3.4 The synergistic effect of CACs+matrix therapy in MI mouse heart is lost when integrin α2 is blocked in CACs. (A) LVEF at baseline (1 week post-MI) and at follow-up (3-wk post-treatment) measured by echocardiography (n=4-7). (B) FS at baseline (1 week post-MI) and at follow-up (3-wk post-treatment) measured by echocardiography (n=4-7). (C) Size of the infarct relative to the entire ventricle area, 3 weeks after treatment (n=4-7). (D) Anterior-to-posterior wall thickness ratio as an indicator of wall thinning, 3 weeks after treatment (n=4-7). (E) Arteriole density and (F) representative images of staining for α-SMA^+ arterioles in tissue sections of MI hearts 3 weeks after treatment; red=α-SMA^+; blue=DAPI nuclei. Scale bar = 50μm (n=4-7).

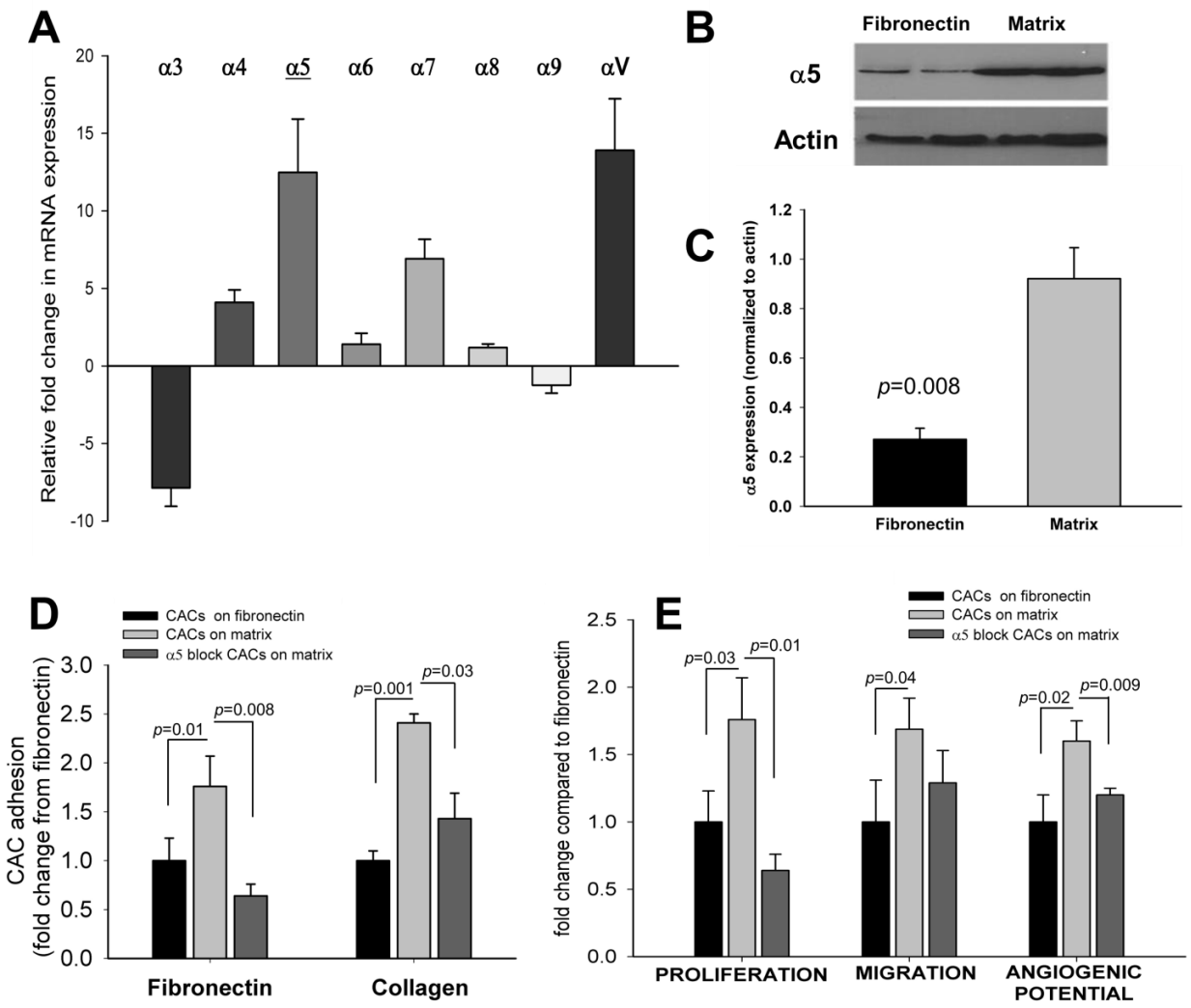

Figure 3.5 Collagen matrix-enhanced function of CACs is dependent on integrin α5. (A) CAC integrin mRNA expression profile after 24h culture on collagen matrix relative to fibronectin (n=6). (B) Representative immunoblot of α5 protein expression in CACs after 24h culture on fibronectin or collagen matrix, with β-actin as a loading control. (C) Quantification of α5 protein expression in CACs after 24h culture on fibronectin or collagen matrix (n=3). (D) CACs were cultured on fibronectin or collagen matrix for 4 days. Cells were then lifted and re-plated onto either fibronectin or collagen matrix with or without Itgα5 blocking (α5 block) and adhesion was assessed after 1h (n=3). (E) Proliferation assessed by counting Ki-67^{+} cells (n=3); migration

towards a VEGF stimulus (n=4); and angiogenic potential of CACs (n=4) were evaluated for cells cultured on fibronectin, matrix, or matrix+α5 block.

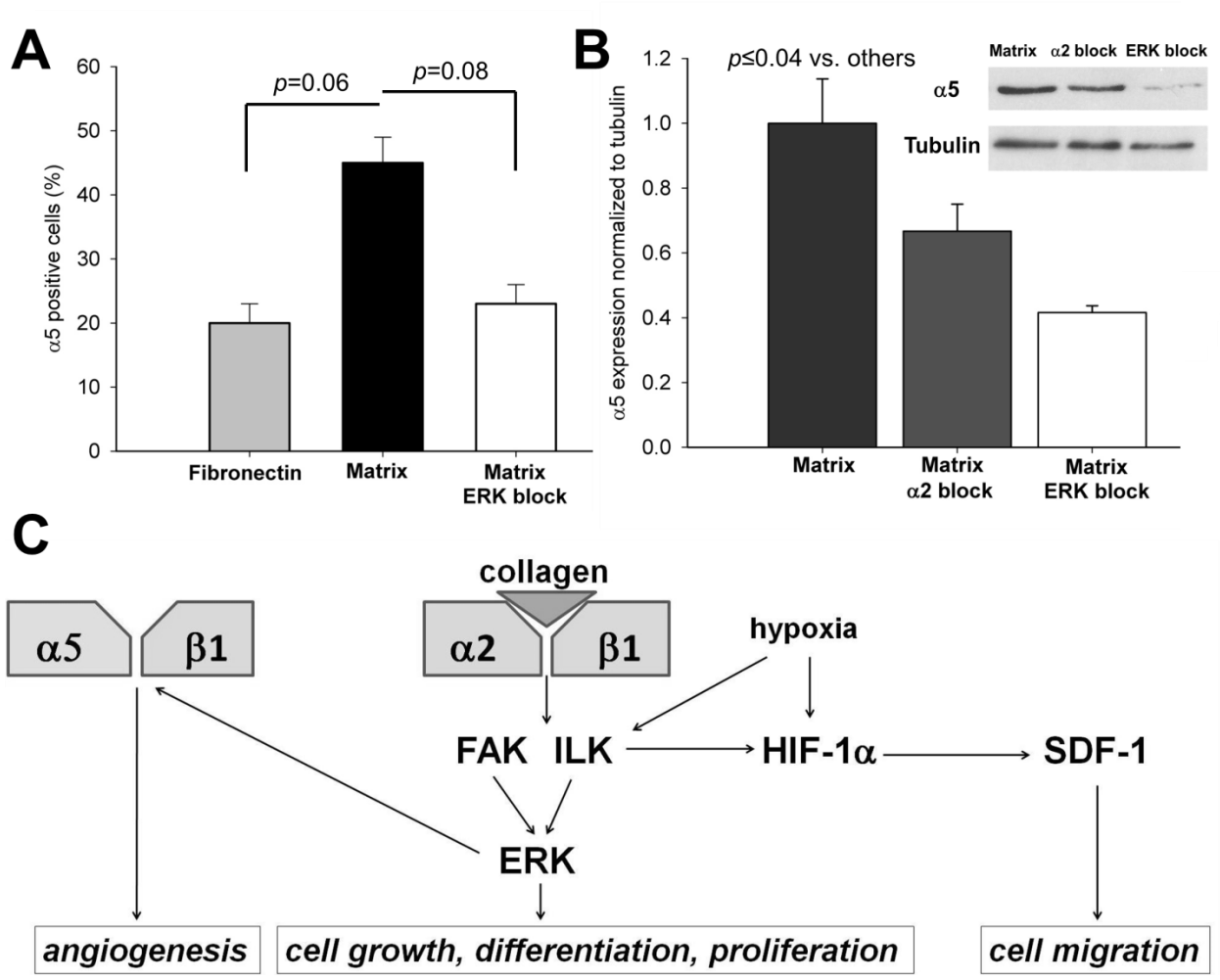

Figure 3.6 Collagen matrix-enhanced integrin α5 expression involves Itgα2 signaling and the ERK pathway. (A) Flow cytometry analysis for the percentage of Itgα5^{+} CACs after 24h culture; matrix-cultured CACs were first treated with or without an ERK/MEK blocker (n=4). (B) Quantification of α5 protein in CACs cultured on matrix ± Itgα2β1 block or ERK/MEK block (n=3). Upper right: Representative immunoblot of α5 expression in CACs with tubulin as a loading control. (C) Schematic figure depicting the signaling cascade activated upon CAC adhesion to collagen matrix.

3.7 Discussion

Injectable hydrogels made from naturally-occurring ECM components appear ideal for improving the persistence and function of transplanted cells applied for cardiac regeneration therapy. Through the provision of natural ligand sites, such biomaterials are expected to interact with the transplanted cells through adhesion molecules to enhance cell attachment/retention and guide tissue regeneration (Kuraitis et al., 2012b, Lutolf et al., 2009). However, this is putative as such mechanisms of action have not been elucidated in the context of *in vivo* regeneration. Focusing on integrin-mediated interactions, we present here the first study of biomaterial-enhanced cell treatment for MI that identifies the mechanisms responsible for the synergistic effect of cells+matrix therapy.

Notably, we showed that cell-matrix interaction was required to improve the function of the MI mouse heart following treatment with CACs+matrix therapy. Specifically, we established that integrin α2β1, primarily a collagen-binding protein (McCall-Culbreath and Zutter, 2008), is essential for CACs to adhere to the matrix, and to mediate matrix-enhanced CAC proliferation and SDF-1 production, which is similar to its role in regulating the proliferative and angiogenic potential of endothelial cells (Chung et al., 2004). Most importantly, blocking Itgα2 in CACs abolished the synergistic benefit of CAC+matrix therapy in the infarcted heart. While integrins can initiate many different signaling cascades, here we demonstrated that the matrix increased ILK expression in CACs, which was reduced by blocking Itgα2. These results are consistent with other studies showing that ILK over-expression in CACs conferred superior proliferation and survival *in vitro* and enhanced angiogenesis *in vivo* (Cho et al., 2005, Werner et al., 2008), and that endothelial cells respond to hypoxia by increasing SDF-1 expression via an ILK mechanism (Lee et al., 2006). Through the use of a matrix, we have observed the same functional responses

in the present study and in previous work where matrix-cultured CACs had increased Akt phosphorylation, resistance to cell death and angiogenic potential (Kuraitis et al., 2011a).

In examining the α-integrins that are not traditionally associated with collagen binding, we obtained unexpected mechanistic insight into how the matrix controls CAC function. Specifically, Itgα5 was up-regulated in collagen matrix-cultured CACs, even though it is a high affinity fibronectin-binding integrin (Pytela et al., 1985). Blocking Itgα5 prevented the matrix from enhancing the adhesive, migratory and angiogenic potential of CACs. Co-culture with hypoxia-treated endothelial cells can similarly result in increased Itgα5 expression in CACs, which was associated with improved migration and angiogenic properties (Bellik et al., 2008). Interestingly, inhibiting either Itgα2 or ERK in matrix-cultured CACs reduced Itgα5 expression. Therefore, we believe that an Itgα2/ERK-dependent mechanism controls the up-regulation of Itgα5, which is indispensable for promoting the matrix-enhanced angiogenic function of CACs. While the importance of Itgα5 for angiogenesis is well-known (Caiado and Dias, 2012, Choi et al., 2009), we have shown here a mechanism for its up-regulation in CACs through interaction with a collagen matrix. Our results suggest that CACs bind to the collagen matrix through Itgα2, thereby activating downstream ILK and ERK signaling and up-regulating the surface expression of Itgα5, all contributing to the therapeutic benefits of CACs+matrix therapy.

We demonstrated that CACs+matrix treatment increased vascularization and reduced adverse remodeling in the MI mouse heart. Furthermore, perfusion, glucose uptake and cardiac output of MI hearts were significantly better when CACs+matrix therapy was administered. Others have shown that treatment with decellularized ECM and SDF-1-primed endothelial progenitors increased perfusion in MI hearts, and suggested that this was responsible for maintaining a more viable myocardium, which was less susceptible to ventricular dysfunction (Frederick et al.,

2010). Our study directly links improved vascularity, perfusion and LV function to increased glucose utilization (viability) following a combined cells+matrix therapy. PET ^{18}F-FDG imaging demonstrated increased FDG uptake in the myocardium with CACs+matrix treatment, indicating a greater area of viable myocardium. This observed increase in myocardial viability may have resulted from myocardial repair and regeneration through: 1) the rescue of hibernating myocardium, which consists of viable cardiomyocytes with low metabolic activity (Giordano et al., 2013a); or 2) the replacement of lost myocardial cells from pools of resident cardiac stem cells and/or proliferating adult cardiomyocytes (Beltrami et al., 2003, Malliaras et al., 2013). A recent study has identified that alterations in ECM composition play an important role in directing adult cardiomyocyte proliferation (Williams et al., 2014). This raises the attractive possibility that biomaterial therapy may be used to modify the cardiac environment to promote the rescue and/or regeneration of cardiomyocytes, and constitutes a future mechanistic direction for our CACs+matrix therapy research.

3.8 Conclusion

In this study, we demonstrate the collagen matrix does not simply provide passive delivery of CACs, but rather, it interacts with the cells through integrin α2β1 to activate intracellular signaling leading to superior proliferation, adhesion, cytokine production, integrin α5 expression and angiogenic potential. This interaction was essential for the synergistic therapeutic benefit of CACs+matrix treatment in MI mouse hearts. Advancing our understanding of the mechanisms of action for injectable biomaterial-enhanced cell therapies, particularly *in vivo*, may lead to improved regenerative strategies for treating myocardial infarction, as well as multiple other diseases and injury.

Acknowledgements

We thank Suzanne Crowe, Rick Seymour, Gregory Cron, Tayebeh Hadizad, Tanja Sofrenovic, and Céline Giordano for technical assistance with this work. Support came from the Canadian Institutes of Health Research (CIHR; grant MOP-77536 to MR and EJS), the Heart & Stroke Foundation of Ontario (HSFO; program grant, PRG 6242 to RSB; and grant-in-aid T6793 to EJS) and the Ottawa Heart Institute Cardiac Surgery Endowed Chair (to MR). RSB is a Career Investigator of the HSFO. BM was the recipient of the Ottawa Heart Institute Lawrence Soloway Research Fellowship, BV, ST and DK were supported by Canadian Graduate Scholarships from the CIHR.

3.9 Supplementary Section

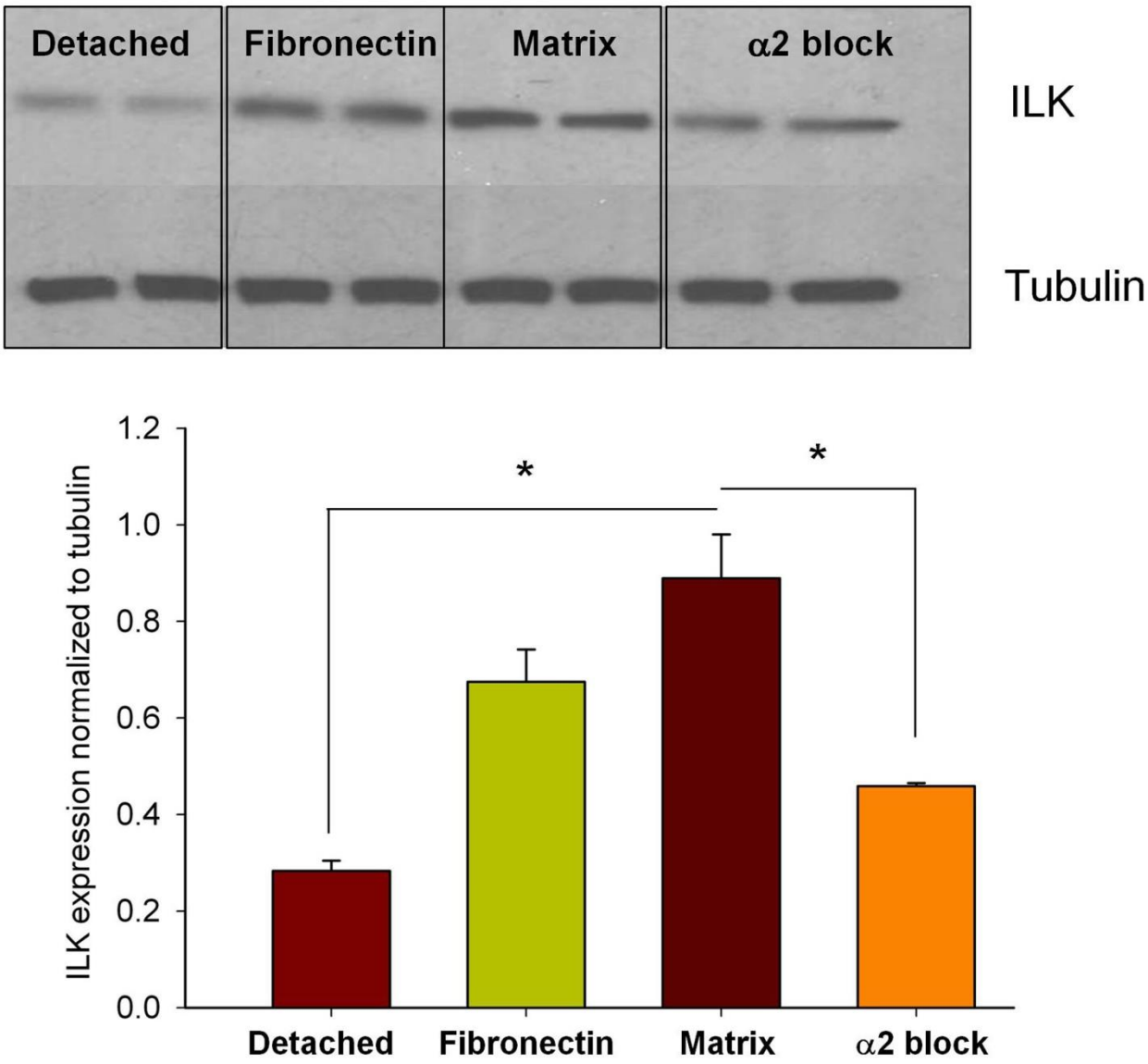

Supplementary Figure 3.1 Integrin α2 is required for increased ILK expression in matrix-cultured mouse BM-CACs. Upper panels: Representative immunoblots of ILK protein expression in CACs cultured in 4 different conditions, with tubulin as a loading control. Lower panel: ILK expression (normalized to tubulin) in detached, fibronectin and collagen matrix (± Itgα2 blocking antibody) culture conditions (*****$p \leq 0.01$; n=3).

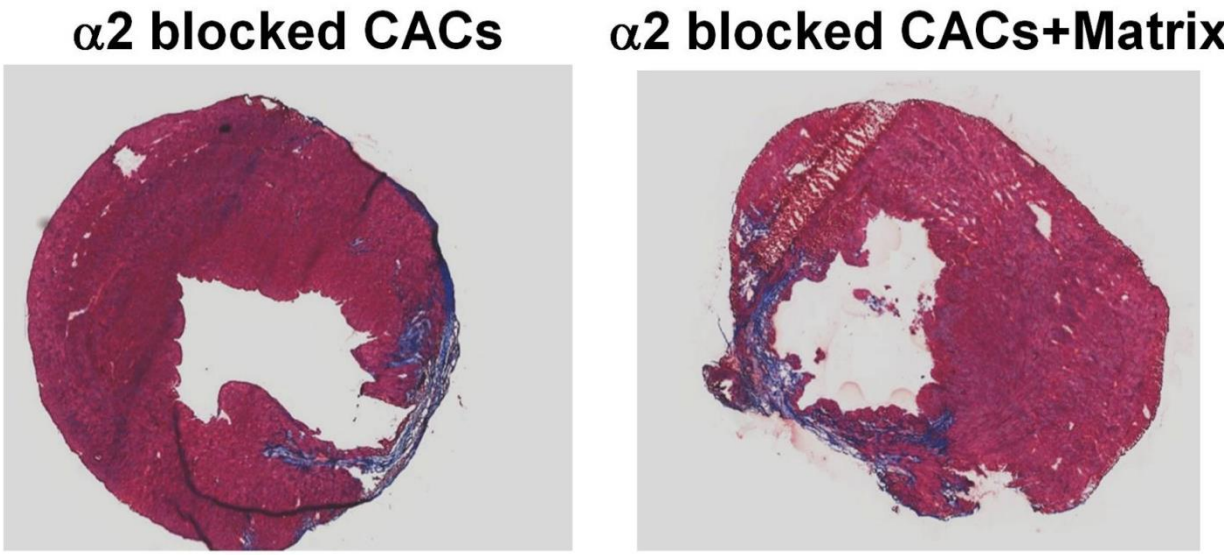

Supplementary Figure 3.2 The ability of CACs+matrix therapy to limit adverse remodeling is inhibited when itgα2 is blocked in CACs**.** Representative Masson Trichrome-stained transverse myocardial mid-papillary (3.8mm from the apex) sections of hearts treated with Itgα2-blocked CACs or Itgα2-blocked CACs+matrix.

Supplemental Table 3.1 Summary of qPCR primers

Symbol	Forward	Reverse
Itga1	CGTGGATAGACTGGCCAAA	CATTTATCATGGAAGTGGCAAG
Itga2	GCCGAGCTTCCATAAAATTG	ACCTGATGAGAAAGCCGAAG
Itga3	ACTCCAAGCCACATGTCCTC	GGACTGGTGCTGTGTACCTG
Itga4	CATGAACAGTCAGCTTAACCTCA	TTAGCTTTCTCCTGGATGTGAG
Itga5	CTGGAGGCTTGAGCTGAGT	CAAGGCAGAAGGCAGCTATG
Itga6	GAACCTGAGTGCCTGCATTT	TGGAACAGCACATTTCTAGAGG
Itga7	TTGGCGCTCAAAGAAGTAGG	CGGCTTTGGCTACTCACTG
Itga8	TTCGGAGTTGCCCAAATAAC	TATGCTCTTGCATCCCTGGT
Itga9	GAGGGATGATGCAGGGAGT	TCGACTCTCATCTGGTGGTG
Itga10	TTGAAGCACCAGGTCTGTGA	ACAAAAGCTGGTCCCCTTCT
Itga11	TGCAAATTCAATGCCAAATG	AGGTCTGTAAAAGATGTGGTGGA
ItgaV	TCTGACTGCTGGTGCACACT	GCCAGGTGGTATGTGACCTT
Chrom-Y	TTTTGCCTCCCATAGTAGTATTTCCT	TGTACCGCTCTGCCAACCA
Ilk	GCTCAGGATTTTCTCGCATC	ATACGGCATCCAGTGTGTGA
18S	CGGCTACCACATCCAAGG	CTGGAATTACCGCGGCT
Gapdh	TGAAGGGGTCGTTGATGG	AAAATGGTGAAGGTCGGTGT

Supplementary Video 3.1 (related to Figure 3.1). The video provides representative echocardiograms demonstrating improved LV wall contractility in hearts treated with CACs+matrix, but not PBS, for which data is reported in Figure 3.1. [data available online; *Biomaterials, Volume 35, Issue 17, June 2014, Pages 4749–4758*]

Chapter 4:

A Collagen-Chitosan Injectable Hydrogel Improves Cardiac Remodeling in a Mouse Model of Myocardial Infarction

Ali Ahmadi; Marc Ruel, Erik J. Suuronen

4.1 Notes on Chapter

Dr. Suuronen's lab has modified the collagen matrix by the addition of chitosan, in order to improve its ability to support angiogenesis. Chitosan is a biocompatible polysaccharide derived from the shell of crustaceans; the optimum mixture of collagen and chitosan has been shown to be superior to collagen-only matrix in terms of supporting endothelial cells and inducing angiogenesis *in vitro*. When implanted subcutaneously in mice, the collagen-chitosan matrix recruited a greater number of progenitor cells and enhanced vascular formation. Chitosan also has long been known for its wound healing properties which is ascribed, at least partially, by chitosan-fibroblast interaction. The focus of this chapter is to evaluate the use of the collagen-chitosan matrix as a therapy for the infarcted myocardium.

4.2 Contribution of Co-authors

M. Ruel was in involved in experimental planning and provided a clinical perspective on the data.

E.J. Suuronen was involved in experimental planning, analysis and manuscript writing/editing.

4.3 Abstract

Background- Cardiac fibroblasts constitute the predominant cell type in the interstitium of the remodeling heart and play an essential role in the response to infarction. In this study, the effects of the collagen-chitosan matrix on cardiac fibroblast phenotype (*in vitro*) and cardiac remodeling (*in vivo*) were investigated.

Methods and Results- Cardiac fibroblasts were cultured on fibronectin, collagen-chitosan matrix or collagen matrix, and myofibroblast differentiation was assessed. Myocardial infarction (MI) was induced in mice by left anterior descending coronary artery ligation. Two weeks post-MI (baseline), mice were randomly allocated to receive myocardial injections of collagen-chitosan, collagen or phosphate buffered saline (PBS). Cardiac function was assessed at baseline and at the end of study (3wk follow-up) by echocardiography. The assessment of α-SMA$^+$ cells per field-of-view (FOV) and in fibroblast cultures showed more myofibroblast differentiation on fibronectin (6.5±1.1/FOV) and collagen matrix (4.4±1.0/FOV) compared to the collagen-chitosan matrix (1.8±0.5/FOV). Also, collagen deposition was increased by ≥2.3-fold in fibronectin and collagen matrix cultures versus the collagen-chitosan matrix-cultured fibroblasts. At 3-wk post-treatment, ejection fraction (EF) and fractional shortening (FS) were improved only in the collagen-chitosan group by 9.9±1.4% and 6.8±1.2%, respectively, whereas they decreased in mice treated with collagen matrix (ΔEF=-7.1±1.5%; ΔFS=-2.5±0.8%) or PBS (ΔEF=-11.6±0.9%; ΔFS=-7.6±1.0%). Concurrently, the collagen-chitosan group showed smaller infarct size (12.8±0.9%) and higher arteriole density (3.4±0.2 /FOV) compared to collagen (22.3±1.4%; 2.2±0.3/FOV) and PBS (19.5±1.8%; 1.3±0.2/FOV) groups. At 1wk post-treatment, only the collagen-chitosan group showed reduced CD68$^+$ cell infiltration (2.5±0.4 fold),

decreased matrix metalloprotease-9 (MMP9) (6.3±1.7 fold) and elevated tissue inhibitor of metalloproteinase-2 (TIMP2) (10.2±0.5 fold) compared to PBS.

Conclusions- The collagen-chitosan matrix reduced cardiac myofibroblast differentiation *in vitro*. Also, collagen-chitosan therapy applied to an established post-MI scar resulted in improved cardiac function, increased arteriole density, and decreased $CD68^+$ inflammatory cell infiltration and favorably affected the MMP/TIMP profile and LV remodeling. The collagen-chitosan matrix shows promise as a stand-alone therapy for remodeling MI hearts.

4.4 Introduction

Cardiac remodeling occurs progressively after myocardial infarction (MI) and is characterized by acute LV dilation, wall thinning, infarct expansion, collagen deposition and scar formation (Gajarsa and Kloner, 2011). Several cellular and extracellular alterations contribute to the post-MI remodeling process during and after the early inflammatory phase. These alterations include degradation of the extracellular matrix (ECM), an acute cellular immune response, cytokine secretion and eventually proliferation and maturation of macrophages and fibroblasts (Spinale, 2007). In the healing heart, cardiac fibroblasts play an important role in regulating inflammation (cytokine secretion) and matrix metabolism (protease production) (Chen and Frangogiannis, 2013). These processes are mainly mediated by the migration of cardiac fibroblasts to the infarcted region and their subsequent differentiation to myofibroblasts which proliferate, generate matrix metalloproteases (MMPs) and deposit collagen resulting in LV remodeling (Souders et al., 2009). Initially, cardiac fibroblast/myofibroblast activation is critical for myocardial healing; however, as this process continues, it leads to a maladaptive response which is associated with extended fibrosis and impaired cardiac function (Souders et al., 2009).

The field of tissue engineering has introduced new potential therapies for treating maladaptive remodeling in the post-MI myocardium. This includes the use of injectable hydrogels with or without progenitor cells or growth factors that can be delivered directly to the infarcted myocardium to stimulate myocardial repair and reduce the heart failure progression (Johnson and Christman, 2013). In this context, chitosan (a chitin-derived deacetylated N-acetylglucosamine) biomaterials have shown promise to interact with fibroblasts and maintain cardiac structure by enhancing the polarity and morphology of cardiomyocytes (Hussain et al., 2013). Another study has demonstrated that the delivery of a chitosan hydrogel carrying immobilized fibroblast growth

factor-2 (FGF-2) to a rabbit model of chronic MI was associated with significant improvement of myocardial function, viability and blood vessel density (Fujita et al., 2005). A chitosan skin patch has also been shown to interact with fibroblasts, improve wound healing and reduce scar formation in a rabbit model (Revi et al., 2013). Also, chitosan-based matrices have shown the ability to serve as an effective vehicle for the delivery of progenitor cells (Wang and Stegemann, 2010) or cardioprotective peptides (Chiu et al., 2012) to MI hearts. Also, chitosan matrices, as a standalone therapy, have been shown to scavenge reactive oxygen species (ROS) and recruit SDF-1 to the heart microenvironment in a rat MI model (Liu et al., 2012). The collagen-chitosan combination has shown enhanced biostability and improved angiogenic potential *in vitro* and *in vivo* compared to collagen-only or chitosan-only hydrogels (Deng et al., 2010). Furthermore, the addition of chitosan to collagen has been shown to improve the infiltration of fibroblasts into the matrix and to maintain an enhanced interaction between this cell type and the matrix (Ma et al., 2003).

The objective of this study was to study the effects of chitosan addition to a collagen matrix on cardiac fibroblast differentiation *in vitro* and its therapeutic benefits on cardiac remodeling in a mouse MI model.

4.5 Methods

Collagen-chitosan matrix preparation

Collagen matrix was prepared as described before (Kuraitis et al., 2011a). Briefly, the matrix was a mixture (pH = 7.2) of blended neutralized type 1 rat tail tendon collagen (0.375%, wt/vol; Becton Dickinson) and chondroitin 6-sulfate (1:6, wt/wt; Sigma), cross-linked with 0.02%

(vol/vol) glutaraldehyde. A glycine solution (20%) was added as a last step to scavenge unreacted aldehyde groups.

The collagen-chitosan matrix consisted of a 1:1 mixture of chitosan and type 1 collagen (0.375% wt/vol). Chitosan (448869; Sigma) was dissolved in 0.2 M HCl (0.5%, wt/vol). Dissolving was accelerated by increasing the temperature to 90°C for 20mins. The solution was then sterilized by filtering. After adjusting the collagen-chitosan mixture pH to 7.2, it was blended with chondroitin 6-sulfate (1:6, wt/wt; Sigma) and cross-linked with 0.02% (vol/vol) glutaraldehyde. A glycine solution (20%) was added to scavenge unreacted aldehyde groups. Matrix solutions were kept on ice until use.

Mouse fibroblast isolation and culture

It has previously been shown that MI modifies cardiac fibroblasts in C57BL/6 mice (Carlson et al., 2011). For this reason cardiac fibroblasts were obtained from MI mice sacrificed 2 weeks after MI surgery to coincide with the timing of treatment delivery. Hearts were perfused with ice cold PBS and harvested under sterile conditions in an isolation hood. Each heart was placed in 5 ml of ice cold calcium and bicarbonate free Hank's with HEPES buffer (136.9 mM NaCl, 5.36 mM KCl, 0.81 mM $MgSO_4.7H_2O$, 5.55 mM Glucose, 0.44 mM KH_2PO_4, 0.31 Na_2HPO_4, 20 mM HEPES; pH=7.4). Hearts were minced and a collagenase solution (30 mg collagenase type II (Roche) and 10 mg porcine trypsin (Sigma) in 10 ml of Hank's + HEPES Buffer) was applied to digest the tissue for 1h at 37^oC with gentle shaking. The mixture is spun briefly and the pellet was resuspended in the collagenase solution for a second digest under the same conditions. Samples were centrifuged, the supernatant was discarded, and the pellet was resuspended in DMEM/F12 media supplemented by HEPES 25 mmol/L (Invitrogen, 11330-032). Cells were

plated on 10cm Petri dishes for 2h, after which the non-adherent cells were removed by gentle shaking and the adherent cells (mostly cardiac fibroblasts) were kept and fed with complete media (DMEM/F12 + 10% FBS), which was replaced every 2 days. Upon reaching confluence (within 5-7 days), cells were lifted using 0.25% trypsin-EDTA (Invitrogen, 25200-056) and passaged further. Passage 3 (P3) cells were seeded on fibronectin (control), collagen matrix, or collagen-chitosan matrix in 12-well plates at a density of 1.0×10^5 cells/well. At this time, the cells were treated with 10 ng/ml of mouse transforming growth factor-β1 (TGF-β1; Cell Signaling; 5231) to induce myofibroblast differentiation. After 5 days, the cells were fixed with 4% paraformaldehyde and kept at 4^oC until immunostaining.

Animal model and surgical procedure and injection

All experimental procedures were performed in accordance with the National Institute of Health Guide for the Care and Use of Laboratory Animals. MI was induced in 9-wk old female C57BL6/J mice by ligation of the left anterior descending coronary artery. Two weeks after MI (baseline), the mice were randomly allocated to receive either phosphate buffered saline (PBS), collagen matrix or collagen-chitosan matrix. An ultrasound-guided procedure was used to deliver 5 equivolumetric intramyocardial injections (50 µl total) through a 27 gauge needle to the infarct and peri-infarct areas. Cardiac function was assessed at baseline and at 3-week follow-up by transthoracic echocardiography (Vevo770 System; VisualSonics). Left ventricular ejection fraction (EF) and fractional shortening (FS) were calculated using Vevo 770 V.0.0.3 Software (VisualSonics). The mice were sacrificed at either 1wk or 3wk and the hearts were collected for infarct assessment, immunohistochemistry and immunoblot assays.

Histology and Immunohistochemistry

Mouse hearts were preserved in Tissue-Tek® O.C.T. Compound. The slides were prepared in 10-µm serial cryo-sections. The slides were used either for infarct assessment (Masson Trichrome and hematoxylin phloxine saffron staining) or immunohistochemistry. Infarct assessment was performed using bright field microscopy on sections cut at 3.8mm from the apex. The anterior LV (infarct) and posterior LV (intact) wall thickness at medial and lateral areas was measured and the anterior/posterior ratio was reported. Furthermore, infarct size (% of myocardium) was calculated using Photoshop® software as the pixel area in the myocardial scar divided by the total myocardial pixel area.

Sections were stained with anti-alpha smooth muscle actin (α-SMA) (ab5694; 1:100) and anti-CD68 (ab125212; 1:500) primary antibodies, followed by secondary antibody staining with Texas-red goat anti-rabbit IgG (T1-1000; 1:100; Vector Laboratories). Tissue sections were also treated with 4´,6-di-amidino-2´-phenylindole (DAPI; Sigma) to stain cell nuclei. For *in vitro* fibroblast/myofibroblast experiments, anti-discoidin domain-containing receptor 2 (DDR2) (ab173478; 1:10), anti α-SMA (ab5694; 1:100), and anti-mouse collagen type 1 (ab34710; 1:100) primary antibodies were applied and the Alexa Fluor 488 goat anti-rabbit (A-11008; 1:500) was used as the secondary antibody. The DDR2 and α-SMA results are reported as the number of positive cells per field-of-view (FOV). Collagen type 1 staining results are reported as the fibrillar collagen length (arbitrary unit/FOV) and density (% of plate covered by collagen deposit per FOV).

Western Blot

Hearts were perfused with ice-cold PBS, and the infarct and peri-infarct regions were excised and snap frozen in liquid nitrogen. Ground tissue (25g/heart) was incubated in 400µl of ice cold Radio Immuno Precipitation Assay buffer for 30mins. The lysate was used for BCA protein assay and western blot. Protein extracts (40µg/sample) were electrophoresed and transferred to nitrocellulose membranes, according to standard protocols. The membranes were incubated with metalloproteinase 9 (MMP9) or tissue inhibitor of tissue inhibitor of metalloproteinase 2 (TIMP2) antibodies (ab38898 and ab38973, respectively; 1:1000). Secondary anti-rabbit IgG (Cell Signaling; 7074S; 1:1000) was applied. As a loading control, membranes were also incubated with an α-tubulin Rabbit antibody (Cell Signaling; 2125S; 1:1000). The SuperSignal West Femto Substrate (Thermo Scientific) was used for chemiluminescence. The immunoblot bands were quantified using Quantity One Software (Bio-Rad Laboratories).

Statistical Analysis

Data are expressed as the mean ± SEM. Statistical analyses between groups were performed with a one-way analysis of variance, adjusted for repeat measures. Statistical significance was given for $p<0.05$.

4.6 Results

In Vitro Cardiac Myofibroblast Differentiation and Collagen Deposition

DDR2 staining indicated that fibroblasts constitute 79±3% of cultured cells at the end of passage 2 (Figure 4.1A). After 5 days of TGF-β1 treatment, greater myofibroblast differentiation (determined by the number of α-SMA$^+$ cells) was observed for cultures on fibronectin

(6.5±1.1/FOV) and collagen matrix (4.4±1.0/FOV) compared to the collagen-chitosan matrix (1.8±0.5/FOV) (Figures 4.1B and 4.1D). Similarly, more collagen deposition was observed for fibroblasts on fibronectin (length: 51.0±3.2/FOV; density: 15.8±0.8%) and on collagen matrix (length: 39.6±3.7/FOV; density: 9.1±0.6%) in comparison to the collagen-chitosan matrix (length: 17.4±2.2/FOV; density: 3.9±0.3%; Figures 4.1C, 4.1E and 4.1F). Although the cells were cultured on rat tail collagen type 1, mouse cell collagen deposition assessment was feasible because the immunostaining was performed on confluent mouse cells and the microscopic plane of view adjusted to visualize the cell layer. The background signal emitted from collagen, collagen-chitosan, or fibronectin coated plates was negligible in this plane of view, as measured by fluorescence microscopy (data not shown).

Cardiac Function after Treatment

MI surgery was performed on 18 mice with 100% survival rate. Treatment delivery was associated with a survival rate of 83%; there were a total of 5 mice per treatment group. Baseline cardiac function at 2wk post-MI was equivalent between all groups (pooled average: EF=34.2±0.6%; FS=23.9±0.3%). Three weeks after treatment delivery, EF and FS significantly decreased in PBS-injected mice by 11.6±0.9% and 7.6±1.0%, respectively (Figure 4.2). The collagen matrix group also showed a decrease in EF (-7.1±1.5%) and FS (-2.5±0.8%). In contrast, EF (by 9.9±1.4%) and FS (by 6.8±1.2%) significantly improved over the 3 week follow-up in mice treated with the collagen-chitosan matrix (Figure 4.2).

LV Mass, Arteriole Density and $CD68^+$ Cell Infiltration in Treated MI Hearts

One week after treatment delivery, the anterior-to-posterior wall thickness ratio (PBS=36.3±6.4%; collagen=33.1±4.1; collagen-chitosan=42.4±13.1%) and infarct size

(PBS=15.2±4.3%; collagen=13.2±2.9%; collagen-chitosan=17.1±3.7%) were equivalent between groups (Figure 4.3). The matrix injection was performed at 2wk post-MI, when the endogenous collagen deposition and fibrosis had already commenced; therefore, we could not distinguish between endogenous collagen deposits and exogenous matrix at 1wk after delivery. Three weeks after treatment, the thickness ratio and infarct size were preserved in collagen-chitosan matrix group (37.8±6.2%; 12.8±0.9%) but worsened in the collagen matrix (22.3±1.4%; 19.9±3.2%) and PBS (19.5±1.8%; 21.2±2.8%) groups (Figure 4.3).

At 1wk post-treatment, arteriole density was higher in the hearts that received collagen-chitosan matrix compared to collagen and PBS treatment (5.0±0.2 versus 3.3±0.2 and 3.1±0.3/FOV, respectively). Between 1 and 3 weeks post-treatment, arteriole density decreased within all groups; but it remained highest in the collagen-chitosan matrix group (3.4±0.2 /FOV) compared to collagen matrix (2.2±0.3/FOV) and PBS (1.3±0.2/FOV) injected hearts (Figure 4.4).

One week after treatment, $CD68^+$ cells were more numerous in PBS and collagen matrix injected hearts (17.6±3.0 and 16.6±1.1/FOV) compared to the collagen-chitosan matrix group (7.0±1.7/FOV). At 3 weeks post-treatment, the number of $CD68^+$ cells was reduced to the same level in all groups (4.8±0.9 and 2.5±0.8 versus 2.8±0.4/FOV for PBS, collagen matrix and collagen-chitosan groups, respectively) (Figure 4.5).

ECM Metabolism in Treated MI Hearts

One week post-treatment delivery, MMP9 protein expression was greater in the hearts of PBS and collagen matrix treated groups (by 6.3±1.7 and 3.0±1.2 fold, respectively) compared to the collagen-chitosan matrix injected group. At the 3wk end-point, MMP9 expression was the same in all groups (Figure 4.6A). Furthermore, TIMP2 protein expression was up-regulated in

chitosan-collagen matrix (by 10.2±0.5 fold) and collagen matrix injected hearts (by 6.0±1.5 fold) compared to PBS at 1 week post-treatment; but no difference was observed between groups at 3 weeks post-treatment (Figure 4.6B).

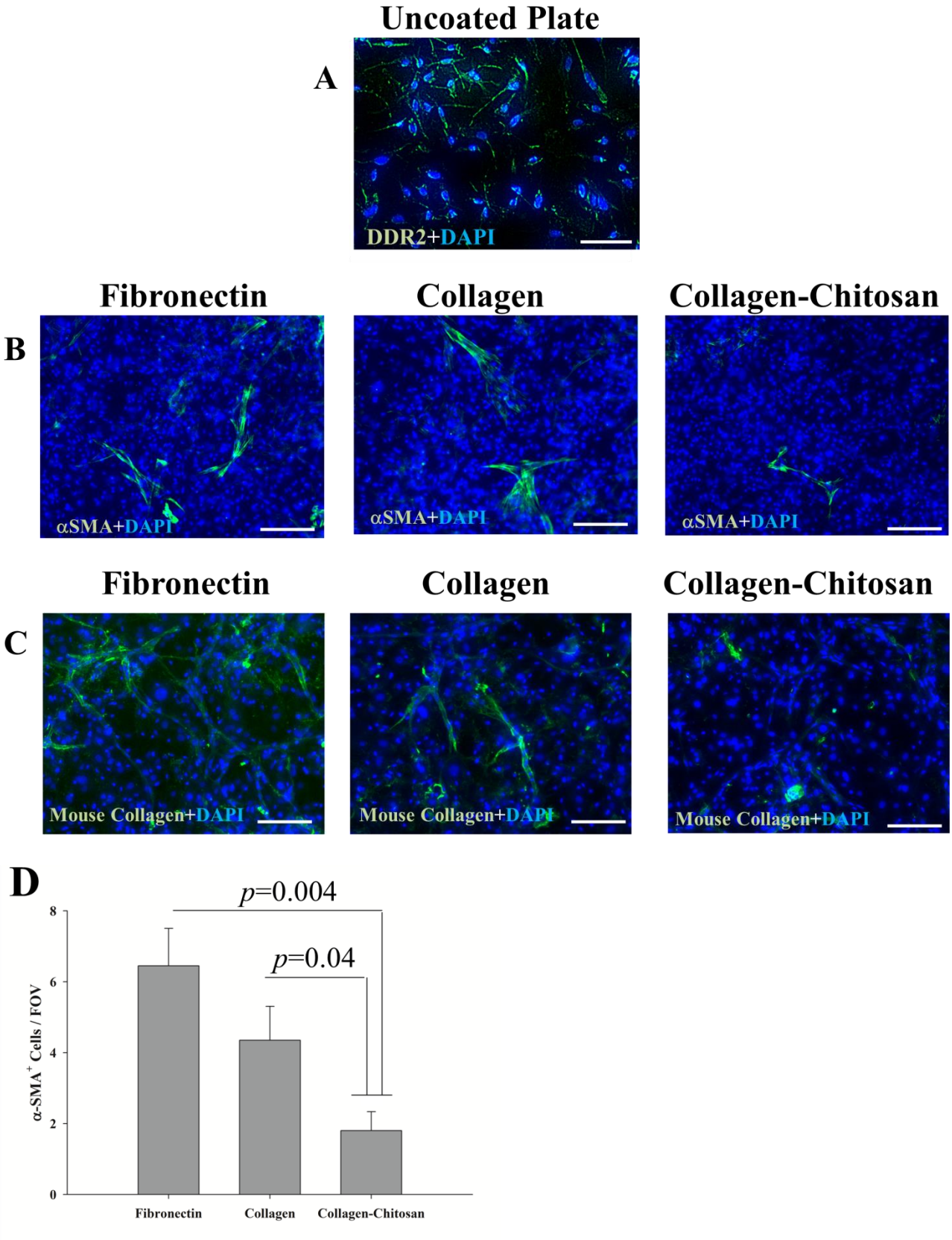
Uncoated Plate
A
DDR2+DAPI
Fibronectin
Collagen
Collagen-Chitosan
B
αSMA+DAPI
αSMA+DAPI
αSMA+DAPI
Fibronectin
Collagen
Collagen-Chitosan
C
Mouse Collagen+DAPI
Mouse Collagen+DAPI
Mouse Collagen+DAPI
D
p=0.004
p=0.04
α-SMA+ Cells / FOV
0
2
4
6
8
Fibronectin
Collagen
Collagen-Chitosan

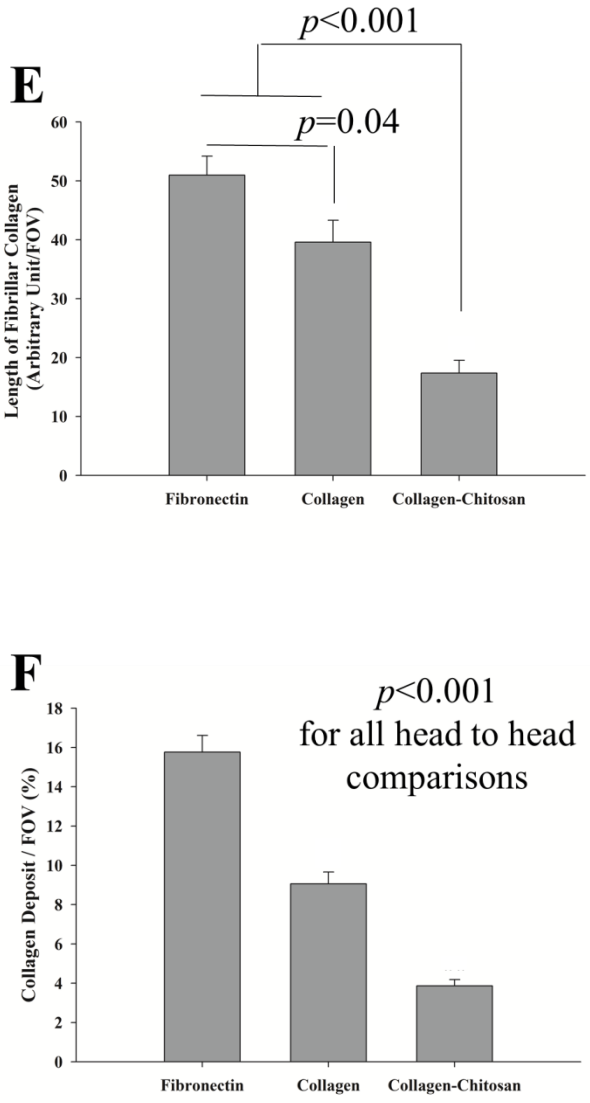

Figure 4.1 Cardiac fibroblast culture. (A) DDR2 staining confirmed the phenotype of cells at the end of passage 2. (B and C) Representative images of cardiac fibroblasts in different culture conditions stained for α-SMA (B) or collagen type 1 (C). (D) α-SMA^{+} cells were less numerous on collagen-chitosan compared to fibronectin and collagen. (E) The length of fibrillar collagen was reduced on collagen-chitosan. (F) The relative surface area of fibrillar collagen was reduced on collagen-chitosan (*n=5* for all experiments).

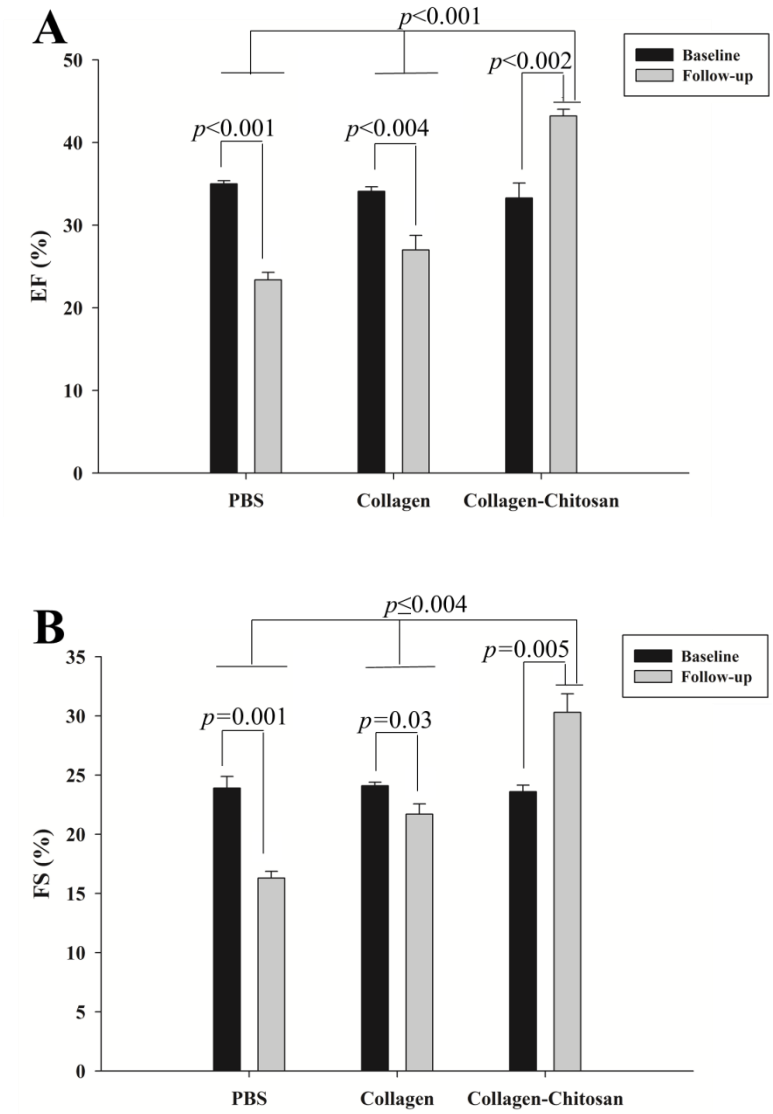

Figure 4.2 Left ventricular EF and FS in MI mice injected with different treatments. (A) In PBS and collagen injected mice, EF decreased from 35.0±0.4% and 34.2±0.6% to 23.4±0.9% and 27.0±1.8%, respectively. In the collagen-chitosan group, EF increased from 33.3±1.8% to 43.2±0.8%. (B) Three weeks after treatment delivery, FS was reduced in the PBS and collagen groups from 23.9±1.0% and 24.2±0.3% to 16.4±0.6% and 21.7±0.9%, respectively. In collagen-chitosan injected hearts, FS increased from 23.6±0.6 to 30.4±1.6% ($n=5$ for all groups).

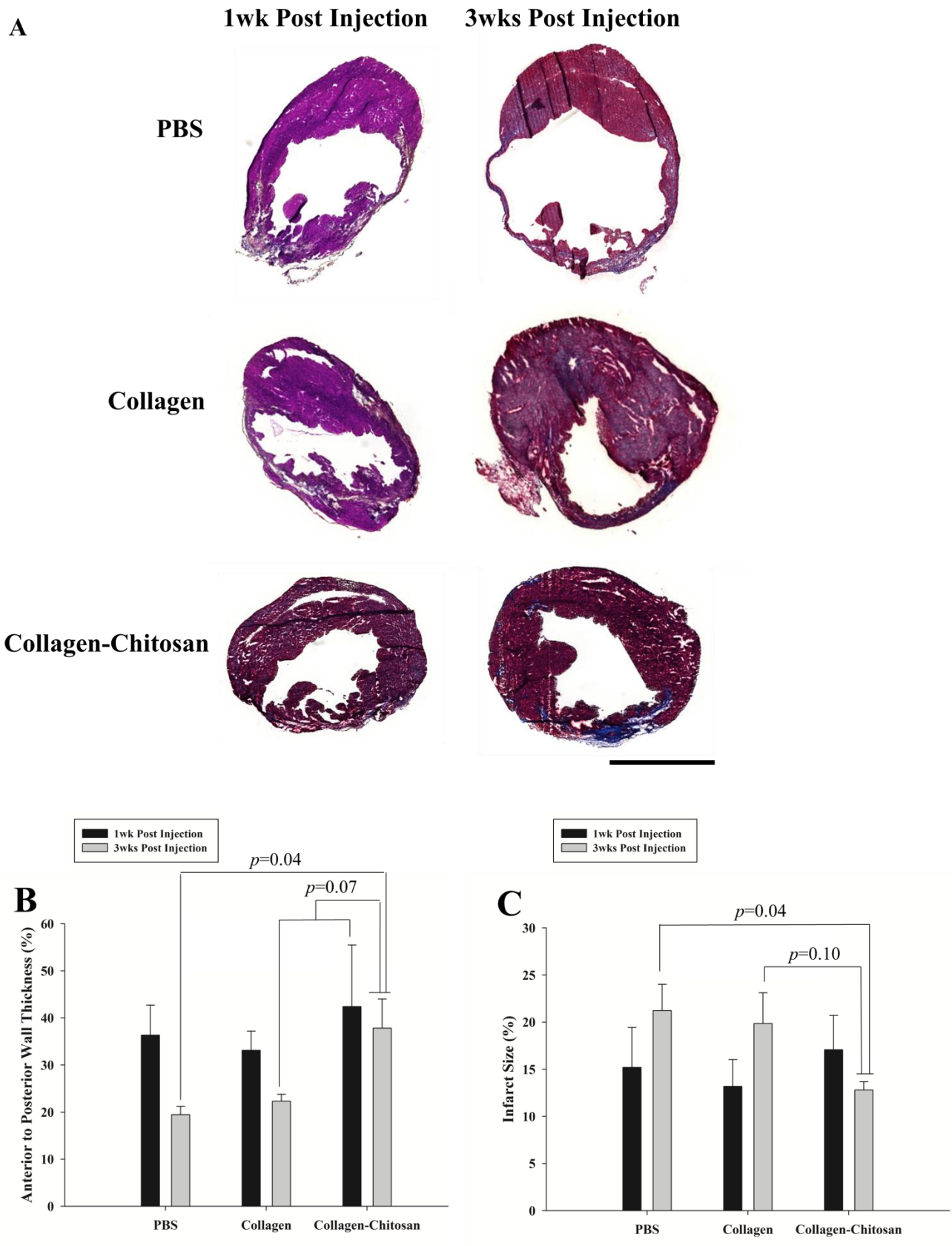
A
1wk Post Injection
3wks Post Injection
PBS
Collagen
Collagen-Chitosan
B
1wk Post Injection
3wks Post Injection
p=0.04
p=0.07
Anterior to Posterior Wall Thickness (%)
0
10
20
30
40
50
60
PBS
Collagen
Collagen-Chitosan
C
1wk Post Injection
3wks Post Injection
p=0.04
p=0.10
Infarct Size (%)
0
5
10
15
20
25
30
PBS
Collagen
Collagen-Chitosan

Figure 4.3 Infarct size assessment 1wk and 3wks after treatment delivery. (A) Representative Masson Trichrome staining of MI mouse hearts sectioned at the same transversal level from the apex (scale bar=2mm). (B) 1wk post-injection, the LV anterior (infarct) to posterior (intact) wall thickness ratio was not significantly different between group (pooled average: 37.3±4.6%). Three weeks post-injection, this ratio was preserved in collagen-chitosan injected hearts vs. PBS group. (C) At 1wk post-injection, the relative infarct size was the same in all groups (pooled average: 15.1±1.9%). At 3wks post-injection, it was smaller in collagen-chitosan treated hearts compared to the PBS group (*n=3* for all groups).

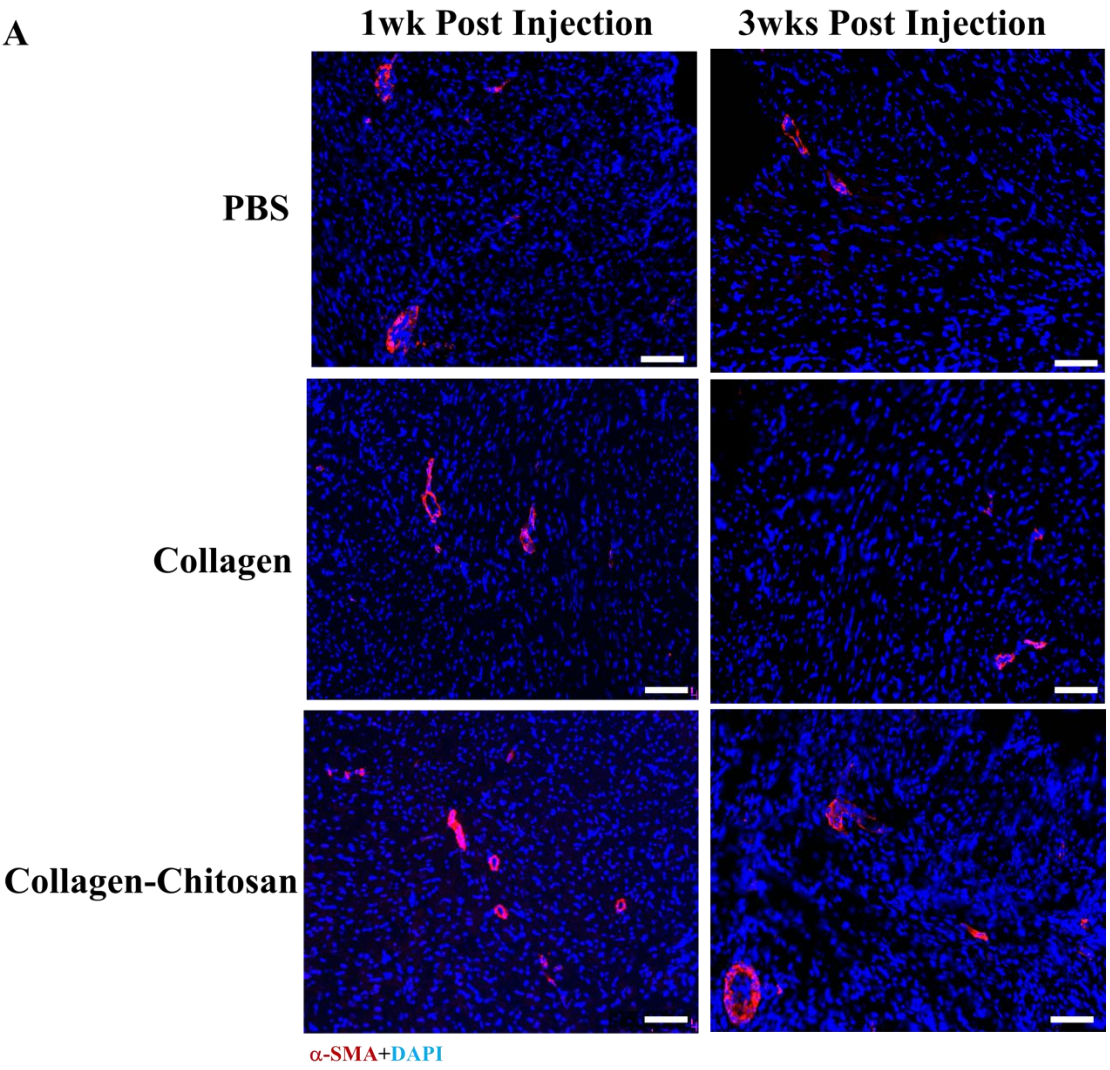
A
1wk Post Injection
3wks Post Injection
PBS
Collagen
Collagen-Chitosan
α-SMA+DAPI

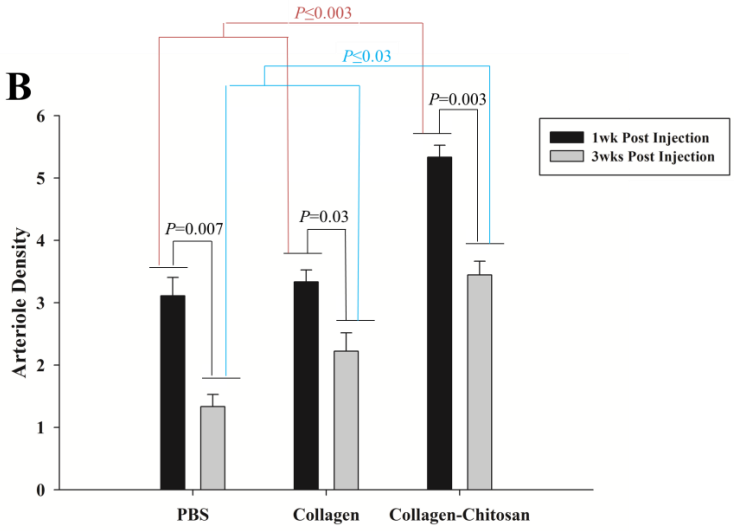
B
P≤0.003
P≤0.03
P=0.003
P=0.007
P=0.03
1wk Post Injection
3wks Post Injection
Arteriole Density
0
1
2
3
4
5
6
PBS
Collagen
Collagen-Chitosan

Figure 4.4 Arteriole density in mouse MI hearts. (A) Representative α-SMA (red) stained MI heart sections (scale bar = 100μm). (B) At 1wk post-injection, the arteriole density was greatest in the collagen-chitosan group compared to all other groups at different time points. Over the 3wk follow-up, the arteriole density was reduced in all groups; at 3 wks post-injection it remained highest in the collagen-chitosan group and lowest in the PBS injected hearts (*n=3* for all groups).

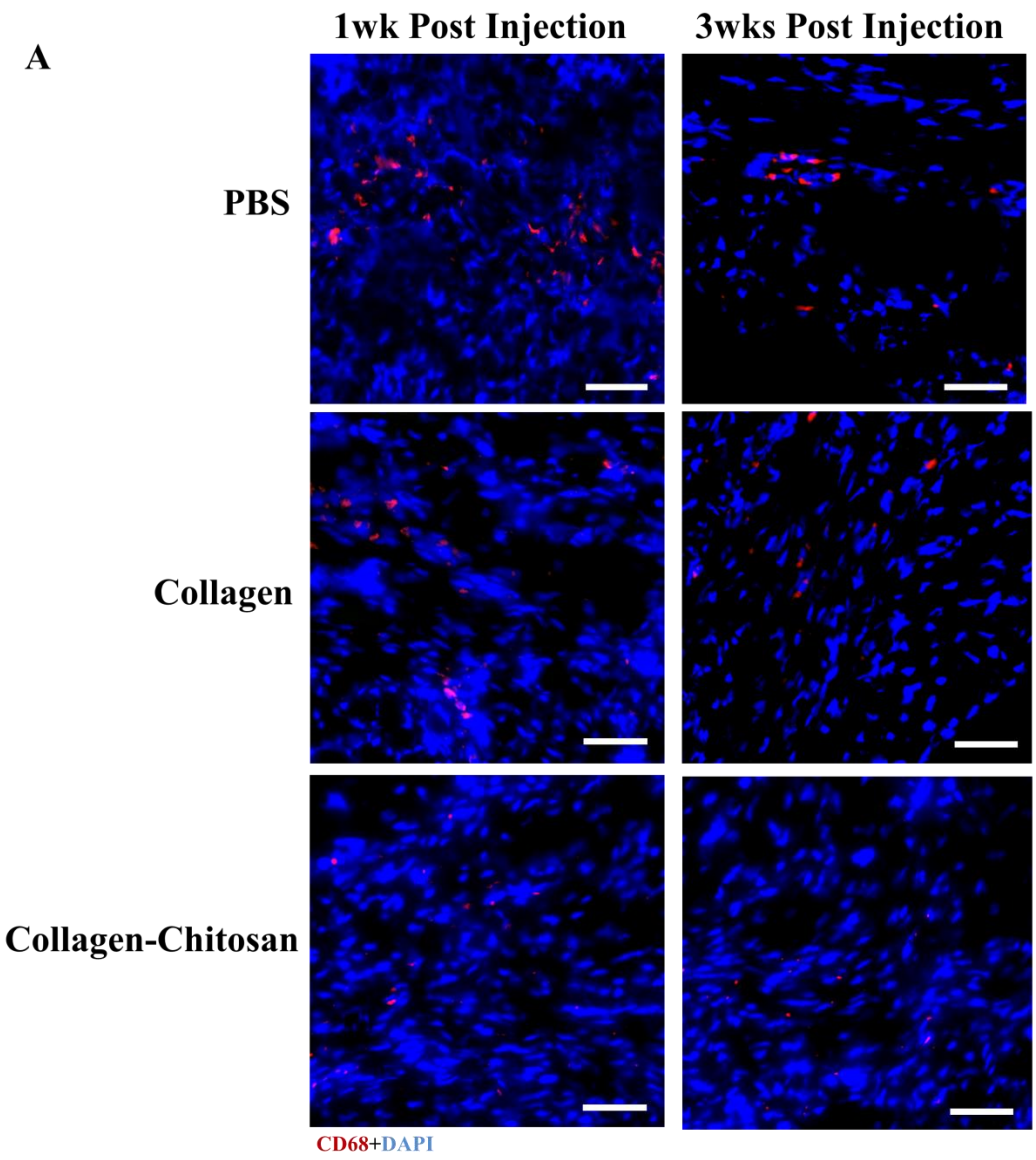
A
1wk Post Injection
3wks Post Injection
PBS
Collagen
Collagen-Chitosan
CD68+DAPI

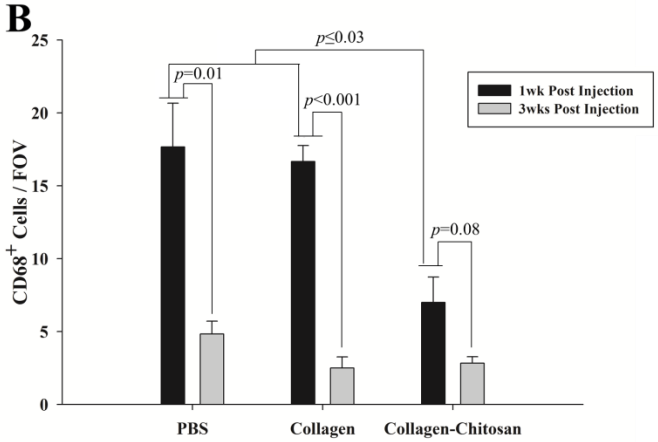
B
p≤0.03
p=0.01
p<0.001
p=0.08
1wk Post Injection
3wks Post Injection
CD68+ Cells / FOV
25
20
15
10
5
0
PBS
Collagen
Collagen-Chitosan

Figure 4.5 $CD68^+$ cells in mouse MI hearts. (A) Representative images of hearts sections stained for $CD68^+$ (scale bar = 50μm). (B) At 1wk post-treatment, $CD68^+$ macrophages were more numerous in the PBS (*$p \leq 0.03$ vs. 1wk collagen-chitosan and 3wk PBS) and collagen treated mouse hearts. After 3 weeks, $CD68^+$ cells were reduced in all groups and there was no significant difference between groups ($n=3$ for all groups).

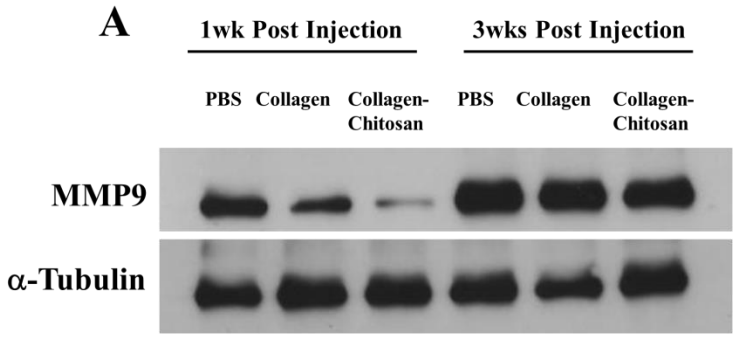
A
1wk Post Injection
3wks Post Injection
PBS
Collagen
Collagen-Chitosan
PBS
Collagen
Collagen-Chitosan
MMP9
α-Tubulin

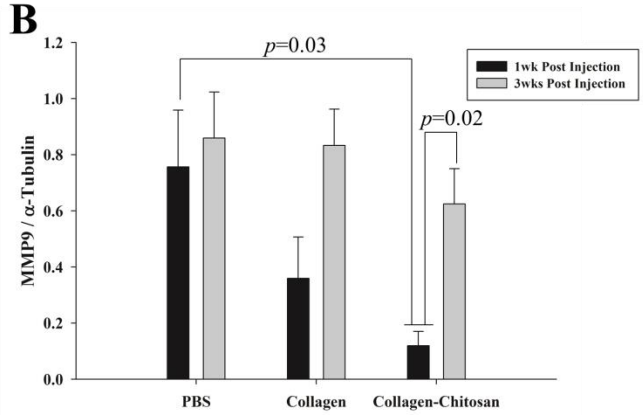
B
p=0.03
p=0.02
1wk Post Injection
3wks Post Injection
MMP9 / α-Tubulin
1.2
1.0
0.8
0.6
0.4
0.2
0.0
PBS
Collagen
Collagen-Chitosan

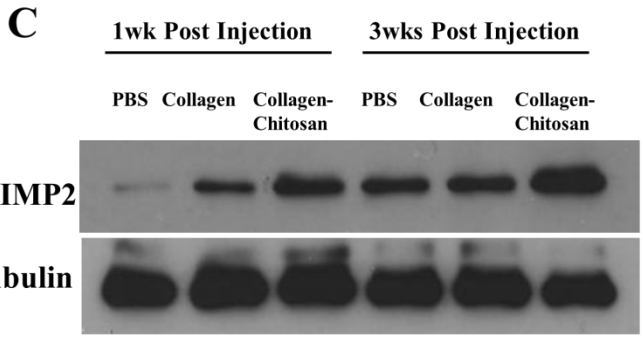
C
1wk Post Injection
3wks Post Injection
PBS
Collagen
Collagen-Chitosan
PBS
Collagen
Collagen-Chitosan
TIMP2
α-Tubulin

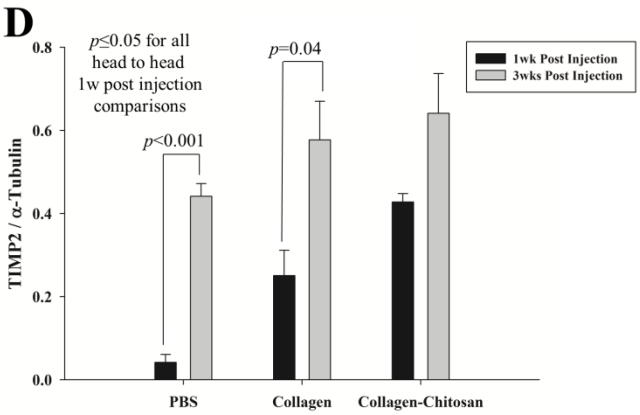
D
p≤0.05 for all head to head 1w post injection comparisons
p<0.001
p=0.04
1wk Post Injection
3wks Post Injection
TIMP2 / α-Tubulin
0.8
0.6
0.4
0.2
0.0
PBS
Collagen
Collagen-Chitosan

Figure 4.6 MMP9 and TIMP2 levels in the treated hearts. (A) At 1wk post-injection, MMP9 expression in the collagen-chitosan group was lower compared to the 1wk PBS mice, and also compared to its expression at 3wks in the collagen-chitosan, and PBS treated mice. (B) At 1wk post-injection, TIMP2 expression was lower in the PBS group compared to all other groups. TIMP2 expression increased from 1 to 3 wks for mice treated with collagen ($n=3$ for all groups).

4.7 Discussion

In this study, a collagen-chitosan matrix was used to treat the established post-MI scar in mice with the aim to positively affect ECM remodeling and improve cardiac function. It was demonstrated *in vitro* that the collagen matrix limits cardiac fibroblast-to-myofibroblast differentiation and the addition of chitosan to the matrix augmented this anti-fibrotic effect. Furthermore, when applied to the mouse heart 2 weeks after MI, the collagen-chitosan matrix improved tissue vascularity, changed the MMP9/TIMP2 expression profile and prevented maladaptive remodeling, resulting in preserved LV mass and improved cardiac function.

Our results indicated that a collagen matrix injection performed at 2 weeks post-MI could lessen, but not attenuate the decline in mouse cardiac function. In comparison, cardiac function improvement was only observed in the collagen-chitosan matrix group. A previous study showed that a collagen hydrogel, as a stand-alone therapy, moderately improved LV function in a rat model if injected 1 week after MI (Dai et al., 2005). Furthermore, we have shown that our matrix applied to the mouse heart 1-week after MI can preserve cardiac function (Ahmadi et al., 2014). The discrepancy in the efficacy of the collagen matrix between these studies and the current one may be attributable to differences in the animal model and more specifically the delivery time-point. These particular collagen matrices may be less therapeutically effective in the setting of an established scar. Our infarct size assessment confirmed that 1 week after treatment, myocardial fibrosis and LV thinning were advanced in all treatment groups and collagen injection is not an efficient therapy to reduce the loss of LV mass and arteriole density. However, the collagen-chitosan matrix therapy impeded the expansion of fibrosis and maintained a higher arteriole density compared to the collagen matrix and PBS control groups.

The addition of chitosan likely improves the outcome of the matrix therapy by more positively regulating the ECM remodeling process. Collagen deposition is strongly associated with myocardial fibrosis, stiffness and cardiac dysfunction (Fan et al., 2012). We have shown that our collagen matrix reduces collagen type 1 production by cardiac fibroblasts *in vitro*. The addition of chitosan to the collagen gel also reduces the differentiation of fibroblasts to myofibroblasts and further reduces collagen type 1 deposition. This is in accordance with a previous study indicating that chitosan decreases collagen type 1 production by keloid fibroblasts (Shi et al., 2006).

In the adult myocardium, the balance between MMPs and TIMPs confers normal ECM homeostasis. Experimental models have revealed that the tissue MMP/TIMP ratio is increased after MI, which contributes to a persistent ECM proteolytic state (Spinale, 2007). Our study showed that the collagen matrix injection decreased MMP9 and increased TIMP2 levels in the infarcted myocardium and that the collagen-chitosan injection further enhanced the MMP9/TIMP2 balance, which suggests decreased ECM degradation. ECM degradation generates pro-inflammatory and chemoattractant fragments that recruit neutrophils and macrophages to the infarcted myocardium (Fan et al., 2012). It has been demonstrated in the post-acute phase of MI that myocardial macrophage infiltration co-localizes with collagen deposition and fibrosis (Nicoletti et al., 1996). Macrophage-secreted TGF-β is one of the main cytokines that may mediate scar formation by stimulating the proliferation and differentiation of cardiac fibroblasts (Yang et al., 2004). This may explain our finding that $CD68^+$ cells (a surface marker for macrophages) were less abundant in the MI heart of the collagen-chitosan matrix group at 1 wk post-injection, which was associated with reduced fibrosis at 3wk compared to the other treatment groups. In the collagen matrix group, however, macrophage infiltration is the

same as the PBS group, which correlated with an equivalent infarct size in collagen matrix and PBS injected hearts.

Our *in vitro* findings indicated that cardiac fibroblasts respond differently to the same concentration of TGF-β depending on their culture substrate. This suggests that the collagen-chitosan matrix may also exert its therapeutic benefit, at least partially, by direct interaction with fibroblasts in the myocardium. Although we have investigated the ECM proteolytic state by measuring the expression of MMP9 and TIMP2, one limitation of this study is that we did not investigate the direct effect of the collagen-chitosan matrix on the cardiac macrophages and their TGF-β secretion. Therefore, it appears that the collagen-chitosan matrix exerts its effects on both macrophages and fibroblasts, yet the interaction between the 2 cell types and how this changes in response to the matrix treatment remains to be elucidated.

In summary, the collagen-chitosan matrix limits adverse remodeling in MI hearts and enhances cardiac function by maintaining arteriole density, improving the ECM proteolytic state and attenuating the macrophage infiltration in the infarcted myocardium. Therefore, the collagen-chitosan matrix may be a promising therapeutic approach for treating established scar in the infarcted heart.

Acknowledgments

The authors wish to thank Branka Vulesevic for her technical help.

Chapter 5:

General Discussion

The studies in this thesis sought to evaluate collagen-based biomaterial strategies for cardiac repair and regeneration. The collagen matrix was used previously to enhance the survival and function of CACs in a rat model of hindlimb ischemia (Suuronen et al., 2006). The positive effect of the collagen matrix on the short-term retention of CACs in this model has been confirmed by use of cell radiolabeling and PET imaging (Zhang et al., 2008b). Furthermore, collagen matrix-cultured CACs have been shown to possess increased angiogenic capacity *ex vivo* and an improved therapeutic potential to restore perfusion in a mouse model of hindlimb ischemia (Kuraitis et al., 2011a). Taken together, these studies suggest that this injectable collagen matrix is suitable as a therapeutic for application in the infarcted myocardium.

In continuation from the previous studies, each section of this thesis provides novel contributions in the evaluation of the collagen matrix for cardiac therapy. In Chapter 2, imaging techniques were applied to evaluate: 1) the efficacy of our minimally invasive delivery method of delivering an injectable collagen matrix to the heart, and 2) the retention and distribution properties of our collagen matrix when delivered to the infarcted mouse myocardium. In chapter 3, the therapeutic benefit and the underlying mechanisms of CAC-collagen matrix treatment in the MI mouse heart were examined. Finally, in chapter 4, the collagen matrix was modified with the addition of chitosan to target fibroblasts and adverse remodeling in the established scar of the infarcted myocardium.

5.1 Minimally Invasive Collagen Matrix Delivery

Previous clinical studies have indicated the feasibility and safety of direct cell delivery using a NOGA mapping injection catheter via femoral or brachial arteries (Banovic et al., 2011, Losordo et al., 2011). Therefore, the development of minimally invasive delivery techniques may address the clinical translation of injectable biomaterials as a treatment for infarcted hearts. However, in applying non-invasive strategies for the delivery of injectable hydrogels, there are still some considerations to be made. For example, if the gel product is injected through a transendocardial or intracoronary catheter, the matrix will flow a relatively long distance through the catheter to the heart, which may lead to matrix solidification in the catheter (Radisic and Christman, 2013). In contrast, if the gelling time is designed to offer a longer sol-phase time frame, the risk of gel leakage to the chamber would be increased. The direct injection of the hydrogel (e.g. during bypass surgery) is an alternative technique, but is limited to the patients who are undergoing open chest surgery, thus restricting the delivery time point to a narrow window. Furthermore, the depth of open chest injection to the myocardium may not be consistent in all patients since the myocardial thickness is altered in post-MI remodeling hearts, which may not be visible to the naked eye (Jessup and Brozena, 2003).

Direct ultrasound-guided injection of microspheres to the normal mouse myocardium using a 30 gauge needle was shown previously (Springer et al., 2005). Herein, we applied this technique with a modified setup for the injection of our collagen biomaterials: (1) we performed the injections to mouse hearts at 7 days post-MI; (2) the viscosity of the collagen matrix required the application of a 27 gauge needle, which is comparable with mouse LV wall thickness; (3) treatment was delivered by 5 injections (10 μL each) which was performed in a rostrocaudal

order into the LV wall; and (4) the injections were made halfway between the endocardium and epicardium to minimize the risk of leakage.

To our knowledge, this is the first study that showed the feasibility of ultrasound-guided injections for myocardial biomaterial delivery. Moreover, despite applying various injectable hydrogels for cardiac regeneration (Rane and Christman, 2011), it is the first time that the leakage/retention ratio of an injectable hydrogel has been reported. The two modalities (PET radiotracer and Qdot labeling) that were used in this study, show the potential to be applied for detecting the leakage/retention ratio of other injectable hydrogels.

In summary, the study presented in Chapter 2 of this thesis indicated that our collagen matrix has optimum gelling properties for delivery and application in the MI heart. The gel is injected directly from a syringe (without the need of catheterization) and it solidifies completely within a short period of time (10-20 min) to minimize leakage out of constantly beating myocardium, while allowing for uniform distribution throughout the target tissue. Considering these results, we sought to apply the collagen matrix as an enhancement strategy for CAC therapy.

5.2 Collagen Matrix as Enhancement Strategy for CAC Therapy

As expected, the study presented in Chapter 3 demonstrated that the engraftment of CACs 3wks after delivery to the MI heart was improved by delivery within the collagen matrix. Notably, the collagen matrix not only acts as a vehicle for delivery of the cells, but also interacts with them leading to enhanced angiogenic function by activating integrin-ILK signaling pathways. ILK signaling has previously been shown to be involved in the angiogenic capacity of CACs in ischemic tissues (Lee et al., 2006, Werner et al., 2008). Therefore, the therapeutic effects of CACs+matrix, to some extent, can be ascribed to improved survival/angiogenic potential of

transplanted cells. This is further supported by the observation that cardiac perfusion improved ($^{13}NH_3$ PET scans) and transplanted CACs were seen to express endothelial markers and incorporate into the vasculature (immunohistochemistry).

It has recently been shown that myocardial ECM composition undergoes radical changes that are initiated soon after MI that is characterized by a decrease in collagen type 1, increased fibronectin content and a reduction in SDF-1 secretion from progenitor cells (Sullivan et al., 2014). As collagen type 1 is the most abundant protein molecule in the normal ECM, the quantitative and qualitative alterations in this ECM component would affect the integrin signaling cascade in different cardiac cells including progenitor cells. Moreover, it has been shown that ILK activates SDF-1 up-regulation in hypoxic CACs (Lee et al., 2006). In the current study, we have shown that CACs secrete more SDF-1 upon adhesion to the collagen matrix compared to fibronectin *in vitro.* We have also shown that the fibrotic area is significantly smaller in the CACs+matrix treated MI mouse heart, which indicates a preserved ECM structure. This suggests that CACs+matrix therapy potentially enhances the recruitment of progenitor cells by paracrine signals and also maintaining normal ECM components.

We also related cardiac function improvement with ILK signaling activity in transplanted CACs: ILK was down-regulated in CACs by blocking Itgα2, which resulted in the loss of engraftment and therapeutic benefits. Moreover, we identified Itgα5 as a downstream component of the ILK pathway which is up-regulated in matrix-cultured CACs in an Itgα2-dependent manner. In summary, Chapter 3 provides evidence that our collagen-based matrix can promote cardiac repair/regeneration through integrin-mediated support of CAC engraftment and function.

5.3 Optimum Timing of Intervention after MI

The optimum time frame for intervention in the dynamic process of MI is controversial. Within the first few hours after the onset of infarction, the release of pro-inflammatory cytokines and infiltration of inflammatory cells generate an unfavorable condition for transplanted cells. By the end of the first week after MI, a granulation tissue is formed and the inflammation subsides, which provides the opportunity for survival and engraftment of transplanted cells (Kuraitis et al., 2010). In accordance with this, the results presented in this thesis (Chapter 3) demonstrate the therapeutic benefits of cell therapy with or without matrix delivery at 1wk post-MI. The ECM-fibroblast interaction appears to modulate the fibrotic process that develops 1-2wks after MI in the mouse; the optimum timing for matrix-only injection may depend on the dynamics of fibroblast activation, as well as the type of biomaterial applied, as shown in Chapters 3 and 4. The use of the collagen matrix alone to treat MI conferred a modest therapeutic benefit when applied 1wk after MI (Chapter 3); the matrix-only group showed a preservation of LVEF and FS over the 3wks follow-up period, whereas these parameters decreased over time in PBS-treated mice. In contrast, the collagen-only matrix did not protect the heart when administered to hearts 2wks after MI (Chapter 4). In order to improve the therapeutic potential of the matrix for cardiac repair at a later stage of infarct evolution, we added chitosan to the collagen matrix (Chapter 4). The optimum intervention time for MI treatment is defined not only by the myocardial inflammatory, metabolic and fibrotic state, but also by the type of intervention being applied and the cells that the treatment targets. The collagen matrix has been shown to interact with progenitor cells and improve their engraftment, secretory profile and regenerative properties (Kuraitis et al., 2011a, Zhang et al., 2008b, Ahmadi et al., 2014). This corroborates with our finding that collagen injection is more beneficial at 1wk post-MI which overlaps with the

optimum time frame for cell therapy. In contrast, collagen-chitosan matrix may mainly exert its therapeutic effect by interacting with fibroblasts, and modulating their function and scar formation. Therefore, it is expected that collagen-chitosan delivery would be beneficial at a more chronic stage of MI. In this regard, more work is being performed in our lab to test the therapeutic effects of matrix injection before 1wk or after 2wks post-MI.

5.4 Collagen-Based Hydrogels as Cell Therapy Enhancement Strategy or Stand-alone Approach

Cell therapy may be associated with immunogenicity (allograft transplantation from healthy donors) or reduced functionality due to co-morbidities such as coronary artery disease or diabetes (autograft transplantation from the same patient) (Sorrentino et al., 2007, Dimmeler and Leri, 2008). The use of biomaterials alone as a therapy can avoid these potential complications associated with cell therapy. For example, bioengineered collagen-based matrices are biocompatible (Johnson and Christman, 2013) and can be prepared off-the-shelf when needed. However, CACs can produce and generate a wide spectrum of chemokine and growth factors that contribute to myocardial regeneration (Urbich et al., 2005). To address this, injectable matrices may be used to deliver chemoattractants or growth factors, but this approach may be limited in the number of molecules that can be delivered (Chiu et al., 2012, Fujita et al., 2007, Kuraitis et al., 2011b). Furthermore, transplanted cells have the advantage of interacting with host cells and incorporating into the regenerating structures (chapter 3); however, cell therapy is limited by low transplanted cell engraftment and survival (Wollert and Drexler, 2010b). Collagen hydrogels have been shown to stimulate endogenous repair mechanisms, which can mediate maladaptive cardiac remodeling (Chapter 4). In this context, we have compared cell therapy-only, matrix-only and combined cells and matrix therapy. The collagen matrix acts as a scaffold

for transplanted cells and it interacts with the cells and improves their functionality in the myocardial ischemic environment. Therefore, combining cell therapy with collagen-based hydrogels is associated with synergistic therapeutic benefits and yields the best treatment results (Suuronen et al., 2006, Ahmadi et al., 2014). However, the matrix-only approach is also a promising therapy for MI because we have shown that it is as effective as cell therapy in terms of preserving cardiac function (Chapter 3). Moreover, it moderately improves cardiac function and attenuates maladaptive cardiac remodeling if chitosan is added to matrix components at the optimum concentration (Chapter 4).

Growing evidence indicates the therapeutic benefits of collagen-chitosan matrices with cells or growth factors for myocardial regeneration (Chiu et al., 2012, Liu et al., 2012, Reis et al., 2012, Wang and Stegemann, 2010); although to our knowledge, ours is the first study that focused on the application of a collagen-chitosan matrix as a stand-alone therapy for cardiac remodeling. Our major findings were that collagen-chitosan matrix-cultured cardiac fibroblasts showed less aptitude to develop a myofibroblast phenotype *in vitro*, and collagen-chitosan matrix therapy moderately increased cardiac function and improved the ECM degradation state *in vivo*. Fibroblasts/myofibroblasts constitute a putative part of biomaterial-host tissue interaction (Huang et al., 2005, Sullivan and Black, 2013, Venugopal et al., 2012) and the current study suggests that this interaction can be targeted to improve cardiac remodeling. The combined findings from Chapters 3 and 4 demonstrate that biomaterial properties and bioactivity may need to be tailored for optimal function in the infarct environment to which they are applied. In summary, collagen-based matrices hold promise both as enhancement strategy for cell therapy and as stand-alone treatment for infarcted myocardium.

5.5 Future Directions

The ability to track biomaterials with imaging will be a highly useful tool in the development and clinical translation of biomaterial therapy. The PET and in vivo fluorescence imaging methods applied in Chapter 2 of this thesis were able to provide important information on the injectability, retention and distribution properties of the collagen matrix; however, both techniques may be limited to tracking the matrix only early after its delivery. Considering the short half-life of ^{18}F-HFB (half-life=2h), the visualization of the labelled collagen matrix with PET imaging is limited to ~3hrs post-injection. In contrast, Qdot fluorescence can be detected for a longer period of time (days to weeks); however, as the injected matrix degrades, Qdots may be released and scavenged by the host cells (e.g. immune cells), and therefore they may not represent the exact distribution of the collagen matrix over time. Thus, methods to monitor the long-term distribution of the biomaterials within the heart are still needed.

Although the long-term fate of the collagen matrix within the infarcted myocardium is still unknown, the current study indicated that the matrix retains and redistributes in the myocardium in the short-term, which supports the efficient delivery of the cells to the target areas. Multiple mechanisms can be hypothesized for the benefit of CACs+matrix therapy. Herein, we described integrin-ILK signal transduction as an important modulator of the synergistic effects of CACs and collagen matrix, but other mechanisms are also likely involved. The augmented FDG uptake in the myocardium with CACs+matrix treatment is indicative of increased viable myocardium. This may have resulted: 1) from the rescue of hibernating myocardium, consisting of viable cardiomyocytes with low metabolic activity; or 2) from cardiomyogenesis of resident cardiac stem cells (Beltrami et al., 2003). The first hypothesis is supported by results in a porcine hibernating myocardium model, whereby CACs+matrix therapy increased myocardial blood

flow and reduced the extent of hibernating myocardium (Giordano et al., 2013b). To address the second possibility, a preliminary experiment has been performed which showed that the ratio of c-kit$^+$ cells in the infarct region to total ckit$^+$ cells in the myocardium is increased in the CACs+matrix injected hearts (Figure 5.1). A limitation is that the origin of the c-kit$^+$ cells was not determined; however, the lack of a difference in c-kit$^+$ numbers acutely (1wk) (data not shown), and their increased frequency in all groups between 1wk and 3wks, suggests they were of an endogenous source. Although exact mechanisms need to be further elucidated, our results show that CACs+matrix therapy has the potential to rescue and/or regenerate cardiomyocytes and this constitutes a possible direction for future investigations.

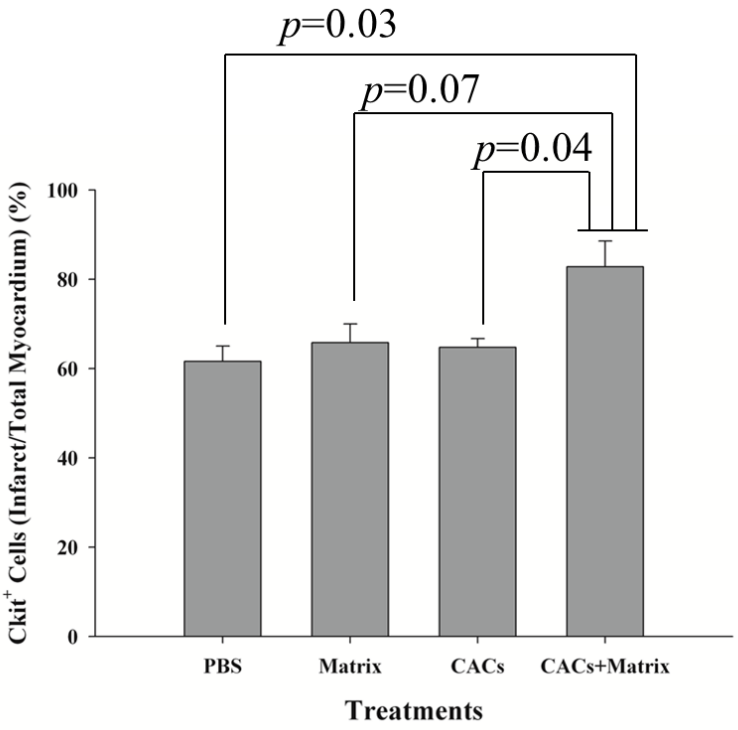

Figure 5.1 Ratio of C-kit$^+$ cells in the infarcted myocardium to the entire ventricles. C-kit$^+$ cells were increased in the infarcted and per-infarcted areas of CACs+matrix injected hearts (82.8±5.8%) compared to CACs-only (64.7±1.9%), matrix-only (65.8±4.1%) and PBS (61.5± 3.4%) (*n=3* per group).

The chemokine-mediated therapeutic benefits of CACs, which are seeded to a biomaterial scaffold and delivered to a rat MI model, have been reported (Frederick et al., 2010). In fact, the paracrine mechanism is believed to be the primary mechanism through which most cell therapies exert their effects (Mirotsou et al., 2011).One plausible axis for expanding the current project is to investigate the role of cytokine signaling, and in particular its role in endogenous progenitor cell recruitment in CACs+matrix hearts. This can be performed by injecting immunocompromised mice with human CACs delivered with or without the collagen matrix. The cell mobilization from the bone marrow into the circulation can be compared between the groups by blood procurement at different time points and characterizing the chemoattractant agents and progenitor cells in the circulation. The levels of cytokines (human vs. mouse) in the infarcted heart can also be assessed over time and compared between the treatment groups, as has been reported by Cho et al (Cho et al., 2007). The paracrine effects of CACs have been highlighted in previous studies which indicated the antioxidative (Yang et al., 2010), angiogenic (Urbich et al., 2005), cardiotrophic (Doyle et al., 2008) and chemoattractant effects of CAC-conditioned media. In the current study, we performed a cytokine array analysis on the serum of mice 3wks after CACs+matrix, CACs-only, matrix-only or PBS injection, as described in Chapter 3. The serum level of VEGF and G-CSF (important progenitor mobilizing agents) were significantly higher in the circulation of CACs+matrix injected mice compared to the PBS group. In the CAC-only injected mice, VEGF was significantly increased and a trend for increased G-CSF was observed compared to the PBS control (Figure 5.2). These results suggest the recruitment of endogenous progenitor cells as a potential mechanism for the therapeutic effects conferred from CACs±matrix.

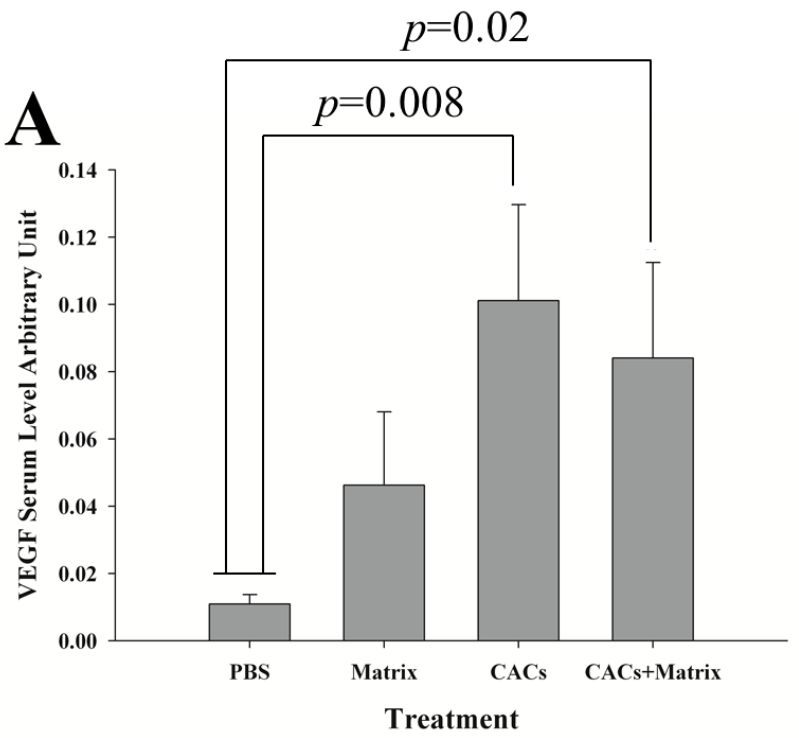
A
p=0.02
p=0.008
VEGF Serum Level Arbitrary Unit
0.14
0.12
0.10
0.08
0.06
0.04
0.02
0.00
PBS
Matrix
CACs
CACs+Matrix
Treatment

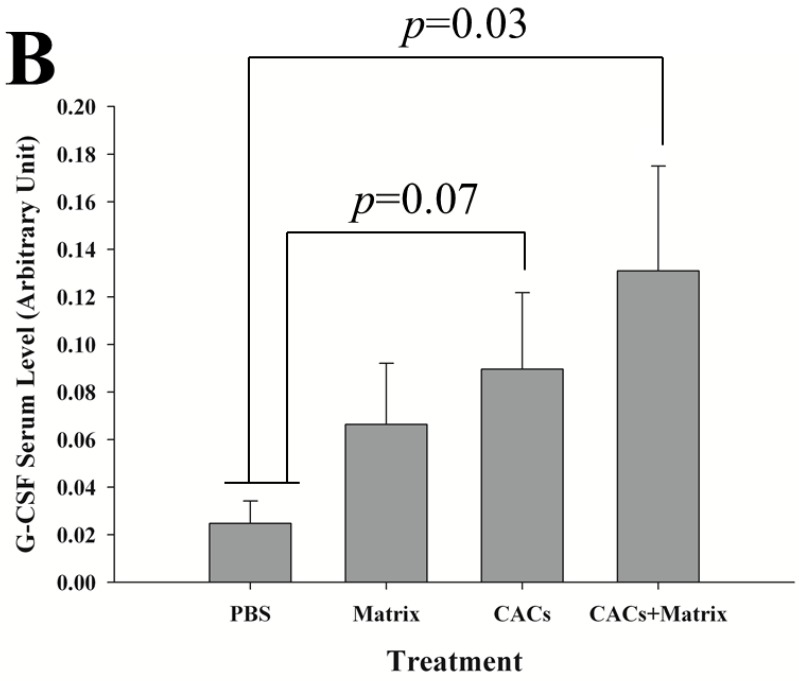
B
p=0.03
p=0.07
G-CSF Serum Level (Arbitrary Unit)
0.20
0.18
0.16
0.14
0.12
0.10
0.08
0.06
0.04
0.02
0.00
PBS
Matrix
CACs
CACs+Matrix
Treatment

Figure 5.2 Circulating serum levels of VEGF and G-CSF in MI mice 3wks after treatment delivery. (A) VEGF was significantly increased in the CACs+matrix and CACs injected mice (8.6±4.1 and 12.4±5.0 fold-change, respectively, compared to PBS). The matrix group had a trend for increased VEGF (by 6.6±4.9-fold) compared to PBS). (B) G-CSF was significantly increased in CACs+matrix injected mice (9.3±2.0 fold-change compared to PBS). In CACs-only and matrix-only groups, a trend for increased G-CSF was observed (5.3±1.0 and 2.1±0.4 fold-change, respectively, compared to control) (*n=7* per group).

In the current study, we showed the importance of Itα2-ILK pathway to the survival and function of CACs *in vitro* and *in vivo*. However, Itg signaling is complex with possible redundant pathways and perhaps cell-matrix interaction may be regulated by this pathway even if ILK is knocked down (Li et al., 2005). One way to address this argument is to use CACs from ILK null mice; however, ILK deletion in the mouse leads to death at the pre-implantation stage (Sakai et al., 2003). Therefore, ILK knockdown in CACs requires an alternative strategy, such as shRNA technology or Cre $ILK^{flox/flox}$ mouse breeding. This type of transgenic mouse does not exist commercially, but theoretically it could be generated by cross breeding UBC – Cre / ERT2 mice (Jackson 008085) to $ILK^{flox/flox}$ mice (Terpstra et al., 2003). The BM cells of these transgenic mice can be used for the generation of CACs, which are then treated with 4-hydroxytamoxifen for ILK deletion (Szabo et al., 2009).

In conclusion we have validated a minimally invasive delivery method which demonstrated the safety and efficient retention/distribution of our collagen matrix when applied to the beating infarcted myocardium. Furthermore, our matrices (collagen and collagen-chitosan hydrogels) have shown several key characteristics of an ideal injectable biomaterial as they positively affected the reparative activity of cells, and improved cardiac function post-MI. While the results are promising, a better understanding of the mechanisms of action of cell+matrix and matrix-alone therapies will help in their optimization and their translation to the clinic.

References

AHMADI, A., MCNEILL, B., VULESEVIC, B., KORDOS, M., MESANA, L., THORN, S., RENAUD, J. M., MANTHORP, E., KURAITIS, D., TOEG, H., MESANA, T. G., DAVIS, D. R., BEANLANDS, R. S., DASILVA, J. N., DEKEMP, R. A., RUEL, M. & SUURONEN, E. J. 2014. The role of integrin alpha2 in cell and matrix therapy that improves perfusion, viability and function of infarcted myocardium. *Biomaterials.*, 35**,** 4749-58. doi: 10.1016/j.biomaterials.2014.02.028. Epub 2014 Mar 14.

AICHER, A., BRENNER, W., ZUHAYRA, M., BADORFF, C., MASSOUDI, S., ASSMUS, B., ECKEY, T., HENZE, E., ZEIHER, A. M. & DIMMELER, S. 2003. Assessment of the tissue distribution of transplanted human endothelial progenitor cells by radioactive labeling. *Circulation,* 107**,** 2134-9.

ALLEN, P., MELERO-MARTIN, J. & BISCHOFF, J. 2011. Type I collagen, fibrin and PuraMatrix matrices provide permissive environments for human endothelial and mesenchymal progenitor cells to form neovascular networks. *J Tissue Eng Regen Med,* 5**,** e74-86.

ALLUKIAN, M., 3RD, XU, J., MORRIS, M., CASKEY, R., DORSETT-MARTIN, W., PLAPPERT, T., GRISWOLD, M., GORMAN, J. H., 3RD, GORMAN, R. C. & LIECHTY, K. W. 2013. Mammalian cardiac regeneration after fetal myocardial infarction requires cardiac progenitor cell recruitment. *Ann Thorac Surg,* 96**,** 163-70.

AMADO, L. C., SALIARIS, A. P., SCHULERI, K. H., ST JOHN, M., XIE, J. S., CATTANEO, S., DURAND, D. J., FITTON, T., KUANG, J. Q., STEWART, G., LEHRKE, S.,

BAUMGARTNER, W. W., MARTIN, B. J., HELDMAN, A. W. & HARE, J. M. 2005. Cardiac repair with intramyocardial injection of allogeneic mesenchymal stem cells after myocardial infarction. *Proc Natl Acad Sci U S A,* 102**,** 11474-9.

ARTZI, N., OLIVA, N., PURON, C., SHITREET, S., ARTZI, S., BON RAMOS, A., GROOTHUIS, A., SAHAGIAN, G. & EDELMAN, E. R. 2011. In vivo and in vitro tracking of erosion in biodegradable materials using non-invasive fluorescence imaging. *Nat Mater,* 10**,** 704-9.

ASAHARA, T., MUROHARA, T., SULLIVAN, A., SILVER, M., VAN DER ZEE, R., LI, T., WITZENBICHLER, B., SCHATTEMAN, G. & ISNER, J. M. 1997. Isolation of putative progenitor endothelial cells for angiogenesis. *Science,* 275**,** 964-7.

ASSMUS, B., FISCHER-RASOKAT, U., HONOLD, J., SEEGER, F. H., FICHTLSCHERER, S., TONN, T., SEIFRIED, E., SCHACHINGER, V., DIMMELER, S., ZEIHER, A. M. & REGISTRY, T.-C. 2007. Transcoronary transplantation of functionally competent BMCs is associated with a decrease in natriuretic peptide serum levels and improved survival of patients with chronic postinfarction heart failure: results of the TOPCARE-CHD Registry. *Circ Res,* 100**,** 1234-41.

ASSMUS, B., HONOLD, J., SCHACHINGER, V., BRITTEN, M. B., FISCHER-RASOKAT, U., LEHMANN, R., TEUPE, C., PISTORIUS, K., MARTIN, H., ABOLMAALI, N. D., TONN, T., DIMMELER, S. & ZEIHER, A. M. 2006. Transcoronary transplantation of progenitor cells after myocardial infarction. *N Engl J Med,* 355**,** 1222-32.

ASSMUS, B., ROLF, A., ERBS, S., ELSASSER, A., HABERBOSCH, W., HAMBRECHT, R., TILLMANNS, H., YU, J., CORTI, R., MATHEY, D. G., HAMM, C. W., SUSELBECK, T., TONN, T., DIMMELER, S., DILL, T., ZEIHER, A. M., SCHACHINGER, V. & INVESTIGATORS, R.-A. 2010. Clinical outcome 2 years after intracoronary administration of bone marrow-derived progenitor cells in acute myocardial infarction. *Circ Heart Fail,* 3**,** 89-96.

BADYLAK, S. F., FREYTES, D. O. & GILBERT, T. W. 2009. Extracellular matrix as a biological scaffold material: Structure and function. *Acta Biomater,* 5**,** 1-13.

BALSAM, L. B. & ROBBINS, R. C. 2005. Haematopoietic stem cells and repair of the ischaemic heart. *Clin Sci (Lond),* 109**,** 483-92.

BANOVIC, M., OSTOJIC, M. C., BARTUNEK, J., NEDELJKOVIC, M., BELESLIN, B. & TERZIC, A. 2011. Brachial approach to NOGA-guided procedures: electromechanical mapping and transendocardial stem-cell injections. *Tex Heart Inst J,* 38**,** 179-82.

BARCZYK, M., CARRACEDO, S. & GULLBERG, D. 2010. Integrins. *Cell Tissue Res,* 339**,** 269-80.

BARDY, G. H., LEE, K. L., MARK, D. B., POOLE, J. E., PACKER, D. L., BOINEAU, R., DOMANSKI, M., TROUTMAN, C., ANDERSON, J., JOHNSON, G., MCNULTY, S. E., CLAPP-CHANNING, N., DAVIDSON-RAY, L. D., FRAULO, E. S., FISHBEIN, D. P., LUCERI, R. M., IP, J. H. & SUDDEN CARDIAC DEATH IN HEART FAILURE TRIAL, I. 2005. Amiodarone or an implantable cardioverter-defibrillator for congestive heart failure. *N Engl J Med,* 352**,** 225-37.

BARTUNEK, J., VANDERHEYDEN, M., VANDEKERCKHOVE, B., MANSOUR, S., DE BRUYNE, B., DE BONDT, P., VAN HAUTE, I., LOOTENS, N., HEYNDRICKX, G. & WIJNS, W. 2005. Intracoronary injection of CD133-positive enriched bone marrow progenitor cells promotes cardiac recovery after recent myocardial infarction: feasibility and safety. *Circulation,* 112**,** I178-83.

BEARZI, C., ROTA, M., HOSODA, T., TILLMANNS, J., NASCIMBENE, A., DE ANGELIS, A., YASUZAWA-AMANO, S., TROFIMOVA, I., SIGGINS, R. W., LECAPITAINE, N., CASCAPERA, S., BELTRAMI, A. P., D'ALESSANDRO, D. A., ZIAS, E., QUAINI, F., URBANEK, K., MICHLER, R. E., BOLLI, R., KAJSTURA, J., LERI, A. & ANVERSA, P. 2007. Human cardiac stem cells. *Proc Natl Acad Sci U S A,* 104**,** 14068-73.

BELLIK, L., MUSILLI, C., VINCI, M. C., LEDDA, F. & PARENTI, A. 2008. Human mature endothelial cells modulate peripheral blood mononuclear cell differentiation toward an endothelial phenotype. *Exp Cell Res,* 314**,** 2965-74.

BELTRAMI, A. P., BARLUCCHI, L., TORELLA, D., BAKER, M., LIMANA, F., CHIMENTI, S., KASAHARA, H., ROTA, M., MUSSO, E., URBANEK, K., LERI, A., KAJSTURA, J., NADAL-GINARD, B. & ANVERSA, P. 2003. Adult cardiac stem cells are multipotent and support myocardial regeneration. *Cell,* 114**,** 763-76.

BELTRAMI, C. A., DI LORETO, C., FINATO, N., ROCCO, M., ARTICO, D., CIGOLA, E., GAMBERT, S. R., OLIVETTI, G., KAJSTURA, J. & ANVERSA, P. 1997. Proliferating cell nuclear antigen (PCNA), DNA synthesis and mitosis in myocytes following cardiac transplantation in man. *J Mol Cell Cardiol,* 29**,** 2789-802.

BERGMANN, O., BHARDWAJ, R. D., BERNARD, S., ZDUNEK, S., BARNABE-HEIDER, F., WALSH, S., ZUPICICH, J., ALKASS, K., BUCHHOLZ, B. A., DRUID, H., JOVINGE, S. & FRISEN, J. 2009. Evidence for cardiomyocyte renewal in humans. *Science,* 324**,** 98-102.

BLEIZIFFER, O., HAMMON, M., NASCHBERGER, E., LIPNIK, K., ARKUDAS, A., RATH, S., PRYYMACHUK, G., BEIER, J. P., STURZL, M., HORCH, R. E. & KNESER, U. 2011. Endothelial progenitor cells are integrated in newly formed capillaries and alter adjacent fibrovascular tissue after subcutaneous implantation in a fibrin matrix. *J Cell Mol Med,* 15**,** 2452-61.

BOHULA, E., LEE, T.R. 2012. Introduction to Cardiac Disease. *In:* ENGEL, F. B. (ed.) *Heart Regeneration: Stem Cell and Beyond.* Singapore: World Scientific Publishing Co.

BUJAK, M. & FRANGOGIANNIS, N. G. 2007. The role of TGF-beta signaling in myocardial infarction and cardiac remodeling. *Cardiovasc Res,* 74**,** 184-95.

BURT, R. K., TESTORI, A., OYAMA, Y., RODRIGUEZ, H. E., YAUNG, K., VILLA, M., BUCHA, J. M., MILANETTI, F., SHEEHAN, J., RAJAMANNAN, N. & PEARCE, W. H. 2010. Autologous peripheral blood CD133+ cell implantation for limb salvage in patients with critical limb ischemia. *Bone Marrow Transplant,* 45**,** 111-6.

CAIADO, F., CARVALHO, T., SILVA, F., CASTRO, C., CLODE, N., DYE, J. F. & DIAS, S. 2011. The role of fibrin E on the modulation of endothelial progenitors adhesion, differentiation and angiogenic growth factor production and the promotion of wound healing. *Biomaterials,* 32**,** 7096-105.

CAIADO, F. & DIAS, S. 2012. Endothelial progenitor cells and integrins: adhesive needs. *Fibrogenesis Tissue Repair,* 5**,** 4.

CARLSON, S., TRIAL, J., SOELLER, C. & ENTMAN, M. L. 2011. Cardiac mesenchymal stem cells contribute to scar formation after myocardial infarction. *Cardiovasc Res,* 91**,** 99-107.

CARMONA, G., CHAVAKIS, E., KOEHL, U., ZEIHER, A. M. & DIMMELER, S. 2008. Activation of Epac stimulates integrin-dependent homing of progenitor cells. *Blood,* 111**,** 2640-6.

CASE, J., MEAD, L. E., BESSLER, W. K., PRATER, D., WHITE, H. A., SAADATZADEH, M. R., BHAVSAR, J. R., YODER, M. C., HANELINE, L. S. & INGRAM, D. A. 2007. Human CD34+AC133+VEGFR-2+ cells are not endothelial progenitor cells but distinct, primitive hematopoietic progenitors. *Exp Hematol,* 35**,** 1109-18.

CHACHQUES, J. C., TRAININI, J. C., LAGO, N., CORTES-MORICHETTI, M., SCHUSSLER, O. & CARPENTIER, A. 2008. Myocardial Assistance by Grafting a New Bioartificial Upgraded Myocardium (MAGNUM trial): clinical feasibility study. *Ann Thorac Surg,* 85**,** 901-8.

CHACHQUES, J. C., TRAININI, J. C., LAGO, N., MASOLI, O. H., BARISANI, J. L., CORTES-MORICHETTI, M., SCHUSSLER, O. & CARPENTIER, A. 2007. Myocardial assistance by grafting a new bioartificial upgraded myocardium (MAGNUM clinical trial): one year follow-up. *Cell Transplant,* 16**,** 927-34.

CHAN, W., DUFFY, S. J., WHITE, D. A., GAO, X. M., DU, X. J., ELLIMS, A. H., DART, A. M. & TAYLOR, A. J. 2012. Acute left ventricular remodeling following myocardial infarction: coupling of regional healing with remote extracellular matrix expansion. *JACC Cardiovasc Imaging,* 5**,** 884-93.

CHAO, H. & HIRSCHI, K. K. 2010. Hemato-vascular origins of endothelial progenitor cells? *Microvasc Res,* 79**,** 169-73.

CHAVAKIS, E., AICHER, A., HEESCHEN, C., SASAKI, K., KAISER, R., EL MAKHFI, N., URBICH, C., PETERS, T., SCHARFFETTER-KOCHANEK, K., ZEIHER, A. M., CHAVAKIS, T. & DIMMELER, S. 2005. Role of beta2-integrins for homing and neovascularization capacity of endothelial progenitor cells. *J Exp Med,* 201**,** 63-72.

CHEKANOV, V., AKHTAR, M., TCHEKANOV, G., DANGAS, G., SHEHZAD, M. Z., TIO, F., ADAMIAN, M., COLOMBO, A., ROUBIN, G., LEON, M. B., MOSES, J. W. & KIPSHIDZE, N. N. 2003. Transplantation of autologous endothelial cells induces angiogenesis. *Pacing Clin Electrophysiol,* 26**,** 496-9.

CHEN, W. & FRANGOGIANNIS, N. G. 2013. Fibroblasts in post-infarction inflammation and cardiac repair. *Biochim Biophys Acta,* 1833**,** 945-53.

CHENG, W., LI, B., KAJSTURA, J., LI, P., WOLIN, M. S., SONNENBLICK, E. H., HINTZE, T. H., OLIVETTI, G. & ANVERSA, P. 1995. Stretch-induced programmed myocyte cell death. *J Clin Invest,* 96**,** 2247-59.

CHIARUGI, P. & GIANNONI, E. 2008. Anoikis: a necessary death program for anchorage-dependent cells. *Biochem Pharmacol,* 76**,** 1352-64.

CHIU, L. L., REIS, L. A., MOMEN, A. & RADISIC, M. 2012. Controlled release of thymosin beta4 from injected collagen-chitosan hydrogels promotes angiogenesis and prevents tissue loss after myocardial infarction. *Regen Med,* 7**,** 523-33.

CHO, H. J., KIM, H. S., LEE, M. M., KIM, D. H., YANG, H. J., HUR, J., HWANG, K. K., OH, S., CHOI, Y. J., CHAE, I. H., OH, B. H., CHOI, Y. S., WALSH, K. & PARK, Y. B. 2003. Mobilized endothelial progenitor cells by granulocyte-macrophage colony-stimulating factor accelerate reendothelialization and reduce vascular inflammation after intravascular radiation. *Circulation,* 108**,** 2918-25.

CHO, H. J., LEE, N., LEE, J. Y., CHOI, Y. J., II, M., WECKER, A., JEONG, J. O., CURRY, C., QIN, G. & YOON, Y. S. 2007. Role of host tissues for sustained humoral effects after endothelial progenitor cell transplantation into the ischemic heart. *J Exp Med,* 204**,** 3257-69.

CHO, H. J., YOUN, S. W., CHEON, S. I., KIM, T. Y., HUR, J., ZHANG, S. Y., LEE, S. P., PARK, K. W., LEE, M. M., CHOI, Y. S., PARK, Y. B. & KIM, H. S. 2005. Regulation of endothelial cell and endothelial progenitor cell survival and vasculogenesis by integrin-linked kinase. *Arterioscler Thromb Vasc Biol,* 25**,** 1154-60.

CHOI, S., LEE, S. A., KWAK, T. K., KIM, H. J., LEE, M. J., YE, S. K., KIM, S. H., KIM, S. & LEE, J. W. 2009. Cooperation between integrin alpha5 and tetraspan TM4SF5 regulates VEGF-mediated angiogenic activity. *Blood,* 113**,** 1845-55.

CHRISTMAN, K. L., FOK, H. H., SIEVERS, R. E., FANG, Q. & LEE, R. J. 2004. Fibrin glue alone and skeletal myoblasts in a fibrin scaffold preserve cardiac function after myocardial infarction. *Tissue Eng,* 10**,** 403-9.

CHRISTMAN, K. L. & LEE, R. J. 2006. Biomaterials for the treatment of myocardial infarction. *J Am Coll Cardiol.,* 48**,** 907-13. Epub 2006 Aug 17.

CHUNG, C. H., WU, W. B. & HUANG, T. F. 2004. Aggretin, a snake venom-derived endothelial integrin alpha 2 beta 1 agonist, induces angiogenesis via expression of vascular endothelial growth factor. *Blood,* 103**,** 2105-13.

CUNHA-REIS, C., EL HAJ, A. J., YANG, X. & YANG, Y. 2011. Fluorescent labeling of chitosan for use in non-invasive monitoring of degradation in tissue engineering. *J Tissue Eng Regen Med,* 7**,** 39-50.

DAI, W., WOLD, L. E., DOW, J. S. & KLONER, R. A. 2005. Thickening of the infarcted wall by collagen injection improves left ventricular function in rats: a novel approach to preserve cardiac function after myocardial infarction. *J Am Coll Cardiol,* 46**,** 714-9.

DAVIS, D. R., RUCKDESCHEL SMITH, R. & MARBAN, E. 2010. Human cardiospheres are a source of stem cells with cardiomyogenic potential. *Stem Cells,* 28**,** 903-4.

DELEWI, R., ANDRIESSEN, A., TIJSSEN, J. G., ZIJLSTRA, F., PIEK, J. J. & HIRSCH, A. 2013. Impact of intracoronary cell therapy on left ventricular function in the setting of acute myocardial infarction: a meta-analysis of randomised controlled clinical trials. *Heart,* 99**,** 225-32.

DENG, B., SHEN, L., WU, Y., SHEN, Y., DING, X., LU, S., JIA, J., QIAN, J. & GE, J. 2014. Delivery of alginate-chitosan hydrogel promotes endogenous repair and preserves cardiac function in rats with myocardial infarction. *J Biomed Mater Res A*.

DENG, C., ZHANG, P., VULESEVIC, B., KURAITIS, D., LI, F., YANG, A. F., GRIFFITH, M., RUEL, M. & SUURONEN, E. J. 2010. A collagen–chitosan hydrogel for endothelial differentiation and angiogenesis. *Tissue Eng Part A,* 16**,** 3099-109.

DES JARDINS, T. 2008. *Cardiopulmonary Anatomy and Physiology: Essentials for Respiratory Care*, Clifton Park, NY, Thomson Delmar Learning.

DI SANTO, S., YANG, Z., WYLER VON BALLMOOS, M., VOELZMANN, J., DIEHM, N., BAUMGARTNER, I. & KALKA, C. 2009. Novel cell-free strategy for therapeutic angiogenesis: in vitro generated conditioned medium can replace progenitor cell transplantation. *PLoS One,* 4**,** e5643.

DIMMELER, S., BURCHFIELD, J. & ZEIHER, A. M. 2008. Cell-based therapy of myocardial infarction. *Arterioscler Thromb Vasc Biol,* 28**,** 208-16.

DIMMELER, S. & LERI, A. 2008. Aging and disease as modifiers of efficacy of cell therapy. *Circ Res,* 102**,** 1319-30.

DING, L., DONG, L., CHEN, X., ZHANG, L., XU, X., FERRO, A. & XU, B. 2009. Increased expression of integrin-linked kinase attenuates left ventricular remodeling and improves cardiac function after myocardial infarction. *Circulation,* 120**,** 764-73.

DOBACZEWSKI, M., GONZALEZ-QUESADA, C. & FRANGOGIANNIS, N. G. 2010. The extracellular matrix as a modulator of the inflammatory and reparative response following myocardial infarction. *J Mol Cell Cardiol,* 48**,** 504-11.

DOYLE, B., SORAJJA, P., HYNES, B., KUMAR, A. H., ARAOZ, P. A., STALBOERGER, P. G., MILLER, D., REED, C., SCHMECKPEPER, J., WANG, S., LIU, C., TERZIC, A., KRUGER, D., RIEDERER, S. & CAPLICE, N. M. 2008. Progenitor cell therapy in a porcine acute myocardial infarction model induces cardiac hypertrophy, mediated by paracrine secretion of cardiotrophic factors including TGFbeta1. *Stem Cells Dev,* 17**,** 941-51.

ERBS, S., LINKE, A., SCHACHINGER, V., ASSMUS, B., THIELE, H., DIEDERICH, K. W., HOFFMANN, C., DIMMELER, S., TONN, T., HAMBRECHT, R., ZEIHER, A. M. & SCHULER, G. 2007. Restoration of microvascular function in the infarct-related artery by intracoronary transplantation of bone marrow progenitor cells in patients with acute myocardial infarction: the Doppler Substudy of the Reinfusion of Enriched Progenitor Cells and Infarct Remodeling in Acute Myocardial Infarction (REPAIR-AMI) trial. *Circulation,* 116**,** 366-74.

FADINI, G. P., LOSORDO, D. & DIMMELER, S. 2012. Critical reevaluation of endothelial progenitor cell phenotypes for therapeutic and diagnostic use. *Circ Res,* 110**,** 624-37.

FAN, D., TAKAWALE, A., LEE, J. & KASSIRI, Z. 2012. Cardiac fibroblasts, fibrosis and extracellular matrix remodeling in heart disease. *Fibrogenesis Tissue Repair,* 5**,** 15.

FREDERICK, J. R., FITZPATRICK, J. R., MCCORMICK, R. C., HARRIS, D. A., KIM, A. Y., MUENZER, J. R., MAROTTA, N., SMITH, M. J., COHEN, J. E., HIESINGER, W., ATLURI, P. & WOO, Y. J. 2010. Stromal cell-derived factor-1alpha activation of tissue-engineered endothelial progenitor cell matrix enhances ventricular function after myocardial infarction by inducing neovasculogenesis. *Circulation,* 122**,** S107-17.

FRIEDMAN, S. L. 2010. Extracellular Matrix. *Signaling Pathways in Liver Diseases.* Springer Berlin Heidelberg.

FRIEDRICH, E. B., WALENTA, K., SCHARLAU, J., NICKENIG, G. & WERNER, N. 2006. CD34-/CD133+/VEGFR-2+ endothelial progenitor cell subpopulation with potent vasoregenerative capacities. *Circ Res,* 98**,** e20-5.

FUJITA, M., ISHIHARA, M., MORIMOTO, Y., SIMIZU, M., SAITO, Y., YURA, H., MATSUI, T., TAKASE, B., HATTORI, H., KANATANI, Y., KIKUCHI, M. & MAEHARA, T. 2005. Efficacy of photocrosslinkable chitosan hydrogel containing fibroblast growth factor-2 in a rabbit model of chronic myocardial infarction. *J Surg Res,* 126**,** 27-33.

FUJITA, M., ISHIHARA, M., SHIMIZU, M., OBARA, K., NAKAMURA, S., KANATANI, Y., MORIMOTO, Y., TAKASE, B., MATSUI, T., KIKUCHI, M. & MAEHARA, T. 2007. Therapeutic angiogenesis induced by controlled release of fibroblast growth factor-2 from injectable chitosan/non-anticoagulant heparin hydrogel in a rat hindlimb ischemia model. *Wound Repair Regen,* 15**,** 58-65.

GAJARSA, J. J. & KLONER, R. A. 2011. Left ventricular remodeling in the post-infarction heart: a review of cellular, molecular mechanisms, and therapeutic modalities. *Heart Fail Rev,* 16**,** 13-21.

GARBERN, J. C., MINAMI, E., STAYTON, P. S. & MURRY, C. E. 2011. Delivery of basic fibroblast growth factor with a pH-responsive, injectable hydrogel to improve angiogenesis in infarcted myocardium. *Biomaterials,* 32**,** 2407-16.

GEHLING, U. M., ERGUN, S., SCHUMACHER, U., WAGENER, C., PANTEL, K., OTTE, M., SCHUCH, G., SCHAFHAUSEN, P., MENDE, T., KILIC, N., KLUGE, K., SCHAFER, B., HOSSFELD, D. K. & FIEDLER, W. 2000. In vitro differentiation of endothelial cells from AC133-positive progenitor cells. *Blood,* 95**,** 3106-12.

GEIGER, B., SPATZ, J. P. & BERSHADSKY, A. D. 2009. Environmental sensing through focal adhesions. *Nat Rev Mol Cell Biol,* 10**,** 21-33.

GIORDANO, C., KURAITIS, D., BEANLANDS, R. S., SUURONEN, E. J. & RUEL, M. 2013a. Cell-based vasculogenic studies in preclinical models of chronic myocardial ischaemia and hibernation. *Expert Opin Biol Ther,* 13**,** 411-28.

GIORDANO, C., THORN, S. L., RENAUD, J. M., AL-ATASSI, T., BOODHWANI, M., KLEIN, R., KURAITIS, D., DWIVEDI, G., ZHANG, P., DASILVA, J. N., ASCAH, K. J., DEKEMP, R. A., SUURONEN, E. J., BEANLANDS, R. S. & RUEL, M. 2013b. Pre-Clinical Evaluation of Biopolymer-Delivered Circulating Angiogenic Cells in a Swine Model of Hibernating Myocardium. *Circ Cardiovasc Imaging*.

GNECCHI, M., ZHANG, Z., NI, A. & DZAU, V. J. 2008. Paracrine mechanisms in adult stem cell signaling and therapy. *Circ Res,* 103**,** 1204-19.

GRANT, F. D., FAHEY, F. H., PACKARD, A. B., DAVIS, R. T., ALAVI, A. & TREVES, S. T. 2008. Skeletal PET with 18F-fluoride: applying new technology to an old tracer. *J Nucl Med,* 49**,** 68-78.

GUNSILIUS, E., DUBA, H. C., PETZER, A. L., KAHLER, C. M., GRUNEWALD, K., STOCKHAMMER, G., GABL, C., DIRNHOFER, S., CLAUSEN, J. & GASTL, G. 2000. Evidence from a leukaemia model for maintenance of vascular endothelium by bone-marrow-derived endothelial cells. *Lancet,* 355**,** 1688-91.

HANNIGAN, G., TROUSSARD, A. A. & DEDHAR, S. 2005. Integrin-linked kinase: a cancer therapeutic target unique among its ILK. *Nat Rev Cancer,* 5**,** 51-63.

HERPEL, E., PRITSCH, M., KOCH, A., DENGLER, T. J., SCHIRMACHER, P. & SCHNABEL, P. A. 2006. Interstitial fibrosis in the heart: differences in extracellular matrix proteins and matrix metalloproteinases in end-stage dilated, ischaemic and valvular cardiomyopathy. *Histopathology,* 48**,** 736-47.

HIRSCH, A., NIJVELDT, R., VAN DER VLEUTEN, P. A., TIO, R. A., VAN DER GIESSEN, W. J., MARQUES, K. M., DOEVENDANS, P. A., WALTENBERGER, J., TEN BERG, J. M., AENGEVAEREN, W. R., BIEMOND, B. J., TIJSSEN, J. G., VAN ROSSUM, A. C., PIEK, J. J. & ZIJLSTRA, F. 2008. Intracoronary infusion of autologous mononuclear bone marrow cells in patients with acute myocardial infarction treated with primary PCI: Pilot study of the multicenter HEBE trial. *Catheter Cardiovasc Interv,* 71**,** 273-81.

HSIEH, P. C., SEGERS, V. F., DAVIS, M. E., MACGILLIVRAY, C., GANNON, J., MOLKENTIN, J. D., ROBBINS, J. & LEE, R. T. 2007. Evidence from a genetic fate-mapping study that stem cells refresh adult mammalian cardiomyocytes after injury. *Nat Med,* 13**,** 970-4.

HUANG, N. F., YU, J., SIEVERS, R., LI, S. & LEE, R. J. 2005. Injectable biopolymers enhance angiogenesis after myocardial infarction. *Tissue Eng,* 11**,** 1860-6.

HUIKURI, H. V., KERVINEN, K., NIEMELA, M., YLITALO, K., SAILY, M., KOISTINEN, P., SAVOLAINEN, E. R., UKKONEN, H., PIETILA, M., AIRAKSINEN, J. K., KNUUTI, J., MAKIKALLIO, T. H. & INVESTIGATORS, F. 2008. Effects of intracoronary injection of mononuclear bone marrow cells on left ventricular function, arrhythmia risk profile, and restenosis after thrombolytic therapy of acute myocardial infarction. *Eur Heart J,* 29**,** 2723-32.

HUR, J., YOON, C. H., KIM, H. S., CHOI, J. H., KANG, H. J., HWANG, K. K., OH, B. H., LEE, M. M. & PARK, Y. B. 2004. Characterization of two types of endothelial progenitor cells and their different contributions to neovasculogenesis. *Arterioscler Thromb Vasc Biol,* 24**,** 288-93.

HUSSAIN, A., COLLINS, G., YIP, D. & CHO, C. H. 2013. Functional 3-D cardiac co-culture model using bioactive chitosan nanofiber scaffolds. *Biotechnol Bioeng,* 110**,** 637-47.

IKEUCHI, M., TSUTSUI, H., SHIOMI, T., MATSUSAKA, H., MATSUSHIMA, S., WEN, J., KUBOTA, T. & TAKESHITA, A. 2004. Inhibition of TGF-beta signaling exacerbates

early cardiac dysfunction but prevents late remodeling after infarction. *Cardiovasc Res,* 64**,** 526-35.

INCE, H., PETZSCH, M., KLEINE, H. D., ECKARD, H., REHDERS, T., BURSKA, D., KISCHE, S., FREUND, M. & NIENABER, C. A. 2005. Prevention of left ventricular remodeling with granulocyte colony-stimulating factor after acute myocardial infarction: final 1-year results of the Front-Integrated Revascularization and Stem Cell Liberation in Evolving Acute Myocardial Infarction by Granulocyte Colony-Stimulating Factor (FIRSTLINE-AMI) Trial. *Circulation,* 112**,** I73-80.

JEEVANANTHAM, V., BUTLER, M., SAAD, A., ABDEL-LATIF, A., ZUBA-SURMA, E. K. & DAWN, B. 2012. Adult bone marrow cell therapy improves survival and induces long-term improvement in cardiac parameters: a systematic review and meta-analysis. *Circulation,* 126**,** 551-68.

JESSUP, M. & BROZENA, S. 2003. Heart failure. *N Engl J Med,* 348**,** 2007-18.

JOHNSON, T. D. & CHRISTMAN, K. L. 2013. Injectable hydrogel therapies and their delivery strategies for treating myocardial infarction. *Expert Opin Drug Deliv,* 10**,** 59-72.

JONG, P., VOWINCKEL, E., LIU, P. P., GONG, Y. & TU, J. V. 2002. Prognosis and determinants of survival in patients newly hospitalized for heart failure: a population-based study. *Arch Intern Med,* 162**,** 1689-94.

JOSHI, N. V., VESEY, A. T., WILLIAMS, M. C., SHAH, A. S., CALVERT, P. A., CRAIGHEAD, F. H., YEOH, S. E., WALLACE, W., SALTER, D., FLETCHER, A. M., VAN BEEK, E. J., FLAPAN, A. D., UREN, N. G., BEHAN, M. W., CRUDEN, N. L.,

MILLS, N. L., FOX, K. A., RUDD, J. H., DWECK, M. R. & NEWBY, D. E. 2014. 18F-fluoride positron emission tomography for identification of ruptured and high-risk coronary atherosclerotic plaques: a prospective clinical trial. *Lancet,* 383**,** 705-13.

JUJO, K., II, M. & LOSORDO, D. W. 2008. Endothelial progenitor cells in neovascularization of infarcted myocardium. *J Mol Cell Cardiol,* 45**,** 530-44.

KAJSTURA, J., LERI, A., FINATO, N., DI LORETO, C., BELTRAMI, C. A. & ANVERSA, P. 1998. Myocyte proliferation in end-stage cardiac failure in humans. *Proc Natl Acad Sci U S A,* 95**,** 8801-5.

KALKA, C., MASUDA, H., TAKAHASHI, T., KALKA-MOLL, W. M., SILVER, M., KEARNEY, M., LI, T., ISNER, J. M. & ASAHARA, T. 2000. Transplantation of ex vivo expanded endothelial progenitor cells for therapeutic neovascularization. *Proc Natl Acad Sci U S A,* 97**,** 3422-7.

KANNEL, W. B. 2000. Incidence and epidemiology of heart failure. *Heart Fail Rev,* 5**,** 167-73.

KATZ, A. M. 2006. *Physiology of the Heart,* Philadelphia, PA, Lippincot Williams & Wilkins.

KAWAMOTO, A., TKEBUCHAVA, T., YAMAGUCHI, J., NISHIMURA, H., YOON, Y. S., MILLIKEN, C., UCHIDA, S., MASUO, O., IWAGURO, H., MA, H., HANLEY, A., SILVER, M., KEARNEY, M., LOSORDO, D. W., ISNER, J. M. & ASAHARA, T. 2003. Intramyocardial transplantation of autologous endothelial progenitor cells for therapeutic neovascularization of myocardial ischemia. *Circulation,* 107**,** 461-8.

KELLAR, R. S., LANDEEN, L. K., SHEPHERD, B. R., NAUGHTON, G. K., RATCLIFFE, A. & WILLIAMS, S. K. 2001. Scaffold-based three-dimensional human fibroblast culture provides a structural matrix that supports angiogenesis in infarcted heart tissue. *Circulation,* 104**,** 2063-8.

KICHULA, E. T., WANG, H., DORSEY, S. M., SZCZESNY, S. E., ELLIOTT, D. M., BURDICK, J. A. & WENK, J. F. 2013. Experimental and Computational Investigation of Altered Mechanical Properties in Myocardium after Hydrogel Injection. *Ann Biomed Eng*.

KIM, K. L., HAN, D. K., PARK, K., SONG, S. H., KIM, J. Y., KIM, J. M., KI, H. Y., YIE, S. W., ROH, C. R., JEON, E. S., KIM, D. K. & SUH, W. 2009. Enhanced dermal wound neovascularization by targeted delivery of endothelial progenitor cells using an RGD-g-PLLA scaffold. *Biomaterials,* 30**,** 3742-8.

KLEIN, R., BEANLANDS, R. S. & DEKEMP, R. A. 2010. Quantification of myocardial blood flow and flow reserve: Technical aspects. *J Nucl Cardiol,* 17**,** 555-70.

KOYANAGI, M., DIMMELER, S. 2012. Repopulation of the Heart with New Cardiomyocytes: Circulating Progenitor Cells. *In:* ENGEL, F. B. (ed.) *Heart Regeneration: Stem Cells and Beyond.* Singapore: World Scientific Publishing Co.

KURAITIS, D., GIORDANO, C., RUEL, M., MUSARO, A. & SUURONEN, E. J. 2012a. Exploiting extracellular matrix-stem cell interactions: a review of natural materials for therapeutic muscle regeneration. *Biomaterials,* 33**,** 428-43.

KURAITIS, D., GIORDANO, C., RUEL, M., MUSARÒ, A. & SUURONEN, E. J. 2012b. Exploiting extracellular matrix-stem cell interactions: a review of natural materials for therapeutic muscle regeneration. *Biomaterials,* 33**,** 428-43.

KURAITIS, D., HOU, C., ZHANG, Y., VULESEVIC, B., SOFRENOVIC, T., MCKEE, D., SHARIF, Z., RUEL, M. & SUURONEN, E. J. 2011a. Ex vivo generation of a highly potent population of circulating angiogenic cells using a collagen matrix. *J Mol Cell Cardiol,* 51**,** 187-97.

KURAITIS, D., SUURONEN, E. J., SELLKE, F. W. & RUEL, M. 2010. The future of regenerating the myocardium. *Curr Opin Cardiol,* 25**,** 575-82.

KURAITIS, D., ZHANG, P., ZHANG, Y., PADAVAN, D. T., MCEWAN, K., SOFRENOVIC, T., MCKEE, D., ZHANG, J., GRIFFITH, M., CAO, X., MUSARÒ, A., RUEL, M. & SUURONEN, E. J. 2011b. A stromal cell-derived factor-1 releasing matrix enhances the progenitor cell response and blood vessel growth in ischaemic skeletal muscle. *Eur Cell Mater,* 22**,** 109-23.

LAMOUREUX, M., THORN, S., DUMOUCHEL, T., RENAUD, J. M., KLEIN, R., MASON, S., LORTIE, M., DASILVA, J. N., BEANLANDS, R. S. & DEKEMP, R. A. 2012. Uniformity and repeatability of normal resting myocardial blood flow in rats using [13N]-ammonia and small animal PET. *Nucl Med Commun,* 33**,** 917-25.

LANGONE, A. J. & HELDERMAN, J. H. 2003. Disparity between solid-organ supply and demand. *N Engl J Med,* 349**,** 704-6.

LEE, L. C., WALL, S. T., KLEPACH, D., GE, L., ZHANG, Z., LEE, R. J., HINSON, A., GORMAN, J. H., 3RD, GORMAN, R. C. & GUCCIONE, J. M. 2013. Algisyl-LVR with coronary artery bypass grafting reduces left ventricular wall stress and improves function in the failing human heart. *Int J Cardiol,* 168**,** 2022-8.

LEE, S. P., YOUN, S. W., CHO, H. J., LI, L., KIM, T. Y., YOOK, H. S., CHUNG, J. W., HUR, J., YOON, C. H., PARK, K. W., OH, B. H., PARK, Y. B. & KIM, H. S. 2006. Integrin-linked kinase, a hypoxia-responsive molecule, controls postnatal vasculogenesis by recruitment of endothelial progenitor cells to ischemic tissue. *Circulation,* 114**,** 150-9.

LEOR, J., TUVIA, S., GUETTA, V., MANCZUR, F., CASTEL, D., WILLENZ, U., PETNEHAZY, O., LANDA, N., FEINBERG, M. S., KONEN, E., GOITEIN, O., TSUR-GANG, O., SHAUL, M., KLAPPER, L. & COHEN, S. 2009. Intracoronary injection of in situ forming alginate hydrogel reverses left ventricular remodeling after myocardial infarction in Swine. *J Am Coll Cardiol,* 54**,** 1014-23.

LI, B., POZZI, A. & YOUNG, P. P. 2011. TNFalpha accelerates monocyte to endothelial transdifferentiation in tumors by the induction of integrin alpha5 expression and adhesion to fibronectin. *Mol Cancer Res,* 9**,** 702-11.

LI, S., BORDOY, R., STANCHI, F., MOSER, M., BRAUN, A., KUDLACEK, O., WEWER, U. M., YURCHENCO, P. D. & FASSLER, R. 2005. PINCH1 regulates cell-matrix and cell-cell adhesions, cell polarity and cell survival during the peri-implantation stage. *J Cell Sci,* 118**,** 2913-21.

LI, S. H., LAI, T. Y., SUN, Z., HAN, M., MORIYAMA, E., WILSON, B., FAZEL, S., WEISEL, R. D., YAU, T., WU, J. C. & LI, R. K. 2009. Tracking cardiac engraftment and distribution of implanted bone marrow cells: Comparing intra-aortic, intravenous, and intramyocardial delivery. *J Thorac Cardiovasc Surg,* 137**,** 1225-33.e1.

LIBBY, P. 2002. Inflammation in atherosclerosis. *Nature,* 420**,** 868-74.

LIBBY, P., RIDKER, P. M. & MASERI, A. 2002. Inflammation and atherosclerosis. *Circulation,* 105**,** 1135-43.

LIN, Y. D., YEH, M. L., YANG, Y. J., TSAI, D. C., CHU, T. Y., SHIH, Y. Y., CHANG, M. Y., LIU, Y. W., TANG, A. C., CHEN, T. Y., LUO, C. Y., CHANG, K. C., CHEN, J. H., WU, H. L., HUNG, T. K. & HSIEH, P. C. 2010. Intramyocardial peptide nanofiber injection improves postinfarction ventricular remodeling and efficacy of bone marrow cell therapy in pigs. *Circulation,* 122**,** S132-41.

LIU, Z., WANG, H., WANG, Y., LIN, Q., YAO, A., CAO, F., LI, D., ZHOU, J., DUAN, C., DU, Z., WANG, Y. & WANG, C. 2012. The influence of chitosan hydrogel on stem cell engraftment, survival and homing in the ischemic myocardial microenvironment. *Biomaterials,* 33**,** 3093-106.

LOFFREDO, F. S., STEINHAUSER, M. L., GANNON, J. & LEE, R. T. 2011. Bone marrow-derived cell therapy stimulates endogenous cardiomyocyte progenitors and promotes cardiac repair. *Cell Stem Cell,* 8**,** 389-98.

LOSORDO, D. W., HENRY, T. D., DAVIDSON, C., SUP LEE, J., COSTA, M. A., BASS, T., MENDELSOHN, F., FORTUIN, F. D., PEPINE, C. J., TRAVERSE, J. H., AMRANI,

D., EWENSTEIN, B. M., RIEDEL, N., STORY, K., BARKER, K., POVSIC, T. J., HARRINGTON, R. A., SCHATZ, R. A. & INVESTIGATORS, A. C. 2011. Intramyocardial, autologous CD34+ cell therapy for refractory angina. *Circ Res,* 109**,** 428-36.

LOSORDO, D. W., SCHATZ, R. A., WHITE, C. J., UDELSON, J. E., VEERESHWARAYYA, V., DURGIN, M., POH, K. K., WEINSTEIN, R., KEARNEY, M., CHAUDHRY, M., BURG, A., EATON, L., HEYD, L., THORNE, T., SHTURMAN, L., HOFFMEISTER, P., STORY, K., ZAK, V., DOWLING, D., TRAVERSE, J. H., OLSON, R. E., FLANAGAN, J., SODANO, D., MURAYAMA, T., KAWAMOTO, A., KUSANO, K. F., WOLLINS, J., WELT, F., SHAH, P., SOUKAS, P., ASAHARA, T. & HENRY, T. D. 2007. Intramyocardial transplantation of autologous CD34+ stem cells for intractable angina: a phase I/IIa double-blind, randomized controlled trial. *Circulation,* 115**,** 3165-72.

LUNDE, K., SOLHEIM, S., AAKHUS, S., ARNESEN, H., ABDELNOOR, M., EGELAND, T., ENDRESEN, K., ILEBEKK, A., MANGSCHAU, A., FJELD, J. G., SMITH, H. J., TARALDSRUD, E., GROGAARD, H. K., BJORNERHEIM, R., BREKKE, M., MULLER, C., HOPP, E., RAGNARSSON, A., BRINCHMANN, J. E. & FORFANG, K. 2006. Intracoronary injection of mononuclear bone marrow cells in acute myocardial infarction. *N Engl J Med,* 355**,** 1199-209.

LUTOLF, M. P., GILBERT, P. M. & BLAU, H. M. 2009. Designing materials to direct stem-cell fate. *Nature,* 462**,** 433-41.

MA, L., GAO, C., MAO, Z., ZHOU, J., SHEN, J., HU, X. & HAN, C. 2003. Collagen/chitosan porous scaffolds with improved biostability for skin tissue engineering. *Biomaterials,* 24**,** 4833-41.

MAHADEVAN, V. 2012. Anatomy of the Heart. *Surgery (Oxford),* 30**,** 5-8.

MALLIARAS, K., MAKKAR, R. R., SMITH, R. R., CHENG, K., WU, E., BONOW, R. O., MARBAN, L., MENDIZABAL, A., CINGOLANI, E., JOHNSTON, P. V., GERSTENBLITH, G., SCHULERI, K. H., LARDO, A. C. & MARBAN, E. 2014. Intracoronary cardiosphere-derived cells after myocardial infarction: evidence of therapeutic regeneration in the final 1-year results of the CADUCEUS trial (CArdiosphere-Derived aUtologous stem CElls to reverse ventricUlar dySfunction). *J Am Coll Cardiol,* 63**,** 110-22.

MALLIARAS, K., ZHANG, Y., SEINFELD, J., GALANG, G., TSELIOU, E., CHENG, K., SUN, B., AMINZADEH, M. & MARBAN, E. 2013. Cardiomyocyte proliferation and progenitor cell recruitment underlie therapeutic regeneration after myocardial infarction in the adult mouse heart. *EMBO Mol Med,* 5**,** 191-209.

MCBRIDE, C., GAUPP, D. & PHINNEY, D. G. 2003. Quantifying levels of transplanted murine and human mesenchymal stem cells in vivo by real-time PCR. *Cytotherapy,* 5**,** 7-18.

MCCALL-CULBREATH, K. D. & ZUTTER, M. M. 2008. Collagen receptor integrins: rising to the challenge. *Curr Drug Targets,* 9**,** 139-49.

MENASCHE, P., ALFIERI, O., JANSSENS, S., MCKENNA, W., REICHENSPURNER, H., TRINQUART, L., VILQUIN, J. T., MAROLLEAU, J. P., SEYMOUR, B., LARGHERO, J., LAKE, S., CHATELLIER, G., SOLOMON, S., DESNOS, M. & HAGEGE, A. A. 2008. The Myoblast Autologous Grafting in Ischemic Cardiomyopathy (MAGIC) trial: first randomized placebo-controlled study of myoblast transplantation. *Circulation,* 117**,** 1189-200.

MENASCHE, P., HAGEGE, A. A., VILQUIN, J. T., DESNOS, M., ABERGEL, E., POUZET, B., BEL, A., SARATEANU, S., SCORSIN, M., SCHWARTZ, K., BRUNEVAL, P., BENBUNAN, M., MAROLLEAU, J. P. & DUBOC, D. 2003. Autologous skeletal myoblast transplantation for severe postinfarction left ventricular dysfunction. *J Am Coll Cardiol,* 41**,** 1078-83.

MENDEZ, G. F. & COWIE, M. R. 2001. The epidemiological features of heart failure in developing countries: a review of the literature. *Int J Cardiol,* 80**,** 213-9.

MERTENS, M. E., HERMANN, A., BUHREN, A., OLDE-DAMINK, L., MOCKEL, D., GREMSE, F., EHLING, J., KIESSLING, F. & LAMMERS, T. 2014. Iron oxide-labeled collagen scaffolds for non-invasive MR imaging in tissue engineering. *Adv Funct Mater,* 24**,** 754-762.

MEYER, G. P., WOLLERT, K. C., LOTZ, J., STEFFENS, J., LIPPOLT, P., FICHTNER, S., HECKER, H., SCHAEFER, A., ARSENIEV, L., HERTENSTEIN, B., GANSER, A. & DREXLER, H. 2006. Intracoronary bone marrow cell transfer after myocardial infarction: eighteen months' follow-up data from the randomized, controlled BOOST

(BOne marrOw transfer to enhance ST-elevation infarct regeneration) trial. *Circulation,* 113**,** 1287-94.

MILLER, R., DAVIES, N. H., KORTSMIT, J., ZILLA, P. & FRANZ, T. 2013. Outcomes of myocardial infarction hydrogel injection therapy in the human left ventricle dependent on injectate distribution. *Int J Numer Method Biomed Eng,* 29**,** 870-84.

MINAMI, E., LAFLAMME, M. A., SAFFITZ, J. E. & MURRY, C. E. 2005. Extracardiac progenitor cells repopulate most major cell types in the transplanted human heart. *Circulation,* 112**,** 2951-8.

MIROTSOU, M., JAYAWARDENA, T. M., SCHMECKPEPER, J., GNECCHI, M. & DZAU, V. J. 2011. Paracrine mechanisms of stem cell reparative and regenerative actions in the heart. *J Mol Cell Cardiol,* 50**,** 280-9.

MURRY, C. E., SOONPAA, M. H., REINECKE, H., NAKAJIMA, H., NAKAJIMA, H. O., RUBART, M., PASUMARTHI, K. B., VIRAG, J. I., BARTELMEZ, S. H., POPPA, V., BRADFORD, G., DOWELL, J. D., WILLIAMS, D. A. & FIELD, L. J. 2004. Haematopoietic stem cells do not transdifferentiate into cardiac myocytes in myocardial infarcts. *Nature,* 428**,** 664-8.

MURRY, C. E., WISEMAN, R. W., SCHWARTZ, S. M. & HAUSCHKA, S. D. 1996. Skeletal myoblast transplantation for repair of myocardial necrosis. *J Clin Invest,* 98**,** 2512-23.

NABEL, E. G. & BRAUNWALD, E. 2012. A tale of coronary artery disease and myocardial infarction. *N Engl J Med,* 366**,** 54-63.

NADAL-GINARD, B., KAJSTURA, J., LERI, A. & ANVERSA, P. 2003. Myocyte death, growth, and regeneration in cardiac hypertrophy and failure. *Circ Res,* 92**,** 139-50.

NICOLETTI, A., HEUDES, D., MANDET, C., HINGLAIS, N., BARIETY, J. & MICHEL, J. B. 1996. Inflammatory cells and myocardial fibrosis: spatial and temporal distribution in renovascular hypertensive rats. *Cardiovasc Res,* 32**,** 1096-107.

NOWBAR, A. N., MIELEWCZIK, M., KARAVASSILIS, M., DEHBI, H. M., SHUN-SHIN, M. J., JONES, S., HOWARD, J. P., COLE, G. D., FRANCIS, D. P. & GROUP, D. W. 2014. Discrepancies in autologous bone marrow stem cell trials and enhancement of ejection fraction (DAMASCENE): weighted regression and meta-analysis. *BMJ,* 348**,** g2688.

OPIE, L. H. 2004. *Heart Physiology From Cell to Circulation,* Philadelphia, PA, Lippincot Williams & Wilkins.

PENN, M. S., MENDELSOHN, F. O., SCHAER, G. L., SHERMAN, W., FARR, M., PASTORE, J., ROUY, D., CLEMENS, R., ARAS, R. & LOSORDO, D. W. 2013. An open-label dose escalation study to evaluate the safety of administration of nonviral stromal cell-derived factor-1 plasmid to treat symptomatic ischemic heart failure. *Circ Res,* 112**,** 816-25.

POZZOBON, M., BOLLINI, S., IOP, L., DE GASPARI, P., CHIAVEGATO, A., ROSSI, C. A., GIULIANI, S., FASCETTI LEON, F., ELVASSORE, N., SARTORE, S. & DE COPPI, P. 2010. Human bone marrow-derived CD133(+) cells delivered to a collagen patch on cryoinjured rat heart promote angiogenesis and arteriogenesis. *Cell Transplant,* 19**,** 1247-60.

PYTELA, R., PIERSCHBACHER, M. D. & RUOSLAHTI, E. 1985. Identification and isolation of a 140 kd cell surface glycoprotein with properties expected of a fibronectin receptor. *Cell,* 40**,** 191-8.

QIN, J. & WU, C. 2012. ILK: a pseudokinase in the center stage of cell-matrix adhesion and signaling. *Curr Opin Cell Biol,* 24**,** 607-13.

QUAINI, F., URBANEK, K., BELTRAMI, A. P., FINATO, N., BELTRAMI, C. A., NADAL-GINARD, B., KAJSTURA, J., LERI, A. & ANVERSA, P. 2002. Chimerism of the transplanted heart. *N Engl J Med,* 346**,** 5-15.

RADHAKRISHNAN, J., KRISHNAN, U. M. & SETHURAMAN, S. 2014. Hydrogel based injectable scaffolds for cardiac tissue regeneration. *Biotechnol Adv*.

RADISIC, M. & CHRISTMAN, K. L. 2013. Materials science and tissue engineering: repairing the heart. *Mayo Clin Proc,* 88**,** 884-98.

RANE, A. A. & CHRISTMAN, K. L. 2011. Biomaterials for the treatment of myocardial infarction: a 5-year update. *J Am Coll Cardiol,* 58**,** 2615-29.

RANE, A. A., CHUANG, J. S., SHAH, A., HU, D. P., DALTON, N. D., GU, Y., PETERSON, K. L., OMENS, J. H. & CHRISTMAN, K. L. 2011. Increased infarct wall thickness by a bio-inert material is insufficient to prevent negative left ventricular remodeling after myocardial infarction. *PLoS One,* 6**,** e21571.

REHMAN, J., LI, J., ORSCHELL, C. M. & MARCH, K. L. 2003. Peripheral blood "endothelial progenitor cells" are derived from monocyte/macrophages and secrete angiogenic growth factors. *Circulation,* 107**,** 1164-9.

REIS, L. A., CHIU, L. L., LIANG, Y., HYUNH, K., MOMEN, A. & RADISIC, M. 2012. A peptide-modified chitosan-collagen hydrogel for cardiac cell culture and delivery. *Acta Biomater,* 8**,** 1022-36.

REVI, D., PAUL, W., TV, A. & SHARMA, C. P. 2013. Chitosan Scaffold Co cultured with Keratinocyte and Fibroblast Heals Full Thickness Skin Wounds in Rabbit. *J Biomed Mater Res A.*

RHEE, J. W., SABATINE, M.S., LILLY, L.S. 2011. Acute Coronary Syndromes. *In:* LILLY, L. S. (ed.) *Pathophysiology of Heart Disease.* 5th ed. Philadelphia, PA: Lippincott Williams & Wilkins.

SAIF, J., SCHWARZ, T. M., CHAU, D. Y., HENSTOCK, J., SAMI, P., LEICHT, S. F., HERMANN, P. C., ALCALA, S., MULERO, F., SHAKESHEFF, K. M., HEESCHEN, C. & AICHER, A. 2010. Combination of injectable multiple growth factor-releasing scaffolds and cell therapy as an advanced modality to enhance tissue neovascularization. *Arterioscler Thromb Vasc Biol,* 30**,** 1897-904.

SAKAI, T., LI, S., DOCHEVA, D., GRASHOFF, C., SAKAI, K., KOSTKA, G., BRAUN, A., PFEIFER, A., YURCHENCO, P. D. & FASSLER, R. 2003. Integrin-linked kinase (ILK) is required for polarizing the epiblast, cell adhesion, and controlling actin accumulation. *Genes Dev,* 17**,** 926-40.

SCHACHINGER, V., ASSMUS, B., BRITTEN, M. B., HONOLD, J., LEHMANN, R., TEUPE, C., ABOLMAALI, N. D., VOGL, T. J., HOFMANN, W. K., MARTIN, H., DIMMELER, S. & ZEIHER, A. M. 2004. Transplantation of progenitor cells and regeneration enhancement in acute myocardial infarction: final one-year results of the TOPCARE-AMI Trial. *J Am Coll Cardiol,* 44**,** 1690-9.

SCHACHINGER, V., ERBS, S., ELSASSER, A., HABERBOSCH, W., HAMBRECHT, R., HOLSCHERMANN, H., YU, J., CORTI, R., MATHEY, D. G., HAMM, C. W., SUSELBECK, T., ASSMUS, B., TONN, T., DIMMELER, S., ZEIHER, A. M. & INVESTIGATORS, R.-A. 2006. Intracoronary bone marrow-derived progenitor cells in acute myocardial infarction. *N Engl J Med,* 355**,** 1210-21.

SCHOMIG, A., KASTRATI, A., DIRSCHINGER, J., MEHILLI, J., SCHRICKE, U., PACHE, J., MARTINOFF, S., NEUMANN, F. J. & SCHWAIGER, M. 2000. Coronary stenting plus platelet glycoprotein IIb/IIIa blockade compared with tissue plasminogen activator in acute myocardial infarction. Stent versus Thrombolysis for Occluded Coronary Arteries in Patients with Acute Myocardial Infarction Study Investigators. *N Engl J Med,* 343**,** 385-91.

SEEGER, F. H., TONN, T., KRZOSSOK, N., ZEIHER, A. M. & DIMMELER, S. 2007. Cell isolation procedures matter: a comparison of different isolation protocols of bone marrow mononuclear cells used for cell therapy in patients with acute myocardial infarction. *Eur Heart J,* 28**,** 766-72.

SEGERS, V. F. & LEE, R. T. 2008. Stem-cell therapy for cardiac disease. *Nature,* 451**,** 937-42.

SEGERS, V. F. & LEE, R. T. 2011. Biomaterials to enhance stem cell function in the heart. *Circ Res,* 109**,** 910-22.

SEIF-NARAGHI, S. B., SINGELYN, J. M., SALVATORE, M. A., OSBORN, K. G., WANG, J. J., SAMPAT, U., KWAN, O. L., STRACHAN, G. M., WONG, J., SCHUP-MAGOFFIN, P. J., BRADEN, R. L., BARTELS, K., DEQUACH, J. A., PREUL, M., KINSEY, A. M., DEMARIA, A. N., DIB, N. & CHRISTMAN, K. L. 2013. Safety and efficacy of an injectable extracellular matrix hydrogel for treating myocardial infarction. *Sci Transl Med,* 5**,** 173ra25.

SHEARER, F., LANG, C. C. & STRUTHERS, A. D. 2013. Renin-angiotensin-aldosterone system inhibitors in heart failure. *Clin Pharmacol Ther,* 94**,** 459-67.

SHI, C., ZHU, Y., RAN, X., WANG, M., SU, Y. & CHENG, T. 2006. Therapeutic potential of chitosan and its derivatives in regenerative medicine. *J Surg Res,* 133**,** 185-92.

SHI, Q., RAFII, S., WU, M. H., WIJELATH, E. S., YU, C., ISHIDA, A., FUJITA, Y., KOTHARI, S., MOHLE, R., SAUVAGE, L. R., MOORE, M. A., STORB, R. F. & HAMMOND, W. P. 1998. Evidence for circulating bone marrow-derived endothelial cells. *Blood,* 92**,** 362-7.

SHINTANI, S., MUROHARA, T., IKEDA, H., UENO, T., HONMA, T., KATOH, A., SASAKI, K., SHIMADA, T., OIKE, Y. & IMAIZUMI, T. 2001. Mobilization of endothelial progenitor cells in patients with acute myocardial infarction. *Circulation,* 103**,** 2776-9.

SHUDO, Y., MIYAGAWA, S., FUKUSHIMA, S., SAITO, A., SHIMIZU, T., OKANO, T. & SAWA, Y. 2011. Novel regenerative therapy using cell-sheet covered with omentum flap

delivers a huge number of cells in a porcine myocardial infarction model. *J Thorac Cardiovasc Surg,* 142**,** 1188-96.

SILVA, E. A., KIM, E. S., KONG, H. J. & MOONEY, D. J. 2008. Material-based deployment enhances efficacy of endothelial progenitor cells. *Proc Natl Acad Sci U S A,* 105**,** 14347-52.

SINGELYN, J. M. & CHRISTMAN, K. L. 2010. Injectable materials for the treatment of myocardial infarction and heart failure: the promise of decellularized matrices. *J Cardiovasc Transl Res,* 3**,** 478-86.

SORRENTINO, S. A., BAHLMANN, F. H., BESLER, C., MULLER, M., SCHULZ, S., KIRCHHOFF, N., DOERRIES, C., HORVATH, T., LIMBOURG, A., LIMBOURG, F., FLISER, D., HALLER, H., DREXLER, H. & LANDMESSER, U. 2007. Oxidant stress impairs in vivo reendothelialization capacity of endothelial progenitor cells from patients with type 2 diabetes mellitus: restoration by the peroxisome proliferator-activated receptor-gamma agonist rosiglitazone. *Circulation,* 116**,** 163-73.

SOUDERS, C. A., BOWERS, S. L. & BAUDINO, T. A. 2009. Cardiac fibroblast: the renaissance cell. *Circ Res,* 105**,** 1164-76.

SPINALE, F. G. 2007. Myocardial matrix remodeling and the matrix metalloproteinases: influence on cardiac form and function. *Physiol Rev,* 87**,** 1285-342.

SPRINGER, M. L., SIEVERS, R. E., VISWANATHAN, M. N., YEE, M. S., FOSTER, E., GROSSMAN, W. & YEGHIAZARIANS, Y. 2005. Closed-chest cell injections into

mouse myocardium guided by high-resolution echocardiography. *Am J Physiol Heart Circ Physiol,* 289**,** H1307-14.

STAMM, C., NASSERI, B., CHOI, Y. H. & HETZER, R. 2009. Cell therapy for heart disease: great expectations, as yet unmet. *Heart Lung Circ,* 18**,** 245-56.

STAMM, C., WESTPHAL, B., KLEINE, H. D., PETZSCH, M., KITTNER, C., KLINGE, H., SCHUMICHEN, C., NIENABER, C. A., FREUND, M. & STEINHOFF, G. 2003. Autologous bone-marrow stem-cell transplantation for myocardial regeneration. *Lancet,* 361**,** 45-6.

STRAUER, B.-E. & STEINHOFF, G. 2011. 10 Years of Intracoronary and Intramyocardial Bone Marrow Stem Cell Therapy of the Heart: From the Methodological Origin to Clinical Practice. *J Am Coll Cardiol,* 58**,** 1095-1104.

STROM, J. B., LIBBY, P. 2011. Atherosclerosis. *In:* LILLY, L. S. (ed.) *Pathophysiology of Heart Disease.* 5th ed. Philadelphia, PA: Lippincott Williams & Wilkins.

STUPACK, D. G. & CHERESH, D. A. 2002. Get a ligand, get a life: integrins, signaling and cell survival. *Journal of Cell Science,* 115**,** 3729-3738.

SUH, H. N. & HAN, H. J. 2011. Collagen I regulates the self-renewal of mouse embryonic stem cells through alpha2beta1 integrin- and DDR1-dependent Bmi-1. *J Cell Physiol,* 226**,** 3422-32.

SULLIVAN, K. E. & BLACK, L. D. 2013. The role of cardiac fibroblasts in extracellular matrix-mediated signaling during normal and pathological cardiac development. *J Biomech Eng,* 135**,** 71001.

SULLIVAN, K. E., QUINN, K. P., TANG, K. M., GEORGAKOUDI, I. & BLACK, L. D., 3RD 2014. Extracellular matrix remodeling following myocardial infarction influences the therapeutic potential of mesenchymal stem cells. *Stem Cell Res Ther,* 5**,** 14.

SUURONEN, E. J., PRICE, J., VEINOT, J. P., ASCAH, K., KAPILA, V., GUO, X. W., WONG, S., MESANA, T. G. & RUEL, M. 2007. Comparative effects of mesenchymal progenitor cells, endothelial progenitor cells, or their combination on myocardial infarct regeneration and cardiac function. *J Thorac Cardiovasc Surg,* 134**,** 1249-58.

SUURONEN, E. J., VEINOT, J. P., WONG, S., KAPILA, V., PRICE, J., GRIFFITH, M., MESANA, T. G. & RUEL, M. 2006. Tissue-engineered injectable collagen-based matrices for improved cell delivery and vascularization of ischemic tissue using CD133+ progenitors expanded from the peripheral blood. *Circulation,* 114**,** I138-44.

SUURONEN, E. J., ZHANG, P., KURAITIS, D., CAO, X., MELHUISH, A., MCKEE, D., LI, F., MESANA, T. G., VEINOT, J. P. & RUEL, M. 2009. An acellular matrix-bound ligand enhances the mobilization, recruitment and therapeutic effects of circulating progenitor cells in a hindlimb ischemia model. *FASEB J,* 23**,** 1447-58.

SZABO, E., SOBOLOFF, J., DZIAK, E. & OPAS, M. 2009. Tamoxifen-inducible Cre-mediated calreticulin excision to study mouse embryonic stem cell differentiation. *Stem Cells Dev,* 18**,** 187-93.

TAKAHASHI, T., KALKA, C., MASUDA, H., CHEN, D., SILVER, M., KEARNEY, M., MAGNER, M., ISNER, J. M. & ASAHARA, T. 1999. Ischemia- and cytokine-induced mobilization of bone marrow-derived endothelial progenitor cells for neovascularization. *Nat Med,* 5**,** 434-8.

TAKEHARA, N., TSUTSUMI, Y., TATEISHI, K., OGATA, T., TANAKA, H., UEYAMA, T., TAKAHASHI, T., TAKAMATSU, T., FUKUSHIMA, M., KOMEDA, M., YAMAGISHI, M., YAKU, H., TABATA, Y., MATSUBARA, H. & OH, H. 2008. Controlled delivery of basic fibroblast growth factor promotes human cardiosphere-derived cell engraftment to enhance cardiac repair for chronic myocardial infarction. *J Am Coll Cardiol,* 52**,** 1858-65.

TAYLOR, D. O., EDWARDS, L. B., AURORA, P., CHRISTIE, J. D., DOBBELS, F., KIRK, R., RAHMEL, A. O., KUCHERYAVAYA, A. Y. & HERTZ, M. I. 2008. Registry of the International Society for Heart and Lung Transplantation: twenty-fifth official adult heart transplant report--2008. *J Heart Lung Transplant,* 27**,** 943-56.

TERPSTRA, L., PRUD'HOMME, J., ARABIAN, A., TAKEDA, S., KARSENTY, G., DEDHAR, S. & ST-ARNAUD, R. 2003. Reduced chondrocyte proliferation and chondrodysplasia in mice lacking the integrin-linked kinase in chondrocytes. *J Cell Biol,* 162**,** 139-48.

THIELE, J., VARUS, E., WICKENHAUSER, C., KVASNICKA, H. M., LORENZEN, J., GRAMLEY, F., METZ, K. A., RIVERO, F. & BEELEN, D. W. 2004. Mixed chimerism of cardiomyocytes and vessels after allogeneic bone marrow and stem-cell transplantation in comparison with cardiac allografts. *Transplantation,* 77**,** 1902-5.

TIMMERMANS, F., VAN HAUWERMEIREN, F., DE SMEDT, M., RAEDT, R., PLASSCHAERT, F., DE BUYZERE, M. L., GILLEBERT, T. C., PLUM, J. & VANDEKERCKHOVE, B. 2007. Endothelial outgrowth cells are not derived from CD133+ cells or CD45+ hematopoietic precursors. *Arterioscler Thromb Vasc Biol,* 27**,** 1572-9.

TONGERS, J., LOSORDO, D. W. & LANDMESSER, U. 2011. Stem and progenitor cell-based therapy in ischaemic heart disease: promise, uncertainties, and challenges. *Eur Heart J,* 32**,** 1197-206.

URBANEK, K., QUAINI, F., TASCA, G., TORELLA, D., CASTALDO, C., NADAL-GINARD, B., LERI, A., KAJSTURA, J., QUAINI, E. & ANVERSA, P. 2003. Intense myocyte formation from cardiac stem cells in human cardiac hypertrophy. *Proc Natl Acad Sci U S A,* 100**,** 10440-5.

URBICH, C., AICHER, A., HEESCHEN, C., DERNBACH, E., HOFMANN, W. K., ZEIHER, A. M. & DIMMELER, S. 2005. Soluble factors released by endothelial progenitor cells promote migration of endothelial cells and cardiac resident progenitor cells. *J Mol Cell Cardiol,* 39**,** 733-42.

VAN RAMSHORST, J., BAX, J. J., BEERES, S. L., DIBBETS-SCHNEIDER, P., ROES, S. D., STOKKEL, M. P., DE ROOS, A., FIBBE, W. E., ZWAGINGA, J. J., BOERSMA, E., SCHALIJ, M. J. & ATSMA, D. E. 2009. Intramyocardial bone marrow cell injection for chronic myocardial ischemia: a randomized controlled trial. *JAMA,* 301**,** 1997-2004.

VENUGOPAL, J. R., PRABHAKARAN, M. P., MUKHERJEE, S., RAVICHANDRAN, R., DAN, K. & RAMAKRISHNA, S. 2012. Biomaterial strategies for alleviation of myocardial infarction. *J R Soc Interface,* 9**,** 1-19.

WALL, S. T., WALKER, J. C., HEALY, K. E., RATCLIFFE, M. B. & GUCCIONE, J. M. 2006. Theoretical impact of the injection of material into the myocardium: a finite element model simulation. *Circulation,* 114**,** 2627-35.

WALTER, D. H., RITTIG, K., BAHLMANN, F. H., KIRCHMAIR, R., SILVER, M., MURAYAMA, T., NISHIMURA, H., LOSORDO, D. W., ASAHARA, T. & ISNER, J. M. 2002. Statin therapy accelerates reendothelialization: a novel effect involving mobilization and incorporation of bone marrow-derived endothelial progenitor cells. *Circulation,* 105**,** 3017-24.

WANG, H., ZHANG, X., LI, Y., MA, Y., ZHANG, Y., LIU, Z., ZHOU, J., LIN, Q., WANG, Y., DUAN, C. & WANG, C. 2010. Improved myocardial performance in infarcted rat heart by co-injection of basic fibroblast growth factor with temperature-responsive chitosan hydrogel. *J Heart Lung Transplant,* 29**,** 881-7.

WANG, L. & STEGEMANN, J. P. 2010. Thermogelling chitosan and collagen composite hydrogels initiated with beta-glycerophosphate for bone tissue engineering. *Biomaterials,* 31**,** 3976-85.

WARY, K. K., VOGEL, S. M., GARREAN, S., ZHAO, Y. D. & MALIK, A. B. 2009. Requirement of alpha(4)beta(1) and alpha(5)beta(1) integrin expression in bone-marrow-

derived progenitor cells in preventing endotoxin-induced lung vascular injury and edema in mice. *Stem Cells,* 27**,** 3112-20.

WERNER, C., BOHM, M. & FRIEDRICH, E. B. 2008. Role of integrin-linked kinase for functional capacity of endothelial progenitor cells in patients with stable coronary artery disease. *Biochem Biophys Res Commun,* 377**,** 331-6.

WHITAKER, R. H. 2010. Anatomy of the Heart. *Medicine,* 38**,** 333-335.

WILLIAMS, C., QUINN, K. P., GEORGAKOUDI, I. & BLACK, L. D., 3RD 2014. Young developmental age cardiac extracellular matrix promotes the expansion of neonatal cardiomyocytes in vitro. *Acta Biomater,* 10**,** 194-204.

WOLLERT, K. C. & DREXLER, H. 2010a. Cell therapy for the treatment of coronary heart disease: a critical appraisal. *Nat Rev Cardiol,* 7**,** 204-215.

WOLLERT, K. C. & DREXLER, H. 2010b. Cell therapy for the treatment of coronary heart disease: a critical appraisal. *Nat Rev Cardiol,* 7**,** 204-15.

YANCY, C. W., LOPATIN, M., STEVENSON, L. W., DE MARCO, T., FONAROW, G. C., COMMITTEE, A. S. A. & INVESTIGATORS 2006. Clinical presentation, management, and in-hospital outcomes of patients admitted with acute decompensated heart failure with preserved systolic function: a report from the Acute Decompensated Heart Failure National Registry (ADHERE) Database. *J Am Coll Cardiol,* 47**,** 76-84.

YANG, F., YANG, X. P., LIU, Y. H., XU, J., CINGOLANI, O., RHALEB, N. E. & CARRETERO, O. A. 2004. Ac-SDKP reverses inflammation and fibrosis in rats with heart failure after myocardial infarction. *Hypertension,* 43**,** 229-36.

YANG, Z., VON BALLMOOS, M. W., FAESSLER, D., VOELZMANN, J., ORTMANN, J., DIEHM, N., KALKA-MOLL, W., BAUMGARTNER, I., DI SANTO, S. & KALKA, C. 2010. Paracrine factors secreted by endothelial progenitor cells prevent oxidative stress-induced apoptosis of mature endothelial cells. *Atherosclerosis,* 211**,** 103-9.

YOON, C.-H., HUR, J., PARK, K.-W., KIM, J.-H., LEE, C.-S., OH, I.-Y., KIM, T.-Y., CHO, H.-J., KANG, H.-J., CHAE, I.-H., YANG, H.-K., OH, B.-H., PARK, Y.-B. & KIM, H.-S. 2005a. Synergistic Neovascularization by Mixed Transplantation of Early Endothelial Progenitor Cells and Late Outgrowth Endothelial Cells. *Circulation,* 112**,** 1618-1627.

YOON, C. H., HUR, J., PARK, K. W., KIM, J. H., LEE, C. S., OH, I. Y., KIM, T. Y., CHO, H. J., KANG, H. J., CHAE, I. H., YANG, H. K., OH, B. H., PARK, Y. B. & KIM, H. S. 2005b. Synergistic neovascularization by mixed transplantation of early endothelial progenitor cells and late outgrowth endothelial cells: the role of angiogenic cytokines and matrix metalloproteinases. *Circulation,* 112**,** 1618-27.

ZHANG, Y., DASILVA, J. N., HADIZAD, T., THORN, S., KURAITIS, D., RENAUD, J. M., AHMADI, A., KORDOS, M., DEKEMP, R. A., BEANLANDS, R. S., SUURONEN, E. J. & RUEL, M. 2012. (18)F-FDG cell labeling may underestimate transplanted cell homing: more accurate, efficient, and stable cell labeling with hexadecyl-4-[(18)F]fluorobenzoate for in vivo tracking of transplanted human progenitor cells by positron emission tomography. *Cell Transplant,* 21**,** 1821-35.

ZHANG, Y., THORN, S., DASILVA, J. N., LAMOUREUX, M., DEKEMP, R. A., BEANLANDS, R. S., RUEL, M. & SUURONEN, E. J. 2008a. Collagen-based matrices improve the delivery of transplanted cells: development and demonstration by ex vivo radionuclide labeling of endothelial progenitor cells and their in vivo tracking with micropositron emission tomography. *Circulation: Cardiovascular Imaging,* 1**,** 197-204.

ZHANG, Y., THORN, S., DASILVA, J. N., LAMOUREUX, M., DEKEMP, R. A., BEANLANDS, R. S., RUEL, M. & SUURONEN, E. J. 2008b. Collagen-based matrices improve the delivery of transplanted circulating progenitor cells: development and demonstration by ex vivo radionuclide cell labeling and in vivo tracking with positron-emission tomography. *Circ Cardiovasc Imaging,* 1**,** 197-204.

ZIMMET, H., PORAPAKKHAM, P., PORAPAKKHAM, P., SATA, Y., HAAS, S. J., ITESCU, S., FORBES, A. & KRUM, H. 2012. Short- and long-term outcomes of intracoronary and endogenously mobilized bone marrow stem cells in the treatment of ST-segment elevation myocardial infarction: a meta-analysis of randomized control trials. *Eur J Heart Fail,* 14**,** 91-105.

ZOHLNHOFER, D., DIBRA, A., KOPPARA, T., DE WAHA, A., RIPA, R. S., KASTRUP, J., VALGIMIGLI, M., SCHOMIG, A. & KASTRATI, A. 2008. Stem cell mobilization by granulocyte colony-stimulating factor for myocardial recovery after acute myocardial infarction: a meta-analysis. *J Am Coll Cardiol,* 51**,** 1429-37.

Appendices

Appendix A - Methods for the Figures of Chapter 5

Quantification of c-kit$^+$ cells in MI hearts

1 wk and 3 wks after treatment delivery, the mice were sacrificed and the hearts perfused with ice cold PBS. The infarct and peri-infarct regions were dissected from the intact ventricular areas and digested separately as described before (Pfister et al., 2005). Briefly, hearts were perfused with 10ml of heparin (5U/ml), minced and digested with 1mg/ml collagenase B (Roche), 2.4U/ml Dispase II (Roche), 0.05% trypsin (Sigma) and 2.5mmol/L $CaCl_2$ in Hank's balanced salt solution (HBSS) buffer for 45 minutes at 37^{o}C. Samples were washed with ice cold 2% fetal calf serum in HBSS, filtered through a 70um filter and centrifuged for 5 minutes at 530g. FACSAria flow cytometry (BD bioscience) was performed to detect c-kit using anti-mouse CD117/c-kit-PE antibody (Southern Biotech). A ratio of the number of c-kit$^+$ cells in the infarct and peri-infarct tissue compared to the number of in the intact ventricular area was calculated.

Assessment of Mouse Serum Angiogenic Chemokines

Mouse blood was collected 3 wk after treatment delivery by cardiac puncture. The serum was isolated by centrifugation for 30 minutes at 700g. 100μl of the final concentration was added to the antibody array glass chip (RayBio® G-Series Cytokine Antibody Array (RayBiotech; Cat# AAM-ANG-G1-4)). After 2 hours of incubation at 37^{o}C, a cocktail of biotinylated antibody was added and the samples were incubated at 4^{o}C overnight followed by 1 hour of incubation with labelled streptavidin. The samples were washed between incubation using the Wash buffer provided with the kit. Finally, the signals were detected by GenePix 4000B macroarray scanner

(Molecular Devices). All cytokines were normalized to internal standard on the glass chip and the arbitrary values were calculated based on intensity of fluorescent signal.

Appendix B – Authorizations

Figure 1.1 was reproduced with the general permission from the Massachusetts Medical Society, Publisher of the New England Journal of Medicine which is available online in the following URL: http://www.nejm.org/page/about-nejm/permissions.

Figure 1.2 was reprinted from an open access article after obtaining the permission from Elsevier's Global Rights Department.

Figure 1.3 was reprinted with the following permission:

Order Completed

Thank you very much for your order.

This is a License Agreement between Ali Ahmadi ("You") and Elsevier ("Elsevier"). The license consists of your order details, the terms and conditions provided by Elsevier, and the payment terms and conditions.

Get the printable license.

License Number	3371460380576
License date	Apr 17, 2014
Licensed content publisher	Elsevier
Licensed content publication	Heart, Lung and Circulation
Licensed content title	Cell Therapy for Heart Disease: Great Expectations, As Yet Unmet
Licensed content author	Christof Stamm,Boris Nasseri,Yeong-Hoon Choi,Roland Hetzer
Licensed content date	August 2009
Licensed content volume number	18
Licensed content issue number	4
Number of pages	12
Type of Use	reuse in a thesis/dissertation
Portion	figures/tables/illustrations
Number of figures/tables/illustrations	1
Format	both print and electronic
Are you the author of this Elsevier article?	No
Will you be translating?	No
Title of your thesis/dissertation	Application of Collagen Matrices for Enhancing Cardiac Regeneration
Expected completion date	Apr 2014
Estimated size (number of pages)	200
Elsevier VAT number	GB 494 6272 12
Permissions price	0.00 USD
VAT/Local Sales Tax	0.00 USD / 0.00 GBP
Total	0.00 USD

Chapter 3 was reprinted with following permission:

Order Completed

Thank you very much for your order.

This is a License Agreement between Ali Ahmadi ("You") and Elsevier ("Elsevier"). The license consists of your order details, the terms and conditions provided by Elsevier, and the payment terms and conditions.

Get the printable license.

License Number	3424250937096
License date	Jul 08, 2014
Licensed content publisher	Elsevier
Licensed content publication	Biomaterials
Licensed content title	The role of integrin α2 in cell and matrix therapy that improves perfusion, viability and function of infarcted myocardium
Licensed content author	Ali Ahmadi,Brian McNeill,Branka Vulesevic,Myra Kordos,Laura Mesana,Stephanie Thorn,Jennifer M. Renaud,Emily Manthorp,Drew Kuraitis,Hadi Toeg,Thierry G. Mesana,Darryl R. Davis,Rob S. Beanlands,Jean N. DaSilva,Robert A. deKemp,Marc Ruel,Erik J. Suuronen
Licensed content date	June 2014
Licensed content volume number	35
Licensed content issue number	17
Number of pages	10
Type of Use	reuse in a thesis/dissertation
Portion	full article
Format	both print and electronic
Are you the author of this Elsevier article?	Yes
Will you be translating?	No
Title of your thesis/dissertation	Application of Collagen Matrices for Enhancing Cardiac Regeneration
Expected completion date	Jul 2014

Estimated size (number of pages)	200
Elsevier VAT number	GB 494 6272 12
Permissions price	0.00 USD
VAT/Local Sales Tax	0.00 USD / 0.00 GBP
Total	0.00 USD

Additional Reference

PFISTER, O., MOUQUET, F., JAIN, M., SUMMER, R., HELMES, M., FINE, A., COLUCCI, W. S. & LIAO, R. 2005. CD31- but Not CD31+ cardiac side population cells exhibit functional cardiomyogenic differentiation. *Circ Res*, 97**,** 52-61.